The Paton WELDING JOURNAL

August 2000 # 8

English translation of the monthly «Avtomaticheskaya Svarka» journal published in Russian since 1948

«The Paton Welding Journal» monthly is published by the E.O. Paton Electric Welding Institute of the National Academy of Sciences of Ukraine with the support rendered by the International Association «Welding».

Promotion group:
V.N.Lipodaev, V.I.Lokteva
A.T.Zelnichenko (Exec. director)
Translators:
S.A.Fomina, I.N.Kutianova,
T.K.Vasilenko

Editorial and advertising offices are located at PWI, Dept. 51, 11, Bozhenko str., 03680, Kyiv, Ukraine.
Tel.: (38044) 227 67 57
Fax: (38044) 268 04 86
E-mail: paton@i.kiev.ua

Subscriptions:
$460, 12 issues

«The Paton Welding Journal» Website:
http://www.nas.gov.ua/pwj

CONTENTS

IMPROVEMENT OF CAVITATION-EROSION RESISTANCE OF CLAD PARTS OF HYDRAULIC MACHINERY

O.G. BYKOVSKY, I.V. PINKOVSKY and **A.V. PATYUPKIN**
Zaporizhya State Technical University, Zaporizhya, Ukraine

ABSTRACT

High-temperature impact on the metal surface in cavitation erosion has been confirmed. Application of dispersion-hardening alloys with an unstable structure is recommended for its elimination. Control of thermal cycle and cladding technique enables a considerable improvement of the cavitation-erosion resistance of the deposited metal.

Key words: *cavitation, erosion, specific energy content, wear-resistant cladding, steel, non-ferrous alloys, relative erosion resistance*

The cavitation phenomenon is found with interruption of the continuity in individual portions of the moving liquid flow, that occurs in interaction with shapes or surfaces of machine parts which are difficult to flow around, as well as in boosted operational modes. Performance deterioration, for instance, lowering of the efficiency of propellers of high-speed ships is accompanied by fracture of the working surface.

Other parts of hydraulic machines are also prone to cavitation wear, namely nozzles, needles and cups of the impeller; guide blades and vanes, impeller case walls in the hydraulic turbines; impeller and straightening unit blades, and spiral cases in centrifugal pumps; stop and relief valves in the pipelines and high-pressure systems. Cavitation impacts destroy the water-cooled walls of the jacket clearance chamber of internal combustion engines, high-speed hydrodynamic bearings and thrust bearings, etc.

Depending on the operational conditions, the area of the damaged zone surface can be up to several square meters, and its depth can be from several millimeters up to several tens of centimeters. Sometimes, the fracture can even be a through-thickness one.

Besides visual observation under the operational conditions, study of the materials behaviour at cavitation impact is now also conducted using various units. Of the latter, the rotating disc unit (RDU) and impact-erosion test rig (IETR) have become widely accepted. RDU reproduces the actual cavitation impact of the liquid flow on the metal and is used for quality tests in investigation of the initial stages and mechanism of cavitation erosion [1]. IETR is applied for quantitative comparative testing of surfaced metal samples with the aim of selection of the optimal composition of the alloy [2].

Qualitative tests are conducted on samples of different shape. The studied surface is polished or prepared in the form of a microsection. For quantitative testing only grinding of the samples surface is performed. Deposited metal wear resistance is assessed by the loss of weight or volume in a certain time interval and is compared with the wear resistance of the standard material. Well-studied materials, for instance, steel 45 or an alloy of which the part developing cavitation erosion, is made, are often used as the latter. The initial stages of the damage are studied by surface profilemetry.

The standpoint of cavitation erosion of the solid surface being due to closure of vapour-gas bubbles on it or near it, can now be regarded as universally recognised [3].

The bubbles penetrating into the normal pressure zone, experience multiple pressing, which results in that the pressure and temperature inside them can rise up to values of tens of thousand atmospheres and thousand degrees, respectively. Although no one has so far been successful in direct measurement of these values, there is indirect evidence of such a thermodeformational impact on the metal as will be shown below.

The complexity of studying the cavitation erosion, is due both to a fast running of the cavitation process proper and to the diversity of the phenomena proceeding in different materials exposed to multiple action of the forming bubbles field. Therefore, the nature of cavitation fracture depends, on the one hand, on the energy and concentration of cavitation bubbles, and on the other, on the strength properties of the materials.

Already the first studies of the initial stages of material fracture in RDU provided experimental proof of the assumption put forward by other researchers, on the relationship between the nature of bubbles distribution and their energy content. It was established that the law of cavitation dents distribution reflecting the random nature of their appearance on the sample surface, corresponds to the Rayleigh distribution density, namely a large number of bubbles with a relatively small energy and small number of bubbles with a relatively high energy.

Analysing the nature of surface relief of an aluminium sample, it can be stated that the formed pits are the result of mechanical impacts of varying intensity. The probability of larger pits development decreases, as with the increase of the impact energy the probability of the impact occurring decreases [1].

Other consequences of thermodeformational impact such as microcracks, slip lines, metal strengthening, are the result of closure of bubbles with a smaller energy as they develop much later than the dent-pits.

Assessment of the level of energy consumed in formation of individual erosion dents, was performed by determination of specific energy content in the materials being tested. This was done by the method of local dynamic deformation of the surface with a steel sphere which was «shot at the sample» with the velocity of 50 – 70 m/s.

The thus formed pit has the volume proportional to the applied energy. This is how the distinct relationship between the pulsed impact strength and elasto-plastic properties of the material, is manifested. Knowing the values of the average volume of the pit and the specific energy content, it is possible to calculate the amount of energy consumed in formation of the local deformation.

It is obvious that the destructive impact of the bubbles depends not only on their energy content, but also on their location relative to the surface. Thus, in bursting of a bubble located near the surface, the impact waves propagate from it as a result of contraction and vibration, which having reached an obstacle in the form of a solid wall, transfer part of their energy to it. Depending on the material properties, either plastic flow or brittle cleavage accompanied by strengthening of isolated microvolumes, take place in the surface layers.

Now, if part of the bubbles form on the very surface, which occurs in the case of the bubble touching it in one point, when the equilibrium of the resultant compressive forces is violated, the impact on the surface is made by microjets which rush into the bursting bubble and make a cumulative microimpact effect on the metal surface (Figure 1, *a*). In this case, higher order energy is imparted to the surface, whereas the stresses exceed the ultimate rupture strength of the material, this being sufficient for local pitting formation. Mechanical impact is accompanied by a significant local temperature rise. This is indicated by appearance of temper colours and by a thin fringe of the molten and then the solidified microscopic particles of the metal ejected out of the pitting (Figure 1, *b*). Both materials with a low corrosion resistance (Figure 1, *a*) and alloys with a high corrosion resistance in fresh water, for instance, brasses, are equally susceptible to corrosion-mechanical impact. The performed microanalysis of the composition of the metal at the pitting bottom (Figure 1, *b*) showed a reduction of zinc content by 30 % in this zone, which can certainly be accounted for only by instantaneous evaporation of this element.

The clearly visible remnants of the flows of molten and then solidified metal at the pitting edge are an indication of the high temperature (Figure 1, *c*). During testing in RDU also, the water heated up to 60 – 80 °C already after several minutes of operation, so that the assumptions of a relatively high-temperature impact in bubble closure are not unfounded. Cavitation erosion being due to cyclic corrosion-mechanical fracture, the mechanism of this process can be analysed in terms of the theory of fatigue fracture, taking into account the fact that impact loads with amplitude variation from 0 to ∞ are applied to each microscopic site.

In this case the proposed schematic allows the cavitation fracture to be represented as the result of the integral action of local loads creating hazardous stresses in the surface layers [1, 2].

In the first zone (Figure 2) the stresses do not exceed the ultimate fatigue resistance of the material in the corroding medium, so that a continuous elastic dissipation of the energy applied to the surface proceeds in it, without any visible traces of plastic deformation.

The second region is characteristic of the regular multi-cycle fatigue fracture, when in the first stages the stresses with the amplitude in this range do not cause any visible damage of the surfaces, although the energy is consumed for accumulation of structural defects (dislocations and vacancies) which manifest themselves in appearance of the slip bands.

In the third region plastic deformation of microvolumes of the surface layer of the metal in each loading act prevails, namely formation of dent-pits, as well as accumulation of micropores and mi-

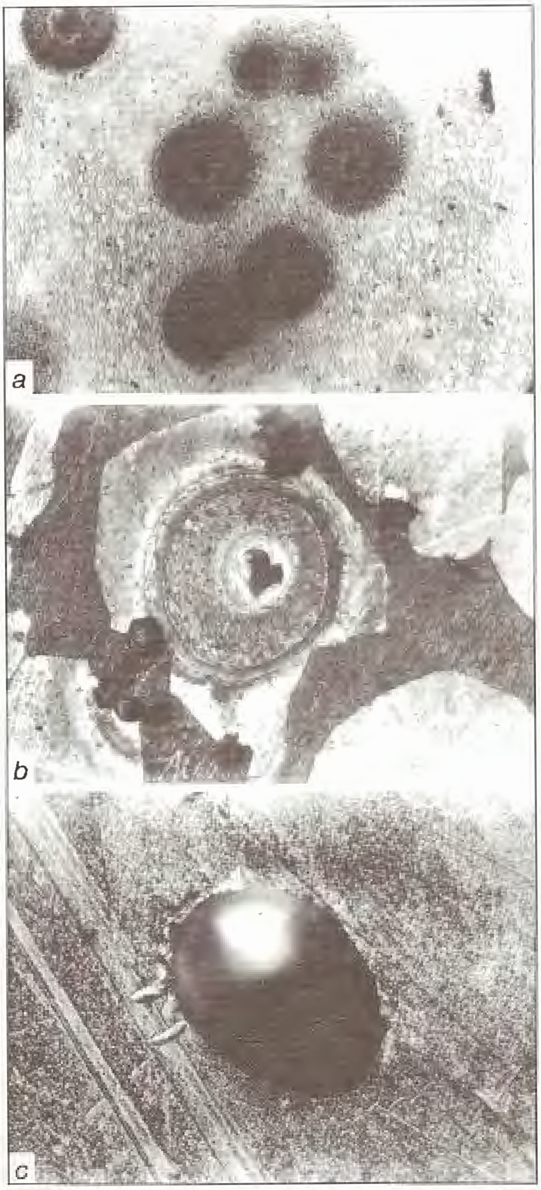

Figure 1. Pitting which results from single impact on samples of St.3 steel (*a*), LMtsZh 55-3-1 brass (*b*) and armco-iron (*c*) (×300) (reduced by 3/5)

crocracks in the slip bands along the twin boundaries with subsequent development of the main cracks in the microvolumes.

In the fourth region the stresses at each impact exceed the ultimate rupture strength of the material, which is expressed in pitting formation after each pulsed impact (Figure 1). The cracks grow and coalesce with time, thus leading to spallation of the alloy macroparticles. Here, the formed macrorelief promotes intensification of fracture, as the number of protrusions acting as microconsoles, increases.

Since that moment the fracture already becomes avalanche-like, and the surface proper loses its working characteristics.

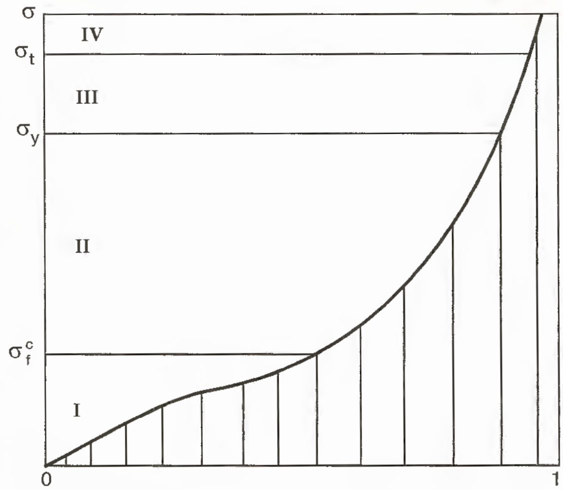

Figure 2. Integral function of stress distribution over the surface with cavitation erosion

Various measures of design and operational nature are applied in order to prevent and reduce the cavitation fracture of the parts of hydraulic machinery. These include deeper location of the impellers; reduction of the number of pump blades; creation of supercavitating propellers; improvement of the profile of parts around which liquids flow; air blowing into the anticipated wear zone; addition of surfactants to the liquid circulating by a closed contour; application of cathode protection, etc.

In the majority of cases, however, these measures result only in partial reduction of fractures, while requiring considerable material expenditure or lowering the working parameters of the units.

Therefore, use of special materials with a high resistance to cavitation fracture for making parts of hydraulic machines, should be regarded as the most effective measure.

Unfortunately, similar to many other cases of wear, the connection between the standard characteristics of mechanical properties of metals and their cavitation-erosion resistance is not in place, thus making the selection of material for fabrication of hydraulic machine parts more difficult.

The energy approach should be regarded as the most rational as it permits considering the process of fracture in cavitation in terms of the general law of conservation of energy, i.e. the wear resistance criterion should be determined by the ability of a body to absorb the fracture energy applied by the cavitating flow.

Statistical processing of the data revealed a relationship between cavitation resistance Δm and specific energy consumption of the material w [1]:

$$\Delta m = 1864.7 - 1983.7w + 718.4w^2 - 86.6w^3.$$

Analysis of this dependence shows that several paths can be chosen in development of materials

Some features of erosion-resistant metal deposited by various processes

Cladding process	*Deposited metal*	*Electrode or welding wire grade*	*Number of layers*	*HV hardness, MPa*	*Relative erosion resistance*
Manual coated-arc	E-10Kh25N13G2B	TsL-9	1	1680	1.20
			2	1630	1.00
	E-08Kh20N9G2B	TsL-11	1	2620	1.80
			2	2290	1.60
			3	2070	1.35
	E-06Kh19N11G2M2	TsL-4	1	3320	7.00
			2	2170	1.50
	E-07Kh20N9	OZL-8	1	3110	6.00
			2	1920	1.50
Manual argon-arc	Br.AN 12-3	PK-Br.AN 14-4	2	2300	61.50
	LK80-3	LK80-3	2	1800	2.60
Semi-automatic argon-arc	Br.AZhN 12-3-5	PK-Br.AZhN 14-4-6	2	2400	30.80
Semi-automatic CO_2	–	Sv-07Kh18N9TYu	1	3100	5.90
			2	1910	1.45
	–	Sv-10Kh18N9T	1	3060	4.03
			2	1810	1.40
Semi-automatic open-arc	10Kh14	PP-AN106	2	43*	18.30
	10Kh15N2GT	PP-AN138	1	2650	1.85
	10Kh12N3R	PP-ZMI-1	1	46*	22.00

Note: 1. *HRC* values are given. 2. The data were generated in IETR.

with the properties guaranteeing the high level of resistance to cyclic microimpact loads.

1. Production of metastable structures in the steels and alloys, capable of a significant strengthening as a result of phase transformations at microplastic deformation. Part of the energy of the cavitating flow is consumed in phase transformations and the resultant strengthening of the subsurface layer and ability to dissipate the internal energy and relieve the stresses. This ability is characteristic of, for instance, chromium-manganese deposited metal of 30Kh10G10 type ($\gamma \rightarrow \alpha$ transformation), chromium-nickel deposited metal of Kh15N7 type with unstable austenite ($\gamma \rightarrow \alpha$ transformation), deposited high-aluminium bronze of Br.A10 type with metastable high-temperature β-phase ($\beta \rightarrow \beta'$ transformation), etc. An additional advantage of the above materials is the ability of their production in the optimal condition without post-cladding heat treatment.

2. Lowering of the packing defects energy in single-phase alloys with a stable structure, thus permitting the wear resistance to be improved due to formation of the substructure in the region of the fatigue loads, hindering crack propagation or development of fracture sites. This was confirmed in testing of a series of copper-aluminium alloys [2]. Now, in transition from pure copper to bronze, the interval between crack initiation and fracture is increased more than 20 times.

3. Strengthening of steels and alloys by fixation (blocking) of dislocations in their alloying with surfactants (boron, zirconium) and elements forming disperse precipitations of the strengthening phases on dislocations and slip lines. The carbides or intermetallics which precipitated in the solid solution, block the dislocations, increase the hardness, elasticity and resistance of microvolumes to microimpacts. This raises the fatigue limit and lowers the probability of local fracture of the surface in «closing» of isolated bubbles, and the boundaries of the zones of corrosion-fatigue and single-impact fracture shift towards higher stress values.

Such properties are found in the clad steels, namely low-carbon maraging chromium-nickel, iron-nickel, and chromium carbon steel of the martensitic class.

All the considered methods are used in practical work to a greater or smaller degree (Table).

Sample claadding was performed in optimal modes in one or two layers. The thickness of each layer was 2 to 3 mm so that the share of the substrate base metal participation did not exceed 20 to 25 %. In cladding with steels the substrate was of St.3 steel and in cladding with aluminium bronze it was LMtsZh 55-3-1 brass.

In testing in IETR, 20Kh13NL steel was taken as the standard for iron alloys, and LMtsZh 55-3-1 brass for copper alloys.

In single- and two-layer cladding (see Table) a higher wear resistance is achieved in the first layer when the deposited metal dilution with the base metal leads to formation in it of compositions with unstable chromium-nickel austenite capable of phase work hardening as a result of $\gamma \rightarrow \alpha$ transformation. In the case of aluminium bronze $\beta \rightarrow \beta'$ self-strengthening is implemented in the same way, when the high-temperature β-phase is almost completely fixed because of the high cooling rates at room temperature. In production trials the improvement of wear resistance is certainly characterised by more moderate numbers. So, while the usual service life of the new propellers or those repaired by cladding with LK80-3 brass does not exceed 200 h of operation, the propellers clad with aluminium bronze have operated during the entire shipping season (600 h), whereas the depth of their erosion damage was not more than 1 mm [2].

Application of the above electrode materials, repair technology and cladding technique in various thermal power stations (Kakhovka, Gorky, Bratsk, Chiryurtskikh cascade) and in other facilities permitted the service life of hydraulic units to be extended by 1.5 to 2 times and tens of thousands of kilowatt-hours of power to be additionally produced both at the expense of shortening the time for repair and improving the wear resistance of the working surfaces [3].

CONCLUSIONS

1. High-temperature impact on the metal surface in cavitation erosion has been experimentally confirmed.

2. An effective measure of controlling the cavitation erosion is application of dispersion-hardening alloys with an unstable structure, capable of self-strengthening at microimpact as a result of phase work hardening.

3. The deposited metal composition and properties can be controlled by changing the thermal cycle and cladding technique.

4. Control of the thermal cycle and cladding technique allows a significant improvement of the cavitation-erosion resistance of the deposited metal.

REFERENCES

1. Pinkovsky, I.V. (1980) *Investigation of cavitation wear and development of sparsely-alloyed cavitation-resistant materials*. Diss. of Cand. of Sci. (Eng.). Zaporozhje.
2. Bykovsky, O.G. (1969) *Investigation of cavitation erosion, development of electrode materials and technology of cladding hydrofoil propellers*. Diss. of Cand. of Sci. (Eng.). Zaporozhje.
3. Milichenko, S.L. (1971) *Repair of cavitation damage of hydraulic turbines*. Moscow: Energia.

COMPOSITE POLYMETALLIC ELECTRODE WIRES

E.V. GAVROV
Zaporizhya State Technical University, Zaporizhya, Ukraine

ABSTRACT

Results of investigations conducted by the Zaporizhya State Technical University for over 30 years in the field of development and practical application of polymetallic wires for welding, surfacing and metallization of copper alloys of different alloying systems are presented. General principles of development of copper-base polymetallic wires which can be successfully used, upon proper correction, for design and manufacture of wires for welding, surfacing and metallization of other alloys are described.

Key words: *aluminium bronze, welding, surfacing, polymetallic wire*

Modern engineering imposes increased requirements on service properties of working surfaces and reliability of welded structures. In many cases a wide application of copper alloys, including aluminium bronzes Br.AZh 9-4, Br.AZhN 10-4-4, Br.AN 12-3, Br.AZhNMts 8.5-4-4-1.5, etc., as well as corresponding electrode wires less than 3.0 mm in diameter, intended for mechanized welding, surfacing and metallization, is indispensable for the fabrication of structures of the required quality. This involves certain problems associated with formability of alloys, which complicates the manufacture of wires of the indicated diameters and required compositions and thus makes production of the required quality of the weld and deposited metal much more difficult.

One of the ways of solving the posed problems is the use of composite polymetallic wires produced by simultaneous drawing of a metal strip-sheath made from an alloy developed and a core consisting of commercial wires to ensure the required alloying system.

Polymetallic wires of different types, combinations and diameters (from 1.2 to 6.0 mm and more) with any content of alloying elements can be manufactured by varying initial sizes and compositions of strips, as well as components of the core. Complicated and labour-consuming processes involved to manufacture all-drawn and flux-cored wires of similar compositions can be replaced by a simpler, more practicable and less labour-intensive process [1]. Wire of the design under consideration is suitable for high-productivity automatic and semi-automatic welding and surfacing performed using standard gas-shielded or submerged-arc welding equipment.

The field of application of the polymetallic wires for the fabrication of welded structures and repair of process equipment has recently been widened to a substantial degree both in Ukraine and abroad. For example, one should mention Japan in the first turn among foreign countries which successfully use polymetallic wires. The experience is available [2] of utilizing composite wires for welding and surfacing aluminium alloys, monel alloy, various grades of aluminium bronzes and steels.

The range of strips and wires manufactured by the national industry is rather wide, which opens up opportunities for developing new polymetallic wires. However, their introduction into industrial practice is hampered by the lack of systematized literature data and information on general principles underlying development, design and study of peculiarities of drawing and melting, as well as potential applications of the polymetallic wires.

This work is the first attempt made to systematize these data and formulate general principles of design and application of the polymetallic wires, which in our opinion will help specialists to develop new compositions and combinations of the wires and reveal the actual industrial demand for such electrode materials.

The choice of a specific combination of components of the wire is based on the necessity of providing the desirable chemical composition and service properties of the weld or deposited metal, as well as parameters of drawing and melting of the wire components. These requirements can be met through a rational selection of sizes and compositions of the components to ensure the selected alloying system and desirable composition of the wire being developed. To decrease the gas content of the deposited or weld metal, in development of the wire it is preferable to select such components which in the initial state have a decreased gas concentration. To suppress gas saturation of metals, it is possible to add powders of the known compounds to cavities existing between the sheath and the core components (up to 40 % at an initial wire diameter of 3.0 mm), i.e. to develop polymetallic flux-cored wires for open-arc welding, welding in active shielding gases, metallization or other purposes. The required continuity of metals (with no pores or slag inclusions, or, if any, of minimum sizes and quantity per unit weld length) is provided by the use of source materials with moisture, grease or different types of contaminants removed by etching in appropriate chemical solutions.

To make a desirable combination, it is necessary to take into account scarcity of the source materials of the components and their sizes specified by standards. The latter makes it possible to use components without preliminary re-drawing of wires of the core to decrease diameter and without cutting of a strip, which means minimizing the manufacture costs of the wires. The practice shows that a rational way of manufacturing a wire is to make the sheath from a material making a base of this wire and vary concentrations of alloying elements by adding wires of certain sizes and compositions to the wire core. So, the selected combination of a polymetallic wire with a preset diameter and composition is determined by sizes of a strip used to make the sheath, diameters of the initial components of the core and chemical composition of the materials involved.

Diameter of a finished polymetallic wire depends upon the application. For example, wire with a diameter of 2.5 – 3.0 mm is employed for gas-shielded, open-arc or submerged-arc welding and surfacing, wire with a diameter of 1.2 – 2.5 mm is utilized for tungsten-electrode welding and wire with a diameter of 1.2 – 2.0 mm is used for plasma surfacing and metallization.

The efficiency of development of welding consumables is known to depends upon the calculation methods employed. Preliminary calculation of initial sizes of the components for the manufacture of the polymetallic wires of preset diameters and compositions can be conducted using methods described in [1, 3, 4]. Compositions of the wires and mechanical properties of the deposited metal at a stage of design can be predicted using mathematical models [5] which provide a substantial reduction of the amount of the exploration works. The models suggested can be utilized for development of both welding and surfacing polymetallic wires of different alloying systems, which are optimal for copper-base alloys.

In making experimental wires, their calculated composition is determined as a ratio of the weight of a unit length of the desired component to the total weight of a length of the wire cut out from its end part. Investigations show that cutting made at the end of a sample for weighing leads, within one necking, to a certain error associated with the so-called «end» effect, this being caused by a non-uniform deformation along the length of the wire. This effect is found to take place as a rule at initial neckings. At later neckings the wire is deformed uniformly along the entire length, with the filling coefficient increased to 0.85 or more. It should be noted that the non-uniformity taking place at earlier neckings is not levelled at later ones. Therefore, the calculated composition should be determined and the wire should be used for practical purposes only after cutting of not less than 2 m from the end. This conclusion is important from the practical standpoint, as the use of the wire which has a heterogeneous composition along its length might lead to a low quality of welded joints. The noted effect is attributable to the absence of the «adhesion bridges» on the mating surfaces of the components participating in joint drawing and, hence, to compression of the sheath along the core. Evolution of this process is greatly affected by diversity of interfaces of the mating surfaces, which do not coincide with a horizontal axis of drawing, because the components ensuring the preset composition have different sizes.

The possibility of providing the deposited or weld metal with a uniform distribution of alloying elements in the case of using polymetallic wires often causes doubts. However, as shown by investigations, these materials provide the weld metal similar to that produced by welding using stick electrodes or solid wires of an identical composition, having preset mechanical properties and high corrosion resistance. As compared with solid wires, in surfacing the polymetallic wires provide wider beads with a smaller penetration depth, other conditions being equal. This is attributable to splitting of the arc into several arcs (formation of the «polyarc») which move over the tip of the polymetallic wire. High-speed filming showed the presence of several glowing spots located at the components that make the wire, irrespective of the surfacing parameters.

The sheath comprises all-drawn wires of different diameters, compositions and thermal-physical properties. This makes investigations of distribution of temperature in a polymetallic wire hardly possible. However, as was established [6], over a wide range of welding parameters the copper-base wire components melt to form a common droplet at the electrode tip, which is caused by the presence of a natural convective heat exchange between them and intensive convective flows in the droplet.

Examples of the developed polymetallic wires and their application fields are given in the Table.

Polymetallic electrode copper-base wires for welding, surfacing and metallization

Deposited metal	*Wire dia., mm*	*Core and copper strip combination*	*Application field*
Br.A	4.0 – 5.0	Aluminium	Manufacture of electrode rods
Br.AN	4.0 – 5.0	Aluminium, nickel	Same
Br.ANT	4.0 – 5.0	Aluminium, nickel, titanium	Submerged-arc surfacing
MN	3.0	Nickel	Same
MNA	3.0	Nickel, aluminium	»
Br.ANTsMtsKhZh	2.8 – 3.0	Aluminium, nickel, zinc, nichrome, steel, manganine	Metal-vapour deposition
Br.AN	1.2 – 2.8	Aluminium, nickel	Welding, surfacing in argon, helium or their mixtures, submerged-arc welding and surfacing, plasma surfacing
Br.AZh	1.2 – 2.8	Aluminium, steel	Same
Br.AZhN	1.2 – 2.8	Aluminium, nickel, steel	»
Br.ANKh	1.2 – 2.8	Aluminium, nickel, nichrome	»
Br.ANMtsZh	2.0 – 3.0	Aluminium, nickel, steel, manganine	»
Br.AZhNMts	1.2 – 3.0	Same	»
Br.AMts	2.0 – 3.0	Aluminium, manganine*	»
NA	1.6 – 2.0	Aluminium**	Plasma-arc metallization

*Sheath made from copper or Br.AMts 9-2 strip.
**Sheath made from nickel strip.

Because they are simple to manufacture and their composition can be readily varied, the polymetallic wires are employed for welding critical structures more than 2 t in weight made from Br.ANMtsZh 8.5-4-4-1.5, and for treatment of working surfaces of the «Camur» rotors, guards of the «Kiesirling» rolling mill and propellers. Positive results were obtained in welding steels 35 and 10Kh18N10T.

The general principles formulated for development of the polymetallic copper-base wires can be successfully used, upon certain correction, for design and manufacture of wires for welding, surfacing and metallization of other alloys.

Further improvement of the technological processes and investigation of the general principles of heating, melting, electrode metal transfer and formation of alloys at the droplet and weld pool stages will help define the scientifically grounded ways of developing new wire compositions, substantially widen their application fields in the national welding industry and satisfy the increasing demands of different industries for multicomponent alloys.

REFERENCES

1. Gavrov, E.V., Aleksandrov, O.A. (1983) Calculation and manufacture of composite wires for mechanized welding and surfacing of copper alloys. In: *Surfacing of wear- and heat-resistant steels and alloys. Surfacing consumables*. Ed. by I.I. Frumin. Kyiv: PWI.
2. Gavrov, E.V. (1986) Composite polymetallic electrode materials in welding industry. *Svarochnoye Proizvodstvo*, **2**, 30 – 31.
3. Gavrov, E.V., Bykovsky, O.G. (1980) Procedure for calculation of a composite wire for welding and surfacing of aluminium bronzes. In: *Topical problems of welding non-ferrous metals*. Kyiv: Naukova Dumka.
4. Bykovsky, O.G., Gavrov, E.V., Kibalchich, A.P. *et al.* (1978) Calculation of a composite electrode wire on the basis of initial sizes of the components. *Avtomaticheskaya Svarka*, **4**, 72 – 73.
5. Gavrov, E.V., Bykovsky, O.G., Zhorzh, V.V. *et al.* (1980) Composite wire for mechanized welding of high-strength bronze of the ANMtsZh type. *Ibid.*, **5**, 39 – 41.
6. Gavrov, E.V., Milichenko, S.L., Bykovsky, O.G. (1981) Composite welding wire Br.ANMtsZh. Ibid., 3, 71 – 72.

MATERIALS AND TECHNOLOGY FOR SURFACING OF MACHINE PARTS OPERATING UNDER CONDITIONS OF IMPACT-ABRASIVE WEAR

V.A. GUK
Zaporizhya State Technical University, Zaporizhya, Ukraine

ABSTRACT

Compositions and structures of deposited metal produced using consumables of different alloying systems were analysed. Performance of the deposited metal under conditions of impact-abrasive wear was evaluated. Composition of a new flux-cored wire ensuring high wear resistance of rotary crusher beaters is suggested.

Key words: *surfacing, wire, alloy, wear*

Capability of metal of resisting fracture under the impact-abrasive effect is a function of many parameters, such as chemical composition, structural state of alloys, sensitivity to structural transformations in the surface layer in interaction with abrasive bodies, conditions of wear, including temperature, value of the impact energy, collision velocity, composition and properties of a material being crushed.

In addition to high resistance to wear in an abrasive environment, properties of the deposited layer depend also upon its composition. An addition of alloying elements to the weld bead can lead to deterioration in welding properties, operational strength and performance of the deposited metal. Resistance of metal to crack formation is decreased most markedly by carbon, which is prone to formation of carbide eutectics distributed along the grain boundaries in the form of clusters. Alloys containing boron are characterized by the effect of low-melting point eutectics Fe–B, which are located at junctions of columnar crystals [1]. Other elements, e.g. manganese (at its content of no more than 4 %), have a positive effect on continuity of metal at a low concentration of carbon, as sulphur is combined to form manganese sulphide and does not form low-melting point sulphide eutectics, such as Fe + FeS [2], which cause a substantial decrease in ductility of the deposited metal.

The rate of growth of tensile strains during solidification of metal plays an important role in initiation and propagation of cracks. Their rate and, hence, susceptibility of the deposited metal to cracking increase with an increase in structural rigidity of billets. For example, inertia-rotary crusher beaters have sufficient rigidity to decrease strains during surfacing, but this rigidity is insufficient to suppress cracking of the deposited wear-resistant layer, especially in the case of violation of the surfacing technology.

This was proved by results of investigations conducted to study the possibility of extending service life of the inertia-rotary crusher beaters using consumables of different alloying systems, as well as of different structures and properties.

In the alloys selected the content of carbon, manganese and chromium varies over wide ranges. For example, the content of carbon is 0.7 – 3.5 % (PP-AN170 and Sormite-1), the content of chromium is 12 – 26 % (VSN-6 and Sormite-1) and that of manganese is 0.3 – 13.0 % (Sormite-1 and PP-G13) (Table).

The majority of extensively applied wear-resistant iron-base alloys have a matrix alloyed with chromium, and chromium increases wear resistance of the alloys. Today the recommended chromium content of the deposited metal is up to 40 %.

Beaters of a special design made from steel St.3 were subjected to surfacing using the consumables under investigation. Because of some drawbacks, beaters of steel 45 used before and beaters treated by the electroslag surfacing method using steel G13 were not investigated.

All surfacing trials were done under constant conditions using electrodes (I_a = 300 – 350 A, U_a = = 32 – 36 V) and flux-cored wires (I_a = 250 – 300 A, U_a = 38 – 40 V, v_w = 21.5 m/h, direct current of reverse polarity, submerged-arc method using flux AN-26S). The indicated wide ranges of the arc voltage values are attributable to large differences in compositions of the consumables investigated.

Industrial tests of the alloys used for surfacing were conducted at a rotation speed of the rotor equal to 985 rpm and capacity of the crusher equal

Composition and hardness of the deposited metal

Surfacing consumable	Chemical composition, %							HV hardness of deposited metal, GPa	Relative wear resistance, ε
	C	Cr	Mn	Ti	Si	B	Others		
PP-G13 (reference)	1.20	–	13.00	–	0.30	–	–	3.95	1.00
PP-U25Kh17T	2.20 – 2.60	16.0 – 18.0	–	0.3 – 0.4	–	–	–	5.13	2.37
VSN-6	1.00 – 1.30	12.0 – 17.0	0.55 – 1.20	–	0.27 – 0.65	–	W 11.0 – 15.0 V 1.4 – 2.0	4.44	1.82
Sormite-1	2.50 – 3.50	23.0 – 26.0	0.30 – 0.50	–	3.20 – 3.60	–	Ni 3.4 – 3.8	6.79	1.98
PP-AN125	2.00	15.0	1.00	0.3	1.50	0.7	–	7.59	1.46
PP-AN170	0.70	20.0	0.60	0.2	0.60	3.0	–	6.62	3.33
UPI-30Kh10G10	0.25 – 0.30	9.0 – 11.0	2.00 – 11.00	–	0.35	–	–	3.25	1.28
PP-IN-1*	1.20 – 2.20	11.0 – 12.0	0.30 – 0.60	–	0.40 – 0.50	2.6 – 4.0	–	7.08 – 7.54	5.20

*Surfacing using the new wire (author's certificate No. 683128).

to 150 t/h. Initial lumps of coal were up to 200 g in weight. Wear of the working edge of the beater equal to 25 – 30 % led to a considerable deterioration of the quality of coal crushing. In practice, this is an indicator that parts with such wear should be replaced.

It is a known fact that only the sharp working edge of the beater provides the required yield of the desirable fraction of coal. It is hard to form the edge of the required geometry by arc welding in 2 or 3 layers using multicomponent wear-resistant alloys. Therefore, welding was done in 1 layer. Dilution of the electrode metal in the first layer led to a decrease in hardness of the deposited metal.

The surfacing alloys were deposited in regions 100 mm long. This arrangement of the deposited beads made it possible to simultaneously test 11 experimental beads and 1 reference bead. As the set of the rotary crusher consists of 3 beaters, wear resistance of a material was evaluated by an average value of wear in cross section of each beater, secured in a specially developed fixture, over the surface areas of the beaters located between profilographic lines before and after the test.

Relative wear resistance of the materials, ε, was determined by the ratio of the wear surfaces in cross sections of the beaters made from the reference and test materials.

Industrial tests of the metal deposited using alloys PP-AN125, Sormite-1 and PP-AN170 with hardness of more than 6 GPa (see the Table) show that an aggregate hardness and an increased content of the hardening phase of an alloy are not always the basic prerequisite of an improved wear resistance of the deposited metal. For example, the metal deposited using PP-AN170 contains about 50 % of the carboboride phase, whereas the Sormite-1 alloy having a lower wear resistance contains 80 % of carbides. The VSN-6 deposited metal contains approximately 50 % of the hardening phase, but its wear resistance is higher than that of the PP-AN125 deposited metal having a content of carbides equal to 60 %.

Maximum wear resistance of the metal deposited with PP-AN170 was achieved probably due to a considerable hardness of the carboboride phase and austenite capable of structural transformations, the content of which in the PP-AN170 deposited metal is almost twice as high as that in the PP-AN125 and Sormite-1 deposited metals. However, as it follows from the Table, sensitivity of metal alloyed with chromium (PP-U25Kh17T) to austenite transformations is higher than that alloyed with manganese (PPG-13 and UPI-30Kh10G10). Therefore, in impact-abrasive wear of the metal deposited on beaters of the inertia-rotary crushers operating in the coal crushing mode, its wear resistance is determined by hardness of the hardening phase and amount of the metastable austenite which can transform into martensite under operational loading. Therefore, in selection of composition of a wear-resistant alloy, optimal for given operating conditions, the preference should be given to iron-base alloys containing carbon, chromium and boron.

The new flux-cored wire of the PP-IN-1 grade was developed on the basis of comparative analysis of compositions and structures of the candidate materials and applicability of the surfacing technology. This wire has a high content (~ 70 %) of the hard carboboride phase which increases the elastic energy potential of the metal and contributes to the energy-intensive process of plastic deformation caused by abrasive bodies.

The metal deposited on the rotary crusher beaters using this wire has wear resistance which is 5 times as high as that of the metal deposited with steel G13 by the electroslag method.

Tests of the metal deposited using the experimental flux-cored wire on bucket teeth of the excavating machines operating with soils of category IV, where the load by impact cutting is higher than that on the crusher beaters, show that wear resistance of the teeth can be increased by no more than 30 %. Further increase in wear resistance is hampered by a decrease in the aggregate hardness of the metal deposited on steel G13 used to make the teeth, as compared with hardness achieved in deposition on plain low-carbon steel, by differences in ductility of steel G13 and the hard alloy, which induce substantial stresses at the fusion boundary and lead to cleavage in the teeth in their interaction with a virgin soil, as well as by crack formation under a temperature effect on steel G13 during the deposition process. The quality of the deposited metal is deteriorated also because of an increased porosity of the metal the teeth are made from, which is caused primarily by casting defects and rust present on their surface.

Therefore, the optimal choice of chemical composition, structure and properties of the metal, as well as the surfacing technology for extending service life of parts should be based in each specific case only on the results of special comprehensive investigations.

REFERENCES

1. Samsonov, G.V., Portnoy, K.I. (1961) *Alloys based on refractory compounds*. Moscow: Oborongiz.
2. Frolov, V.V. (1970) *Theoretical principles of welding*. Moscow: Vysshaya Shkola.

WEAR RESISTANCE OF METAL DEPOSITED ON WORKING PARTS OF ROAD-BUILDING MACHINES DURING THEIR OPERATION

S.N. POPOV
Zaporizhya State Technical University, Zaporizhya, Ukraine

ABSTRACT

Three groups of surfacing alloys characterized by a different content of the hardening phase are considered. The effect of phase composition on physical-mechanical, operational and service properties of alloys is analysed.

Key words: *deposited metal, structural-phase condition, physical-mechanical properties, wear resistance, technological applicability, plastic deformation, abrasive fracture, alloy matrix, carbide phase*

The problem of development of a wear-resistant material for parts of road-building machines operating under specific conditions of abrasive wear is extremely complicated, and this probably is a reason why it has not been solved as yet. The available literature data do not allow a sufficiently grounded selection of structural-phase composition of the material and its physical-mechanical properties for operation under specific service conditions [1 – 3]. Thus, the data given in [4, 5] cover only a small number of materials tested (steel 35L, tellurium-modified gray cast irons, white nickel-chromium cast irons, steel G13L, metal deposited using electrodes TsS-1 (Sormite) and flux-cored wire PP-AN125), they lack systematizing and are rather contradictory in terms of wear resistance of metal under service conditions of the road-building machine mixing blades.

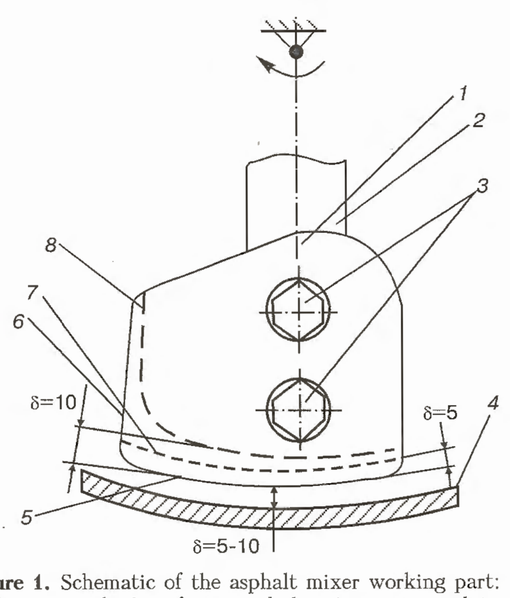

Figure 1. Schematic of the asphalt mixer working part: *1* — blade; *2* — rack; *3* — fastening bolts; *4* — armour plate; *5* — working edge; *6* — end face edge; *7* — contour of permissible wear of the working edge of the blade; *8* — contour of the actually acceptable wear in long-time operation of the asphalt mixer

Development of a wear-resistant material for blades of asphalt mixers (Figure 1) is done by successive resolving of a set of interrelated problems at the basic stages of investigations using a multi-criterial approach [6]. First the wear environment and conditions, as well as character of fracture of the working surface of the blades are investigated and procedure for testing materials to ensure reliable results is developed [7]. Then the effect of a type of the metal matrix and content of the hardening phase (up to 25 %) on wear resistance of cast alloys after heat treatment under service conditions of the blades is studied [8]. Considering sizes of working parts of the mixing equipment and values of permissible wear (up to 5 mm) of the working surfaces [6], electric-arc surfacing with a wear-resistant material has been recognized as the most cost effective method in terms of extending service life of these parts.

On this basis, industrial tests were conducted to estimate applicability of standard surfacing consumables and determine an optimal combination of the type, structural-phase composition of an alloy and amount the hardening phase contained in it to ensure maximum wear resistance of working parts of the asphalt mixers. The most widely applied standard surfacing consumables with a matrix in differing structural conditions were selected for the investigations. These consumables were conditionally subdivided into three groups, depending upon the content of the hardening phase (I — up to 5.3 %, II — 12 – 35 %, III — over 50 %) (Table). The tests were carried out by the procedure described in [7] at the Zaporizhya District Asphalt-

Properties of surfacing consumables and alloys tested under conditions of operation of asphalt mixer working parts

Consumable	*HRC hardness*	*Phase composition, %*				*Content of hardening phase, %*	*Relative wear resistance, ε*	*Microhardness of base HV_{50}, GPa*	*Microhardness of hardening phase HV_{50}, GPa*	*Fitness for purpose*
		Before tests		*After tests*						
		α	γ	α	γ					
Group I										
PP-3Kh2V8	45 – 48	100	–	100	–	2.4	1.32	3.5 – 4.0	–	Good
PP-AN105	12 – 18	–	100	–	100	–	1.60	3.8 – 4.5	–	»
EN-N60	51 – 58	100	–	100	–	5.3	2.10	5.4 – 6.2	–	»
Group II										
PP-Kh12F1	43 – 46	50	50	60	40	12.0	2.15	4.5 – 4.8	–	»
PP-AN140	48 – 51	60	40	65	35	15.0	3.60	4.2 – 4.6	–	»
PP-AN125	50 – 58	90	10	100	–	10.0	3.86	8.5 – 8.7	–	»
PP-AN101	48 – 52	25	75	35	65	35.0	4.20	4.1 – 4.5	–	»
Group III										
TsS-1	45 – 54	70	30	75	25	60.0	5.10	5.3 – 6.1	12.0 – 13.0	Satisfactory
EN-T590	50 – 55	90	10	100	–	50.0	5.40	6.2 – 6.8	14.3 – 16.0	»
EN-T620	50 – 60	65	35	80	20	55.0	5.60	7.1 – 7.9	13.0 – 16.0	»
EN-ITS01	59 – 62	75	25	90	10	65.0	5.90	6.5 – 7.0	15.0 – 16.5	»
KKhB-45	66 – 68	90	10	95	5	70.0	6.20	8.2 – 8.5	16.0 – 18.0	Unsatisfactory
PP-AN170	60 – 63	45	55	60	40	50.0	6.50	7.6 – 8.1	15.0 – 18.0	»
EN-180Kh12R4	62 – 65	70	30	75	25	65.0	7.10	8.0 – 9.5	20.0 – 22.0	»
TZ tungsten carbide	*HRA* 90	–	–	–	–	80.0	13.50	4.5 – 6.0	24.0 – 30.0	»
PP-150Kh13R3F	63 – 65	85	15	90	10	65.0	10.10	8.0 – 8.5	20.0 – 28.0	Satisfactory
250Kh5S2GAT	55 – 65	85	15	100	–	8.0	2.90	6.1 – 8.2	–	Good
Reference — annealed steel 45	*HV* 166					8.73	1.00			

Concrete Plant using the DS-117-2E machine in the process of preparation of an asphalt-concrete mixture containing crushed granite of the 10 – 25 mm fraction with microhardness of HV_{50} 12 GPa and compression strength of σ = 11 – 12 GPa. The initial radial gap between the end face of the blade and the armour plate of the mixer was 5 mm. Surfacing of samples was done using the A-765 semi-automatic device or by manual arc welding at a direct current of reverse polarity under conditions specified in GOST 26101–84. The VS-500 rectifier or PS-1000 transformer was used as the power supply.

The tests showed (see the Table) that alloy PP-3Kh2V8 with a structure consisting of the pearlitic base and an insignificant amount (2.4 %) of the carbide phase had low wear resistance (ε = = 1.32). Materials that provide either purely austenitic structure (PP-AN105) of the deposited metal, because of low microhardness of stable austenite (HV_{50} 3.8 – 4.5 GPa) and absence of the hardening phase, or the martensitic structure (EN-N60) with an insignificant amount of carbides (5.3 %) have low wear resistance. Although the surfacing consumables of group I have good technological and service reliability, they are absolutely unsuitable for the given service conditions. That is why they are no longer in use.

Surfacing consumables of group II provide deposited metal with an austenitic-martensitic structure and a carbide content of 10 – 35 %. Having an approximately identical content of the carbide phase, alloys of this group have wear resistance which is determined by hardness of the matrix. Thus, at α/γ = 50/50 (PP-Kh12F1) wear resistance is 2.15, while at α/γ = 60/40 (PP-AN140) and 90/10 (PP-AN125) it is 3.60 and 3.86, respectively. However, the content of the carbide phase has a more substantial effect than the aggregate hardness increased only due to an increase in hardness of the metal base. An increase in the hardening phase content of up to 35 % (PP-AN101) even at a ratio of α/γ = 25/75 results in an increase in a relative wear resistance of up to ε = 4.20. Alloys of group II are little susceptible to crack formation, have good technological and service reliability, but the amount of the carbide phase contained in structure of the deposited metal is insufficient for en-

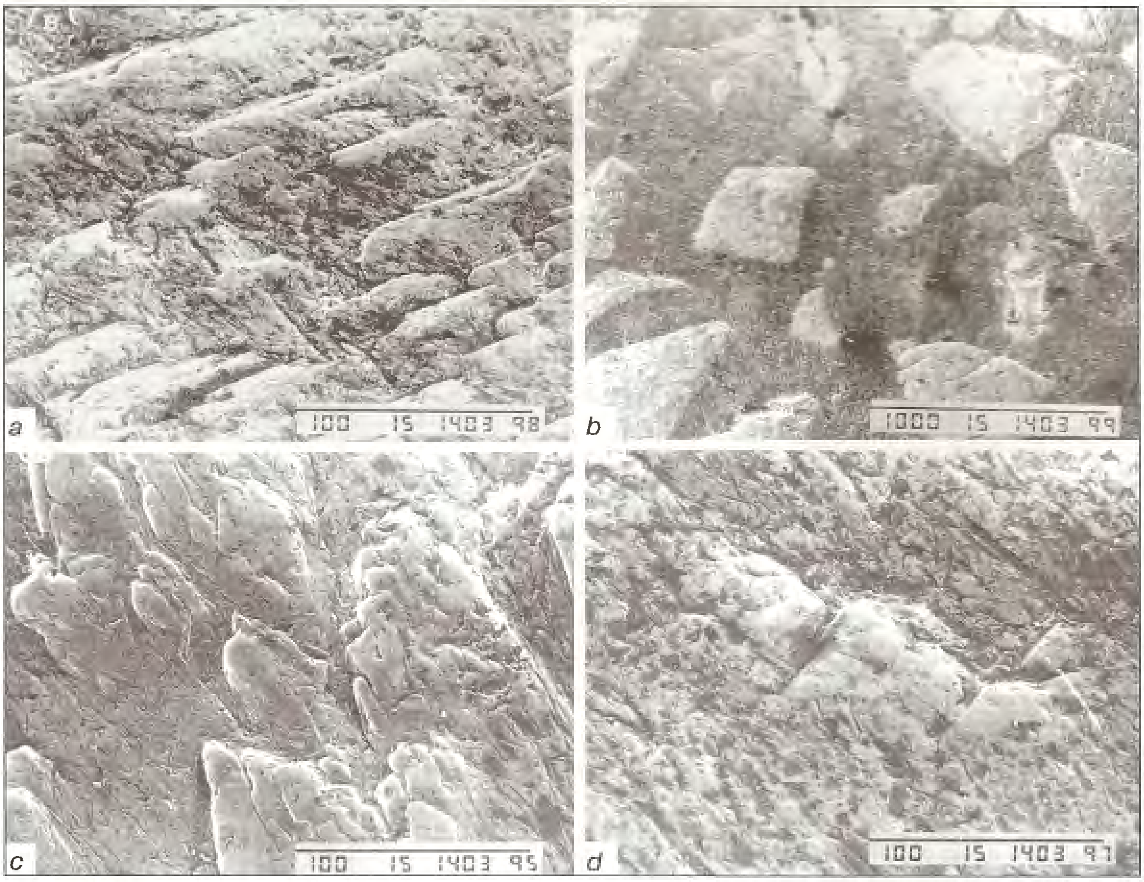

Figure 2. Friction surface of the materials after testing them under service conditions of asphalt mixer blades: *a* — PP-AN170; *b* — TZ tungsten carbide; *c* — EN-ITS01; *d* — TsS-1

suring the required level of wear resistance for service conditions of the blades.

Alloys of group III containing a significant amount of the redundant phase (50 – 80 %) have maximum wear resistance. In this group the deposited metal produced using the TsS-1 electrodes (redundant phase — 60 %) has the lowest wear resistance ($\varepsilon = 5.10$). This is associated with low microhardness of carbides Cr_7C_3 (HV_{50} 12.25 – 13.40 GPa), as compared with that of the abrasive particles (HV_{50} 12 – 14 GPa), which causes low-cycle fracture of the friction surfaces (Figure 2). The metal deposited with the EN-T590 ($\varepsilon = 5.40$) and EN-T620 ($\varepsilon = 5.60$) electrodes has a higher wear resistance. This is associated with additional alloying of the deposited metal with boron, which causes an increase in hardness of the carbide phase and the alloy base. Thus, microhardness of the redundant phase of these materials increases to HV_{50} 14.3 – 16.5 GPa and that of the alloy matrix grows to HV_{50} 6.2 – 7.9 GPa. High wear resistance of the working parts of the mixers under service conditions is ensured by standard surfacing consumables EN-ITS01 ($\varepsilon = 5.90$), KBKh-45 ($\varepsilon = 6.20$), PP-AN170 ($\varepsilon = 6.50$) and experimental alloy EN-180Kh14R4T ($\varepsilon = 7.10$).

An increased wear resistance of this group of the materials is determined by the fact that microhardness of their redundant phases is equal to or higher than that of the abrasive particles (HV_{50} 15 – 18 GPa). Metallography of the worn surfaces (Figure 2) shows that at these values of microhardness an abrasive particle, when it collides with the hardening phase, is destroyed partially or completely. The length of the trace left by plastic deformation and removal of the chip is limited by a distance between two hard inclusions. Microvolumes of metal in the space between particles of the carbide phase, which projects over the surface of the alloy base, are destroyed during the wear process. This results in a rather high wear resistance of such alloys.

At the same time, some of the alloys developed, containing large amounts of coarse redundant inclusions, e.g. EN-180Kh14R4, are hardly suitable for the use under the given wear conditions, as they have high susceptibility to crack formation because of excessive brittleness, which leads to spalling of the deposited metal during operation when the granite particles being mixed are jammed between the blade and casing of the mixer (Figure 3).

Figure 3. Asphalt mixer blade surfaced using the EN-180Kh14R4 electrode after service

Among all the surfacing consumables investigated the cast TZ tungsten carbide alloy (ε = = 13.50), whose microstructure consists of a solid solution with coarse particles of tungsten semi- and monocarbide, has maximum wear resistance. Intensity of wear of this alloy is much lower than that of other materials considered above. This is attributable to a substantial hardness of tungsten carbide, which is approximately 2 times as high as that of the abrasive particles. However, application of tungsten carbide, despite its significant wear resistance, is restricted by a high cost of this material, as well as by low productivity and high labour consumption of the flame surfacing process.

Wear resistance of the deposited metal under conditions of operation of the asphalt mixers depends upon microhardness of the matrix and hard-

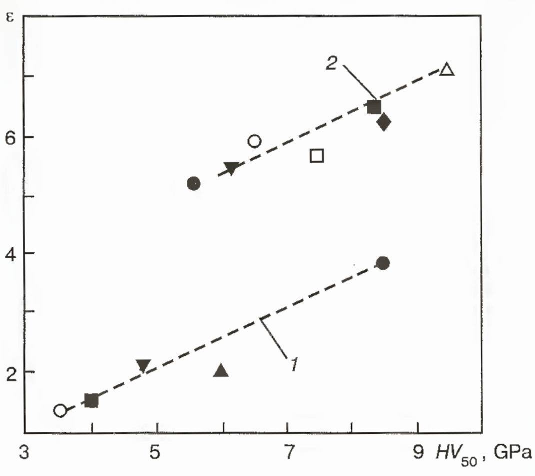

Figure 4. Variations in relative wear resistance (ε) of the investigated surfacing consumables depending upon microhardness of the alloy base, HV_{50}: *1* — alloys with a hardening phase content of less than 13 % (○ — PP-3Kh2V; ■ — PP-AN105; ▼ — PP-Kh12F1; ▲ — EN-N60; ● — PP-AN125); *2* — alloys with a hardening phase content of more than 30 % (● — TsS-1; ▼ — EN-T590; ○ — EN-ITS01; □ — EN-T620; ◆ — KKhB-45; Δ — EN-180Kh12R4; ■ — PP-AN170)

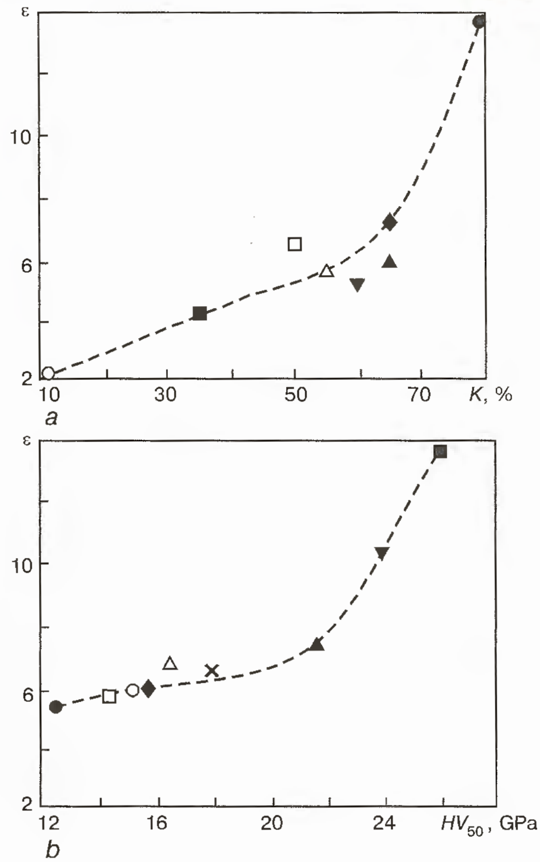

Figure 5. Variations in relative wear resistance (ε) of the investigated surfacing consumables depending upon the content (*K*) (*a*) and microhardness (HV_{50}) (*b*) of the hardening phase: *a* — ○ — PP-Kh12F1; ■ — PP-AN101; Δ — EN-T620; ◆ — EN-180Kh12R4; ● — TZ tungsten carbide; □ — PP-AN170; ▲ — EN-ITS01; ▼ — TsS-1; *b* — ● — TsS-1; □ — EN-T590; ○ — EN-T620; Δ — EN-ITS01; ▲ — EN-180Kh12R4; ■ — TZ tungsten carbide; ◆ — PP-AN170; ▼ — PP-150Kh13R3F; × — KKhB-45

Figure 6. Asphalt mixer blade surfaced using the new PP-150Kh13R3F material after long-time operation

ening phase of the alloy (Figures 4 and 5). The content of the carbide phase being approximately equal, wear resistance depends upon microhardness of the base. However, even at a maximum value of microhardness, HV_{50} 9.5 GPa (see the Table), the alloy base alone cannot ensure high wear resistance, as microhardness of the abrasive particles (HV_{50} 12 – 14 GPa) is 1.2 – 1.4 times as high as that of the matrix.

Thus, as proved by the investigations, the level of wear resistance of the metal deposited with the TsS-1 alloy (Sormite), as well as the EN-T590, EN-T620 and EN-ITS01 electrodes, is 1.8 – 2.0 times higher than that of the blade material (cast iron 250Kh5S2GAT, T_{hard} = 850 – 870 °C). Therefore, they can be applied for deposition of wear-resistant layers on working surfaces of the blades. However, wear resistance of these materials is not maximum achievable for the Fe–C–Cr–B alloying system. This proves the high level of wear resistance provided by such surfacing consumables as PP-AN170, KBKh-45 and EN-180Kh12R4, in which microhardness of the hardening phase amounts to 18 – 22 GPa. Nevertheless, such alloys are hardly suitable for surfacing of the blades, as they are susceptible to crack formation and excessive brittleness, which leads to spalling of the metal during operation.

Analysis of dependencies of the effect of the amount and microhardness of the hardening phase on the ability of metal to resist wear under service conditions of the blades (Figure 5) showed that a substantial increase in wear resistance could be achieved at a content of hard inclusions equal to not less than 50 % and ratio of microhardness of the redundant phase to that of the abrasive equal to or more than 1.5, i.e. at microhardness of carbides (borides) equal to about 19 – 22 GPa. Therefore, in development of a wear-resistant material with a high content of carbides (more than 50 %) the choice of a metal matrix should be based on the possibility to produce the base with a reasonable combination of high microhardness and capability of retaining a stable amount of the hardening phase. The tests showed that the materials science parameters of an alloy should be within the following ranges: aggregate hardness – HRC 62 – 65, content of the hardening phase – K = 50 – 70 %, microhardness of inclusions – HV_{50} 19 – 30 GPa, microhardness of the base – HV_{50} 6 – 8 GPa.

Based on the above requirements for a wear-resistant alloy, we developed a new surfacing consumable PP-150Kh13R3F (author's certificate No. 1587804). Industrial tests of this consumable indicated that wear resistance of the mixer blades surfaced using this material (Figure 6) was 3.5 times higher than that of the parts manufactured by a standard technology.

REFERENCES

1. Popov, V.S., Brykov, N.N. (1996) *Wear resistance of steels and alloys*. Zaporizhya: VPK «Zaporizhya».
2. Tenenbaum, M.M. (1976) *Wear resistance of structural materials and machine parts*. Moscow: Mashinostroyeniye.
3. Budinaki, K.J. (1993) *Tribology. Investigations and applications. USA and CIS experience*. Moscow: Mashinostroyeniye.
4. Bardakh, Ya.E., Bandurov, V.A. (1968) Wear-resistant parts of asphalt mixers. *Avtomobiln. Dorogi*, **9**, 27 – 28.
5. Sementsov, N.Z. (1979) Extension of service life of asphalt mixer blades. *Ibid*., **12**, 27 – 28.
6. Popov, S.N. (1999) Integrated approach to extension of service life of road-building machine parts. In: *Technology for repair of machines, mechanisms and equipment*. Alushta: ATMU.
7. Brykov, N.N., Popov, S.N. (1991) Procedure for testing materials intended for fabrication of asphalt mixing machine rotor blades. *Stroiteln. i Dorozhn. Mashiny*, **3**, 24 – 25.
8. Brykov, N.N., Popov, S.N. (1991) Effect of structure of alloys of the asphalt mixing machine blades in wear resistance. *Ibid*., **2**, 18 – 19.

DEPOSITION OF LAYERS WITH HIGH ADHESION STRENGTH BY THE ARC METALLIZATION METHODS

E.M. MATVIJSHIN
Zaporizhya State Technical University, Zaporizhya, Ukraine

ABSTRACT

Composite wires of the Ni–Al and Fe–Al types with a nickel or steel sheath are suggested. The wires used for electric-arc spraying provide coatings with a high strength of adhesion to the substrate, including to polished surfaces of parts.

Key words: *electric-arc metallization, polished substrate, adhesion strength, composite wire*

Owing to its high cost effectiveness and productivity, electric-arc metallization finds currently an increasingly wide application for deposition of coatings. An important factor in improving reliability and extending life of coated parts is an increase in strength of adhesion of coatings to the workpiece surface, which is achieved by deposition of intermediate layers. This problem is especially pressing for repair of parts made from chilled cast iron, as well as hardened parts the surface of which is hard to treat to produce the required microrelief. In this connection, development of wire materials for electric-arc spraying of layers with a high adhesion strength is of scientific and practical interest.

To deposit such layers by flame or plasma spraying methods, an extensive use is made of thermosensitive bimetal nickel-base flux-cored materials [1, 2].

Metal-ceramic and polymetallic wires of the Ni–Al type with an aluminium sheath are used to deposit coatings using a wire flame-spraying device [3, 4]. Metal-ceramic wires failed to find acceptance in the national industry because of a labour-intensive manufacturing process. The use of polymetallic wires of the «Alyunik» type, which have low rigidity of the sheath and large diameter (> 2 mm), for spraying using electric-arc metallization devices is difficult, and they do not ensure a high adhesion strength of the deposited layers. Therefore, investigations were conducted to study the possibility of using composite wires with a nickel or iron sheath for deposition of layers with an increased adhesion strength by the electric-arc metallization methods. Such wires can be made by drawing a nickel or steel strip through a drawing die simultaneously with aluminium or other wires which make the wire core. Even at a small diameter (< 1.8 mm) they are characterized by sufficient rigidity, can be consistently fed and sprayed using any type of a metallizer.

The investigations included studies of the possibility of depositing layer with a high adhesion strength without preliminary treatment of workpiece surfaces to impart them certain roughness. Strength of adhesion of the coatings to a polished substrate was evaluated by the method of «pin pulling» [5] using a pin 5 mm in diameter.

It was established that the smaller the diameter of a composite wire, the higher and more consistent the adhesion strength of the deposited layers. However, small-diameter wires (< 1.6 mm) made from a thin strip (δ < 0.2 mm) are characterized by low rigidity, poor retention of flux additions in the core and inconsistent feed to the spraying zone. If they are made from a thicker strip (δ > 0.3 mm), this increases the quantity of neckings and labour consumption in the wire manufacture.

Composite wires with a diameter of 1.7 – 1.8 mm turned out to be optimal for electric-arc metallization. Spraying such wires using devices with a different geometry of the blowing system shows that the highest strength of adhesion of the coatings to the polished surface is achieved in the case of using metallizers with the diaphragm-type spraying nozzles (EM-12, EM-14, EM-15). The use of devices with conical nozzles of the reducing type or expanding nozzles which provide supersonic velocity of the air jet results in a substantial decrease in adhesion strength of the layers. This is attributable to more favourable conditions for formation of a homogeneous melt at the tip of the composite wire and a metallization flow of coarser particles in the case of the devices with the diaphragm-type nozzles. All the investigations that followed were carried out using the EM-12 metallization machine with the 8 mm diameter diaphragm nozzle connected to the VS-600 power supply.

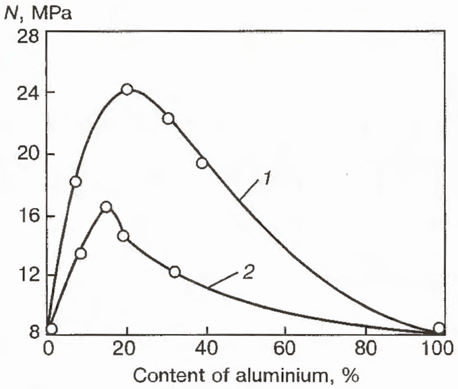

Figure 1. Effect of aluminium content of the composite wire of the Ni–Al (*1*) and Fe–Al (*2*) type on strength of adhesion to the polished substrate of coatings sprayed from distance L = = 180 mm at U_a = 32 V and P = 0.5 MPa

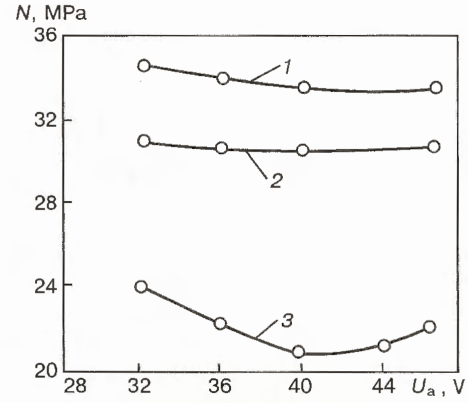

Figure 3. Effect of arc voltage U_a on strength of adhesion of coatings sprayed using the NA-20 nickel-aluminium wire with a different content of zirconium oxide: 6 % (*1*); 2 % (*2*) and 0 % (*3*)

As shown by tests of the coatings sprayed using nickel- and iron-base wires with a different aluminium content, the Ni–Al type wires provide a higher adhesion strength, as compared with the Fe–Al type wires (Figure 1). The Ni–Al type coatings are characterized by a maximum adhesion strength at 18 – 22 % Al and the Fe–Al type coatings — at 8 – 12 % Al.

This character of the relationship persists under different spraying conditions, although adhesion strength of the layers greatly depends upon the process parameters. Thus, variations in the wire feed speed and, hence, the current have almost no effect of the adhesion strength. At the same time, the adhesion strength substantially varies with variations in the arc voltage. Decrease in the voltage leads to an increase in the adhesion strength, although it makes ignition of the arc more difficult and deteriorates stability of its burning.

Ionizing agents in the form of a concentrate of rare-earth metal (REM) oxides were added to the core to increase stability of spraying of the wire at low values of the arc voltage. In addition to cerium oxide (up to 50 %), the concentrate also contained oxides of lanthanum, neodymium, praseodymium, zirconium and hafnium, as well as pure zirconium. The additions were introduced in the form of a paste mixed with binder, which made the process of their proportioning easier and ensured their uniform distribution in the wire core. The investigations showed that the ionizing agents added to the Ni–Al wires with 20 % Al did not only improve the arc burning stability, but also increased strength of adhesion of the coatings to the substrate (Figure 2).

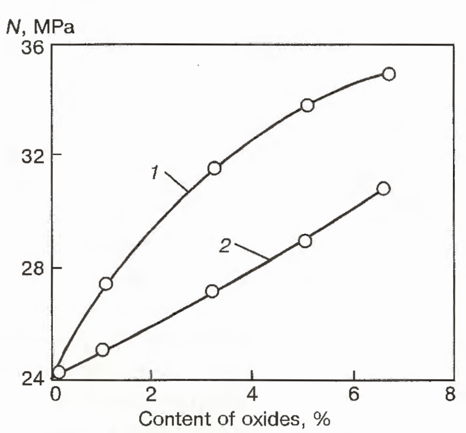

Figure 2. Effect of zirconium (*1*) and REM (*2*) oxide content of the wire of the NA-20 type on strength of adhesion of coatings sprayed at U_a = 32 V, P = 0.5 MPa and L = 150 mm

Addition of zirconium oxide causes a more substantial increase in the adhesion strength, but in this case it hardly depends upon the arc voltage (Figure 3).

The iron-base wires, even those containing additions of zirconium and REM oxides, provide metallized coatings with a lower adhesion strength. Therefore, the investigations were conducted to study the possibility of producing coatings with a high adhesion strength using sparsely alloyed composite wires of the Fe–Al (Figure 4), Fe–Ni–Al and Fe–NiCr–Al systems by adding the nichrome Kh20N80 or nickel Np-2 components to the core of the iron-aluminium wire.

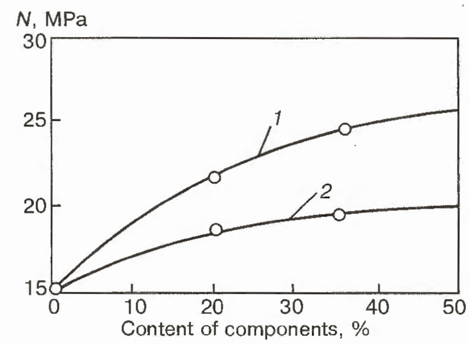

Figure 4. Effect of nichrome (*1*) and nickel (*2*) content of the core of the iron-aluminium wire with 10 % Al on adhesion strength of the coatings

The nichrome addition was found to lead to a more intensive growth of the adhesion strength than the nickel addition.

In adding 2 – 6 % zirconium oxide to the core of the Fe–NiCr–Al type wire the value of strength of adhesion to the polished surface increases to 38 – 45 MPa.

Results of the investigations made it possible to recommend the new composite wires with a nickel or steel sheath [6] for deposition of layers with a high adhesion strength by the electric-arc metallization method. The nickel-aluminium wires are more practicable to manufacture, as in their core they contain one soft metal component. The core of the Fe–NiCr–Al type wires contains harder components, as compared with aluminium, and is characterized by a very high filling coefficient (60 – 70 %), which makes the process of manufacture of such wires labour-consuming and expensive.

The materials suggested have been commercially applied at many enterprises for deposition of the electric-arc metallized coatings (without preliminary formation of the required roughness) on shafts of internal combustion engines and calender shafts made from chilled cast iron, glossing cylinders of paper-making machines, mounting surfaces of rolling bearings and other parts with high surface hardness. In this case working layers of different materials, depending upon service conditions of a part, are deposited on a composite sublayer (δ = = 0.1 mm), most often using high-carbon wires. Long-time operation of parts reconditioned by this method proved their high reliability and good performance.

CONCLUSIONS

1. The suggested composite wires with a nickel or steel sheath provide high strength of adhesion of coatings even to polished surfaces of parts in electric-arc spraying using metallizers with the diaphragm-type nozzles.

2. The use of such wires allows deposition of coatings on parts of chilled cast iron or hardened regions on surfaces without imparting them certain roughness and provides high performance of the coatings.

REFERENCES

1. Dittrich, F., Shepard, B., Shepard, P. *Metallization by spraying in a flame of mixtures entering into exothermic reaction and forming intermetallic compounds*. Pat. **3322515** USA, Int. Cl. 29-191.2. Publ. 30.05.67.
2. Borisov, Yu.S., Kharlamov, Yu.A., Sidorenko, S.L. (1987) *Thermal spray coatings of powder materials*. Kyiv: Naukova Dumka.
3. Dittrich, F., Shepard, B., Shepard P. *Compositions for flame spraying, forming exothermic intermetallic compounds*. Pat. **3436248** USA, Int. Cl. C 23 C 7/00. Publ. 01.04.69.
4. Novinsky, E., Harington, D. *Wire for flame spraying of coatings*. Pat. **4276353** USA, Int. Cl. B 32 B 15/02. Publ. 30.06.81.
5. Hasui, A. (1975) *Spraying technique*. Moscow: Mashinostroyeniye.
6. Matvijshin, E.M., Kononov, G.V., Milichenko, A.S. *Composite wire for deposition of coatings*. Pat. **1803** Ukraine, Int. Cl. C 23 C 4/10. Publ. 25.10.94.

EFFECT OF COMPOSITION OF FERROALLOYS ON THE CONTENT AND SHAPE OF NON-METALLIC INCLUSIONS IN METAL DEPOSITED WITH ELECTRODES UONI-13/55

V.S. POPOV, S.P. BEREZHNYI, I.M. BILONIK and **V.P. PIROZHKOVA**
Zaporizhya State Technical University, Zaporizhya, Ukraine

ABSTRACT

Effect of additions of ferrotitanium and complex ferroalloy of the electroslag melting in the coating of basic electrodes of the UONI-13/55 type on the mechanical properties of the deposited metal and content of non-metallic inclusions and also impurities in it was investigated.

Key words: *welding electrodes, basic coating, complex ferroalloy, electroslag remelting, weld metal, oxide inclusions, mechanical properties*

One of drawbacks of the weld metal which limits the use of welded components under the conditions of dynamic and alternating loads is the presence of uncontrollable impurities and non-metallic inclusions in the deposited metal, thus reducing, as is known, its ductile characteristics.

The basic type of electrodes covers a wide assortment of grades, including also the UONI-13/55 electrodes, designed for welding critical structures of low-alloyed steels. The requirements to the increased strength and toughness are specified to the weld metal of these steels. The basic type electrodes are used in industry over not less than 40 years [1, 2], and many research works were devoted to their comprehensive study [2 – 5]. There are all grounds to consider that the resource of strength and ductile capabilities of the metal, deposited with these electrodes, was maximum exhausted.

After analyzing the state of achievements in the field of study of structure and properties of low-carbon steels and methods of improving their strength and ductile characteristics, A.P. Gulyaev noted [6, 7] that it is possible, in principle, to produce a complex of properties, which is better than that obtained until present time, either by refining the initial grain to No.10 – 12, or at the expense of improving the purity of metal. Such refining can be attained in cooling from the melt at the rate exceeding 650 °C /s [8], that is impossible from the technical point of view in real conditions of welding.

At the same time the problem of decreasing the contamination of the deposited metal with non-metallic inclusions can be solved to a certain degree by the selection or a special preparation of ferromaterials for a coating of the welding electrodes. As the content of impurities in ferroalloys exceeds often that in the welding wire by 5 times, and the content of non-metallic inclusions exceeds by one order, then these ferroalloys are a source of difficult-to-remove impurities and non-metallic inclusions in the weld metal. It is known that to obtain the high values of mechanical properties of welds in welding with UONI-electrodes a complex deoxidation of metal with manganese, silicon and titanium, introduced into the coating of electrodes in the form of ferroalloys, is used. At the same time, from the data of [9], the volume share of inclusions in the ferromanganese used can reach 0.4 %. This is mainly silicates of manganese, while the share of a phosphite and sulphide eutectics is equal to 10 – 20 %. In a ferrosilicium the share of inclusions consisting mainly of the particles of quartz and corundum, can reach 1.0 %. In electrodes UONI-13/55 the ferrotitanium (up to 15 %) produced by an alumothermic method is used [1] as a deoxidizer in parallel with a ferrosilicium and ferromanganese (both by 5 %). This ferrotitanium contains a large amount of impurities of non-ferrous metals (Table 1). Inclusions whose volume share reaches 0.6 % are presented mainly by refractory oxides of aluminium (up to 70 %) and also nitrides of titanium and aluminium [9]. The main amount of impurities and inclusions is transferred to the weld metal and influences negatively its mechanical properties. In this connection we made an attempt to produce special ferromaterials with a low content

Table 1. Composition (mass %) of ferrotitanium of different methods of production

Chemical element	*FTi30A*	*FTSh-45*	*K-2*
Ti	28 – 40	44 – 46	28 – 31
Al	4 – 12	0.1	0.8
Si	< 5	0.17	26 – 28
Mn	1.5	0.6	24 – 25
Cu	0.3 – 1.5	0.02	0.06
Sn	0.01	0.005	0.005
C	0.15	0.08	0.20
S	0.015 – 0.040	0.01	0.030
P	0.02 – 0.04	0.012	0.028
N	0.065	0.04	–
H	0.0065	0.0055	–
O	0.45	0.25	–

Note. FTi30A was produced by alumothermic methods, FTSh-45 and K-2 – by electroslag melting.

Table 2. Composition (mass %) of coating of electrodes

Component	*UONI-13/55 [1]*	*Batch of electrodes*		
		A	*B*	*C*
Marble	54	–	–	–
Dolomite FK-2	–	54	54.0	54
Fluorspar FFS 95	15	15	15.0	15
Quartz sand	9	9	9.0	9
Ferromanganese FMn 1.0	5	5	5.0	–
Ferrosilicium FS 75	5	5	5.8	–
Ferrotitanium FTi30A	12	12	–	–
Ferrotitanium FTSh-45	–	–	11	–
Alloy K-2	–	–	–	18
Iron powder PZhV-2	–	–	–	5
Soluble glass 30*	30*	30*	30*	30*

*In percentage to the sum of rest elements.

of impurities and non-metallic inclusions, to study their effect on structure and mechanical properties of the weld metal. If to take into account that the ferrotitanium is introduced into the coating of the welding electrodes in the amount of up to 15 % than the degree of its contamination and content of inclusions influences the properties of the weld to the highest degree.

Therefore, to manufacture the quality welding electrodes the electroslag method of producing the ferrotitanium using sheet waste of titanium VT1-0 and steel was suggested and realized in practice. At such technology the secondary aluminium was not used as a deoxidizer that prevents the enter of non-ferrous metal impurities to the ferrotitanium. The alloy is characterized by a guaranteed concentration of titanium and low content of aluminium (less than 1 %). This provides a stable composition and mechanical properties of metal deposited with electrodes whose coating contains the above-mentioned ferrotitanium. To manufacture welding electrodes it is most rational to produce alloy with 40 – 48 % titanium content, which can be refined easily. The volume share of inclusions in this ferrotitanium does not exceed 0.18 %.

The study of use of a complex deoxidizer, containing several elements-deoxidizers (silicon, manganese, titanium) during welding presents an interest. As these complex deoxidizers for the electrode coatings are not produced in industry, we have developed the process of an electroslag remelting of a combined electrode of Fe–Ti type with an addition of standard ferromanganese and ferrosilicium. The ratio of these components was calculated to provide a formulated composition of a charge of electrodes UONI-13/55. It was assumed that during remelting the contamination of the produced complex alloy at the expense of refining the introduced components by a special highly-basic flux will decrease. It was established that the use of reactive fluxes refines the industrial ferroalloys both as to the non-metallic inclusions and impurities. The content of sulphur and phosphorous in the alloy was decreased by more than twice as compared with their total content in initial components. The volume share of inclusions which are presented mainly by carbonitrides of titanium, of 10 – 20 μm size, does not exceed 0.22 %. The inclusions of a thialite type of up to 16 μm size are seldom observed that is due to the formation of stable carbonitrides of titanium (ferrosilicium and ferromanganese serve the «suppliers» of carbon and nitrogen).

The study of effect of complex ferroaloy of the electroslag melting, introduced to the coating of the welding electrodes, on the composition and content of non-metallic inclusions in the deposited metal was carried out on electrodes of three pilot batches (Table 2). The industrial UONI-13/55 electrodes were selected as a reference, as they are most widely used for welding critical structures. They are sufficiently well-studied, the results of studies are published and the comparison with electrodes, which have a large amount of statistic data, is advantageous.

Electrodes of batch A were manufactured using industrial ferroalloys produced by formula of UONI-13/55 electrodes [1]. In coating of electrodes of batch B the ferrotitanium FTi30A of an alumothermic method of production was replaced by ferrotitanium FTSh-45 of the electroslag melting. In batch C all the ferroalloys were replaced by one complex alloy K-2 of the electroslag melting. Number of deoxidizers in all batches of electrodes

Table 3. Composition (mass %) of the deposited metal

Batch of electrodes	*C*	*Si*	*Mn*	*S*	*P*
A	0.09	0.50	1.0	0.020	0.020
B	0.10	0.30	0.8	0.020	0.022
C	0.09	0.35	1.0	0.014	0.016
UONI-13/55 (certificate composition)	0.08 – 0.11	0.20 – 0.50	0.6 – 1.2	≤ 0.022	≤ 0.024

was taken from the condition of feasibility of binding the equal amount of oxygen and producing the certificate composition of the deposited metal [2]. Coefficient of mass of coating of the electrode batches examined varied within the ranges of 33 – 34 %. As in coating of batch C the amount of a complex ferroalloy was reduced to 18 % against 22 % in batch A, then an additional 5 % of iron powder was introduced to the charge of electrodes C to preserve a stable mass of the coating.

To assess the effect of composition of ferroalloy in the coating of electrodes on the content of non-metallic inclusions the metallographic and petrographic examinations of ferroalloys and deposited metal were carried out using microscope MIM-8. Central regions of metal of single-layer welds on 10 mm thick steel VSt.3 made with pilot 4 mm diameter electrodes were examined. Welding was performed at direct current of a reversed polarity using the following conditions: I_w = 180 – 190 A, U_a = 22 – 24 V.

It was established that chemical composition of weld metal made with pilot electrodes (Table 3) corresponds to the requirement of a certificate of UONI-13/55 electrodes. In metal deposited with electrodes of a batch C in which a refining complex ferroalloy was used, the content of sulphur and phosphorous is lowest.

The electroslag technology of producing titanium and complex ferroalloy without using the secondary aluminium provides a low content of impurities of non-ferrous metals (copper and tin) in metal deposited with electrodes of batches B and C (Table 4). The technology gives a feasibility to produce the complex ferroalloys of Fe(Ti–Si–Mn) type with a wide range of changing the content of separate components that makes it possible to produce easily the required composition of the ferroalloy for similar grades of the electrodes.

The metal contamination with non-metallic inclusions was determined by GOST 1778–70, method P.

Inclusions in the metal deposited with electrodes of batch A, are similar in shape and composition to those revealed in welds made with electrodes UONI-13/55. Separate silicates in the form of single globules of 2 – 4 μm size, more seldom of 5 – 6 μm, have a glassy structure. These globules possess a higher value of refraction $n \approx 1.520$, than a quartz glass that indicates their complex composition. Oxides unlike the silicates are observed more often in the form of angular, fragmented particles of perovskite and thialite of (10 – 20) × (2 – 4) μm size. There are particles with optical properties which correspond to α-Al_2O_3. Some of inclusions are partially fused and acquired higher reflectivity and value of refraction. Large exogenous inclusions of thialite $Al_2O_3 \cdot TiO_2$, perovskite $CaO \cdot TiO_2$ or corundum α-Al_2O_3 of size (20 – 25) × × (4 – 6) μm size dominate (Figure, batch A). Aluminium and slag particles with a high content of Al_2O_3, entered by ferrotitanium of the alumothermic method of production can serve a source of these inclusions. The volume share of inclusions in the deposited metal is 0.22 %.

Non-metallic inclusions in metal deposited with electrodes of batch B are presented mainly in the form of separate globules of up to 2 μm size, which have both homogeneous and heterogeneous microstructure. The latter is characterized by higher values of refraction which approach those of Fe–Mn glasses with titanium and manganese silicates. Particles of thialite have a size of up to 4 μm and observed more seldom than in metal deposited with electrodes of batch A. There are also rare fine inclusions of irregular shape, corresponding to ilmenite ($FeO \cdot TiO_2$) by optical properties, and also single fine-dispersed inclusions of red-pink colour of a titanium monoxide. Large exogenous particles of type of thialite, perovskite and also corundum

Table 4. Composition (mass %) of gases and impurities of non-ferrous metals in the deposited metal

Batch of electrodes	*O*	*N*	*Ti*	*Cu*	*Sn*
A	0.050	0.0073	0.011	0.10	0.010
B	0.046	0.0062	0.018	0.08	0.005
C	0.040	0.0065	0.020	0.08	0.005

Table 5. Mechanical properties (tests acc. to GOST 6996–75) of weld metal deposited with pilot electrodes

Batch of electrodes	*Ultimate rupture strength, σ_t, MPa*	*Yield strength, σ_y, MPa*	*Elongation, δ, %*	*Impact strength KCU, J/cm²*
A	505 – 545	400 – 420	23 – 27	155 – 205
B	520 – 560	400 – 440	26 – 28	175 – 220
C	540 – 565	420 – 450	27 – 30	210 – 240
UONI-13/55 (certificate data)	≥ 490	≥ 390	≥ 20	≥ 160

α-Al_2O_3 were not revealed on metallographic sections. The volume share of non-metallic inclusions does not exceed 0.16 %.

In metal deposited with electrodes of a batch C, the non-metallic inclusions are presented mainly by up to 4 μm size silicates of a complex composition. In addition, the most silicate inclusions have a globular shape and heterogeneous microstructure (Figure) with a characteristic of refraction which is typical of Fe–Mn glasses with titanium. The volume share of non-metallic inclusions in weld metal does not exceed 0.14 %.

In metal deposited with electrodes of batches B and C the total amount of non-metallic inclusions was reduced. In addition, in metal deposited with electrodes C with a complex ferroalloy of the electroslag melting the total amount of non-metallic inclusions is reduced by 30 % as compared with that of metal deposited with electrodes A (with alumothermic ferrotitanium and separate introduction of ferromanganese and ferrosilicium). In metal of batch B and C there are no large exogenous particles of thialite and perovskite typical of the ferrotitanium of the alumothermic method of production. At reduction of the total amount of inclusions the specific share of silicates of a complex composition with a heterogeneous microstructure is somewhat increased.

The lowest content of oxygen, oxide inclusions and also their typical composition in metal deposited with electrodes of batch C is explained by the effect of a complex deoxidizer which contains three and more active elements (titanium, silicon, manganese, aluminium) that provides the deeper deoxidation of the metal [10]. The application of a complex deoxidizer provides the formation of fusible compositions of deoxidation products, coagulating quickly and removing easier from the molten metal [11, 12].

Results of investigation of mechanical properties of metal deposited with pilot electrodes are given in Table 5.

The use of ferrotitanium FTSh-45 in the electrode coating, which is more pure as to impurities and non-metallic inclusions, made it possible to increase the mean values of elongation by 7 % and impact strength by 9 % as compared with those for electrodes of the batch A.

When all the ferroalloys introduced into the coating of electrodes separately are replaced by a complex ferroalloy K-2 the mean values of elongation are increased by 12 %, and the impact strength — by 18 % as compared with those in case of using electrodes of the batch A, and, consequently, by 8 and 9 % as compared with typical mean values in case of using the electrodes UONI-13/55 [3].

CONCLUSIONS

1. Ferrotitanium of the alumothermic production, which contains aluminium, is a source of contami-

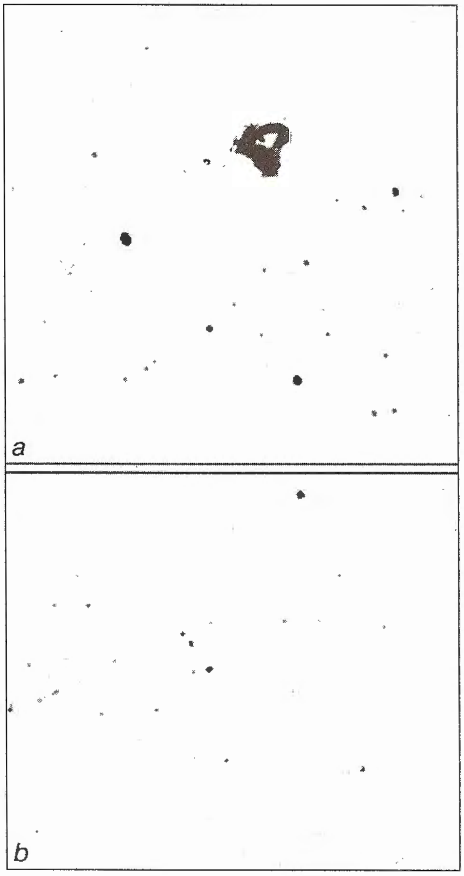

Non-metallic inclusions in metal of electrodes UONI-13/55 of batches A (*a*) and C (*b*) (×60) (reduced by 2/3) nation of weld metal with refractory slag and oxide inclusions. The latter can be eliminated by using the ferrotitanium of the electroslag melting.

2. Application of a refined complex ferroalloy of the electroslag melting in the coating of electrodes can reduce the content of harmful elements (sulphur and phosphorous) and non-metallic inclusions by 30 %, providing the formation of inclusions in the weld metal in the form of silicates of a heterogeneous composition, of more favourable globular shape in particular.

3. Introduction of a complex ferroalloy of the electroslag melting to the composition of coating of electrodes UONI-13/55 reduces the content of impurities and non-metallic inclusions in the weld metal, promotes the improvement of morphology of the latter, thus leading to increase in elongation and impact strength of the weld metal by not less than 10 %.

REFERENCES

1. (1962) *Handbook on welding*. Ed. by E.V. Sokolov. Moscow: GNTI.
2. Petrov, G.L. (1973) *Welding consumables*. Leningrad: Mashinostroyeniye.
3. Tarkhov, N.A., Sidlin, Z.A., Rakhmanov, A.D. (1986) *Manufacture of metallic electrodes*. Moscow: Vysshaya Shkola.
4. Pokhodnya, I.K., Korsun, A.O., Meshkov, Yu.Ya. *et al.* (1986) Peculiarities of brittle fracture of weld metal made by electrodes with a basic type coating. *Avtomaticheskaya Svarka*, **10**, 1 – 5.
5. Pokhodnya, I.K., Korsun, A.O., Meshkov, Yu.Ya. *et al.* (1986) Effect of titanium introduced to the coating of electrodes UONI-13/55 on microstructure and mechanical properties of weld metal. *Ibid.*, **12**, 1 – 7.
6. Gulyaev, A.P. (1983) About strength. *Metalloved. i Termich. Obrabotka Metallov*, **7**, 2 – 6.
7. Gulyaev, A.P. (1975) *Pure steel*. Moscow: Metallurgia.
8. Opalchuk, A.S., Kondratyuk, S.E., Khatra, A. *et al.* (1995) Effect of cooling rate in crystallization of structure formation and properties of tool steels. *Protsessy Litja*, **1**, 69 – 73.
9. Gasik, M.I., Ignatiev, V.S., Khitrik, S.I. (1970) *Gases and impurities in ferroalloys*. Moscow: Metallurgia.
10. Yavoisky, V.I., Rubenchik, Yu.I., Okenko, A.P. (1980) *Non-metallic inclusions and properties of steel*. Moscow: Metallurgia.
11. Gasik, L.N., Ignatiev, V.S., Gasik, M.I. (1975) *Structure and quality of industrial ferroalloys and master alloys*. Kyiv: Tekhnika.
12. Bornatsky, I.I. (1978) *Production of steel*. Moscow: Metallurgia.

EFFECT OF COOLING RATE ON THE STRUCTURE OF HIGH-CARBON DEPOSITED METAL

Yu.M. TKACHENKO
Zaporizhya State Technical University, Zaporizhya, Ukraine

ABSTRACT

Structure of the chromium deposited metal of 120Kh12F1 type used in restoration of dies for production of refractories is examined. It is shown that a ratio of structure austenite-martensite-carbide constituents in the deposits can be preset by a rate of metal cooling.

Key words: *surfacing, structure, transformation, cooling rate*

The structure of the deposited metal is determined both by properties of the alloying system and also by cooling conditions. Chromium carbon materials deposited with a flux-cored wire PP-120Kh12F1 are used for the restoration of dies for the production of refractories. Due to a large variety of types and sizes of the dies the rate of cooling of the deposited metal is varied within wide ranges from 10 to 70 °C/s.

The effect of cooling rate on the structure of metal at its surfacing with a flux-cored wire PP-Kh12F1-0 was investigated using a quick-response high-temperature dilatometer of IMET-DB design [1]. The samples were manufactured from steel Kh12F1, which corresponds by the chemical composition to the deposited metal in the second layer, mass %: C — 1.29; Cr — 11.1; W — 0.81; Mn — 0.52 and Si — 0.4.The metal cooling during surfacing is started from the melting temperature when the metal is in a state close to equilibrium. Therefore, during the dilatometric investigations the Kh12F1 steel samples were heated at a constant rate of 40 °C/s up to the maximum admissible temperature 1215 °C and cooled within the range of 78.00 – 0.95 °C/s rates. From the anisothermal diagram of decomposition of the overcooled austenite (Figure 1), a region of precipitation of a carbide phase from the solid γ-solution and also the values of temperature of a beginning of the martensite transformation M_b for the above-mentioned range of rates were determined.

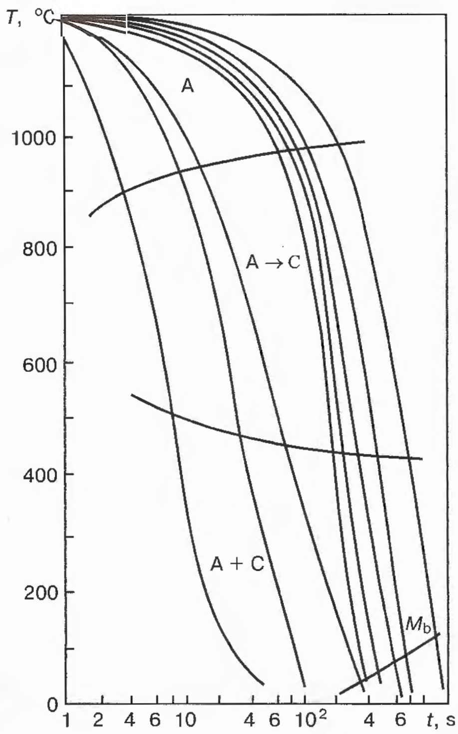

Figure 1. Part of an anisothermal diagram of decomposition of Kh12F1 steel austenite (cooling from 1215 °C)

The results of dilatometric investigations could establish that the structure of the high-carbon alloyed deposited metal during cooling depends greatly on the rate of cooling within the interval of austenite (A) → carbide (C) transformations. In addition, the amount of the forming carbide

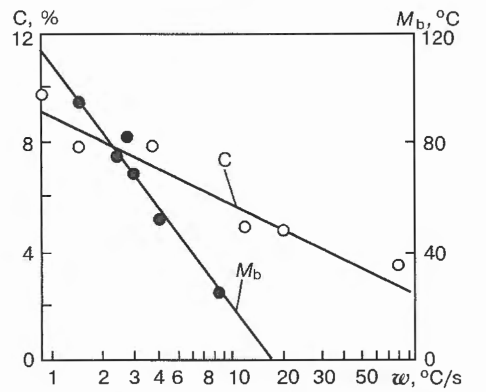

Figure 2. Effect of cooling rate on amount of carbide phase (C) and temperature M_b for Kh12F1 steel

phase C and temperature M_b are interrelated and determined by a rate of cooling samples, w (Figure 2).

The examination of parameters of a residual austenite lattice in the URS-50I type installation showed that, due to proceeding of diffusion processes, a period of the austenite lattice from 0.360 (at $w = 78$ °C/s) to 0.356 nm (at $w = 4$ °C/s) is decreased when the carbide phase is formed in the region of austenite-carbide transformations (Figure 1), thus indicating about its depletion with a carbon. This decrease is higher with a larger time of metal staying in the region of the austenite-carbide transformations. As a result, the stability of the overcooled austenite of the deposited metal is decreased and the favourable conditions are created for the formation of a martensitic phase in the matrix.

Thus, the ratio of constituents of austenite-martensite-carbide matrix can be regulated during surfacing with carbon chromium materials by control of the cooling rate within the interval of A $\rightarrow$ $\rightarrow$ C transformations and producing the deposited metal with the required properties.

REFERENCES

1. Shorshorov, M.Kh., Belov, V.V. (1972) *Phase transformations and changing of steel properties in welding*. Moscow: Nauka.

CORROSION RESISTANCE OF STAINLESS STEEL WELDED JOINTS IN ALKALI SOLUTIONS (REVIEW)

A.G. ALEKSANDROV and **Yu.N. SAVONOV**
Zaporizhya State Technical University, Zaporizhya, Ukraine

ABSTRACT

Corrosion behaviour of stainless steel welded joints in alkali solutions in the production of pulp by a kraft-method has been investigated. The corrosion potential of steels is within the passive region, the region of an active-passive transition or near the transpassive region of potentials. Under these conditions the welded joints are susceptible to a corrosion cracking, while weld metal is prone to a selective corrosion.

Key words: *welded joints, stainless steels, alkali solutions, corrosion cracking, weld metal, general corrosion*

Problem of the corrosive resistance of the equipment used in alkali solutions appeared first at the attempts to intensify the operation of steam boilers [1]. However, the cracks began to be initiated in their joints. This phenomenon was called a caustic brittleness. Later, similar damages were observed in the equipment of a soda [2], alumina [3, 4] and pulp-and-paper making [5]. It is evident that in alkali solutions the equipment under certain conditions is subjected to a corrosion cracking. Origin and mechanism of the corrosion cracking are well-studied only with respect to acid solutions.

To increase the life of the equipment, it is recommended in several productions to replace the low-carbon steels by stainless steels or double-layer steels with a protective stainless steel coating [5].

In the 1970 – 1975 there occurred the failure of the welded technological pipelines made of stainless steel 12Kh18N10T of equipment for a continuous pulp digestion using a kraft-method at the Arkhangelsk and Kotlass pulp-and-paper plants (PPP), where sufficiently low concentrations of alkali solutions (up to 10 – 15 % NaOH) are used. The examination showed that the failure of the pipelines was caused by a corrosion cracking in one cases, while in another cases it was caused by a selective corrosion of the weld metal [6]. In 1980 an explosion occurred in a digester in the USA (Pinehill). Examination showed that this explosion was caused by cracks of a corrosion cracking origin in a circumferential site weld [7].

There are available more than 300 digesters for producing the pulp by a kraft-method. A comprehensive analysis of their condition showed that almost all of them have cracks of a corrosion cracking origin not depending on the grade of steel (low-carbon, stainless or clad) from which they are manufactured [7]. The electrochemical examinations showed that the corrosion cracking in a technological medium (white lye, g/l: 40 – 75 NaOH; 20 – 25 Na_2S; 2 – 4 Na_2SO_4; 10 – 12 Na_2CO_3) at temperatures 90 – 100 °C occurs within the regions of an active-passive or passive-transpassive transition [8]. Increase in concentration of alkali solutions and operating temperature up to the boiling point promotes the increase in corrosion failures of the type of a general corrosion, as, for example, in soda production [2, 9].

Thus, the nature of corrosion failures of the welded equipment depends greatly on the structural material, temperature and concentration of NaOH alkali solutions. At comparatively low concentrations of NaOH and rather high temperatures (equipment for alumina production and pulp making) the corrosion cracking of a transcrystalline nature in stainless steels and an intercrystalline nature in low-carbon steels is a main kind of the failure. General or selective corrosion is observed only at local increases in concentration of the solutions, destroying of an oxide film due to boiling of the solution at the wall during the heat transfer and cavitation phenomena, in case of difference in chemical composition of the parent and deposited metal [9].

At high concentrations (more than 40 % NaOH) and temperatures close to the temperatures of boiling, the general corrosion is a main kind of failure of steels and welds in alkali solutions [9, 10].

Such dependence of the failure nature on the conditions of service is correlated with modern conceptions about the electrochemical origin of the corrosion and the theory of a passivity. In alkali solutions, steels, the same as pure metals, may be in an active state, while in the region of an active-passive transition they are in a passive, transpassive state and also in a state of a secondary passivity [10, 11]. The peak of an active dissolution on a potentiodynamic anodic curve, taken in the solution of a white lye at temperature 92 °C, is located within the region of potentials 0.9 – 1.0 V. At potentials 0.6 – 0.2 V a passive state is formed, and at the further decrease of the potential (below 0.2 – 0.1) – a transpassive state [7, 11].

Depending on concentration, composition and temperature of NaOH solution the steady potential of corrosion is located in the region of an active dissolution (at concentrations of more than 30 % NaOH and values of temperatures of solutions which are close to a boiling point). The higher concentration and temperature of the solution, the more probable occurrence of corrosion by the type of an active dissolution. At such potential of corrosion almost all the metals and alloys, except nickel, are subjected to an active dissolution [12]. Nickel has a high thermodynamic stability and imparts this property to the alloys by increasing their corrosion resistance in alkali solutions [9, 13]. At chromium content of about 30 % a high corrosion resistance under these conditions is provided [9]. Other metals, included to the composition of steels and alloys, have only a negligible influence on the corrosion resistance in alkali. This characteristic in alkali solutions is increased by niobium, copper and vanadium and decreased by manganese and molybdenum. The corrosion resistance is decreased especially by molybdenum which is in a transpassive state and subjected to an intensive dissolution at the potentials lower than 1 V [13 – 15].

The presence of oxidizers in alkali solutions [15], the temperature reduction below the boiling point and decrease in concentration for less than 30 % NaOH transfer steels to a passive state [11, 16]. It is possible to increase the passivity of steel, to improve the passive state and resistance of the oxide film by the alloying with chromium (20 – 30 %) and nickel (12 – 26 %).

Under these conditions, the stainless steel of 12Kh18N10T grade and double-layer steel with a protective layer from austenitic Cr–Ni steels found the wide application for manufacture of the equipment. Examination of the corrosion failures of the equipment made of steel 12Kh18N10T showed that their nature is determined by the service conditions, technology of welding, filler electrode materials, postweld heat treatment.

The main kind of failure of the welded joints in < 30 % NaOH alkali solutions is a corrosion cracking. This was observed in welded joints of the pipelines, at boiler walls, along the welds in welding-on of fins to the transport tyres, rolls, wheels, storage tanks and other technological equipment used at temperatures 70 – 100 °C, i. e. at potentials of an active-passive transition [8].

Increase in temperatures of working and test media to the boiling point and higher even at relatively low concentrations of solutions (25 – 30 % NaOH) leads to the initiation of a general or structural-selective corrosion of the deposited metal. The differences in chemical composition of parent and deposited metals (in particular, molybdenum content in the latter), the increased content of the second phase (δ-ferrite) increases the probability of the general or structural-selective corrosion of the weld metal. Due to a different content of chromium and nickel in austenitic and ferritic structural constituents the increase in δ-ferrite amount leads to the decrease in a corrosion resistance, as the structural-selective corrosion is proceeding with a dominating dissolution of the δ-ferrite [17].

Welds of digesters, a central pipe, distributing pipelines, dash plates of evaporating cycles, made from 12Kh18N10T steel, etc., used in alkali solutions at 100 – 170 °C, are subjected to an intensive general corrosion.

During 1971 – 1999 the investigations were made at the Zaporizhya State Technical University for improving the life of the equipment operating in a white lye and also in 30 – 40 % NaOH alkali solutions and at temperatures 90 – 170 °C.

Digesters of the equipment for a continuous pulp digestion at the Arkhangelsk PPP and Syktyvkar saw-milling plant were repaired using the technology based on the above-conducted investigations. In 1974 – 1985 the new high-pressure pipelines of 325 × 12 mm diameter pipes were manufactured using electrodes of EA-1B (TsL-11) grade and mounted on the equipment. After welding the welds were subjected to heat treatment in muffle furnaces, i.e. austenitization from temperatures (1050 ± 25) °C to homogenize the structure of the deposited metal and to relieve the residual welding stresses [18]. The heat-treated pipelines are used until now, while in nonheat-treated welded pipelines the cracks of a corrosion cracking origin were formed after 3 – 5 years of service. The postweld «stabilizing tempering» of the welded joints (850 – 900 °C, 1 – 2 h soaking) was used in manufacture and repair of large-sized apparatuses for increasing the corrosion resistance [19 – 21].

The further increase in the corrosion resistance of welded joints in alkali solutions was attained by modifying the deposited metal with yttrium [22 – 25]. Modifying of the deposited metal is possible with zerium, calcium and other rare- and alkali-earth metals. However, the deoxidizing and modifying ability of the yttrium is higher than that of other elements [22, 24]. The high natural melting temperature (1525 °C) makes it possible to provide the rather high residual content of yttrium in the deposited metal in arc welding [24]. The corrosion resistance of the Cr–Ni deposited metal, modified with yttrium, is increased [23], that is due to its effect on the characteristics of a passive state: the transition to the passive state is easier, the critical points and current in a passive state are decreased [24]. Two-phase austenitic-ferritic stainless steels of 12Kh21N5T and other grades are the promising structural material for the hardware of the equipment used in 10 – 30 % NaOH alkali solutions [26]. Unlike the austenitic steels, the two-phase austenitic-ferritic steels have a high resistance to a corrosion cracking. Therefore, the welded hardware of the two-phase steels can be used reliably in alkali solutions without postweld heat treatment. However, the welded joints of the austenitic-ferritic steels, made with electrodes of EA-1B, EA-2B types possess the lower resistance of the deposited metal in alkali solutions [27].

It is possible to control the corrosion processes and to influence the corrosion resistance of the deposited metal by changing the phase composition of the weld and HAZ metal [28]. Thus, the increased nickel content in the weld metal to 7 % and chromium up to 24 – 26 %, as compared with those in the parent metal, provides its structure with 35 – 40 % content of the ferritic phase and the corrosion resistance equal to that of the parent metal [27]. The phase composition of the HAZ metal can be controlled by changing the energy input in welding [28].

The increase in tough-plastic properties of the weld metal can be attained by the modifying with yttrium. The effect of yttrium on the properties and corrosion resistance of the austenitic-ferritic deposited metal is similar to its effect on the properties of the austenitic deposited metal [29 – 32].

CONCLUSIONS

1. Welded joints of austenitic Cr–Ni stainless steels in 10 – 30 % NaOH alkali solutions and at high values of temperature are subjected to a corrosion cracking in HAZ and a selective corrosion in weld metal.

2. Heat treatment of welded joints (austenitization from 1050 – 1100 °C, stabilizing tempering at 880 – 890 °C) increases the resistance against the weld metal corrosion cracking.

3. Further increase in resistance can be attained at the expense of an additional alloying with nickel (1 – 2 %) and modifying with yttrium (residual content in deposited metal is ≤ 0.03 – 0.05 %). Yttrium increases the technological strength, ductility and corrosion resistance.

4. Welded joints of two-phase austenitic-ferritic steels have a high resistance to cracking in alkali solutions. The corrosion resistance of the weld metal depends on its chemical composition and structural state. The metal with the structure, containing 35 – 40 % of the ferritic phase, possesses the highest value of the corrosion resistance.

REFERENCES

1. Evans, Yu.R. (1962) *Corrosion and oxidation of metals*. Moscow: Mashgiz.
2. Hike, F. (1974) Corrosion of metallic materials in hot concentrated caustic soda solutions. *Soda to Enso*, **24**, 109 – 136.
3. Steklov, O.I. (1976) *Strength of welded structures in aggressive media*. Moscow: Mashinostroyeniye.
4. Aleksandrov, A.G. (1970) Effect of alloying on resistance of a welded joint metal to corrosion cracking in alkali media. *Fiz.-khim. Mekhanica Materialov*, **3**, 116 – 117.
5. Strom, S. (1993) Crack development and corrosion on continuous kraft digesters. In: *Eng. Sol and Corr. Probl*. Houston.
6. Aleksandrov, A.G., Milichenko, S.L., Kirpik, L.K. *et al.* (1976) Causes and nature of fracture of welded pipelines from Cr–Ni steel. *Svarochnoye Proizvodstvo*, **2**, 30 – 31.
7. Chakrapani, D.C., Czyzewski, H. (1984) Pulp digester cracking afflicts a variaty of alloys. In: *Proc. of Int. Congr. on Metallic Corrosion*, Toronto, 1984, June 5 – 7. Ottawa.
8. Crowe, D.C., Tromans, D. (1984) Caustic cracking of stainless steel. *Can. Metallurgy*, **1**, 99 – 106.
9. Sakaki, T., Simizu, E., Sakiyama, K. (1980) Corrosion of Fe–Cr–Ni alloys in hot concentrated caustic soda solution. *Nihon Kinzoku Gakkaishi*, **5**, 582 – 587.
10. Yasuda, M., Tokunaga, S., Taga, T. *et al.* (1985) Corrosion behaviour of 18-8 stainless steels in hot concentrated caustic soda solutions under heat transfer conditions. *Corrosion-Nace*, **12**, 720 – 727.
11. Aleksandrov, A.G., Gorban, V.A., Langer, N.A. *et al.* (1980) Corrosion and electrochemical properties of welded joints of steel 08Kh18N10T in 30 % NaOH solution. *Avtomaticheskaya Svarka*, **9**, 68 – 69.
12. Yasuda, M., Fukumoto, K., Koizumi, H. *et al.* (1987) On the active dissolution of metals and alloy in hot concentrated caustic soda. *Corrosion-Nace*, **8**, 492 – 498.
13. Aleksandrov, A.G. (1970) Corrosion resistance and resistance to corrosion cracking of Fe–Ni alloys in concentrated solutions of alkali. *Fiz.-khim. Mekhanika Materialov*, **2**, 45 – 48.
14. Aleksandrov, A.G., Savonov, Yu.N., Lazebnov, P.P. *et al.* (1983) Corrosion resistance of metal of welded joints from steel 12Kh18N10T in alkali media. *Svarochnoye Proizvodstvo*, **2**, 24 – 25.
15. Kanevsky, L.S., Kolesnikova, N.N., Shirokova, N.V. *et al.* (1975) Effect of alloying elements on corrosion resistance of Cr–Ni steels in alkali medium. *Zashchita Metallov*, **5**, 781 – 784.
16. Fokin, M.N., Zhuravlyov, V.K., Mosolov, A.V. (1978) About some peculiarities of electrochemical behaviour of stainless steels in NaOH solutions. *Ibid.*, **6**, 690 – 693.
17. Lazebnov, P.P., Aleksandrov, A.G. (1987) Effect of chemical composition on corrosion and electrochemical properties of Cr–Ni deposited metal in alkali media (Review). *Svarochnoye Proizvodstvo*, **7**, 4 – 7.
18. Aleksandrov, A.G., Lazebnov, P.P. (1983) Effect of ferrite on corrosion resistance of austenitic-ferritic deposited metal. *Avtomaticheskaya Svarka*, **10**, 70 – 71.
19. Aleksandrov, A.G., Pinkovsky, I.V., Tsentsiper, B.M. (1978) *Repair of supply pipelines of equipment for a continuous pulp digestion*. Moscow: Lesnaya Promyshlennost.

20. Aleksandrov, A.G., Savonov, Yu.N., Stepakin, A.F. *et al.* (1986) Repair of digesters for sulphite-pulp production. *Bumazhnaya Promyshlennost*, **12**, 6.
21. Aleksandrov, A.G. (1990) Corrosion resistance of welded joints of Cr–Ni steels in alkali media (Review). *Svarochnoye Proizvodstvo*, **5**, 9 – 10.
22. Aleksandrov, A.G., Lazebnov, P.P. (1982) Effect of yttrium on structure and mechanical properties in welding cast iron, steels and alloys. *Avtomaticheskaya Svarka*, **12**, 34 – 37.
23. Aleksandrov, A.G., Lazebnov, P.P., Savonov, Yu.N. *et al.* (1982) Effect of yttrium on corrosion resistance of welded joints of steel 12Kh18N10T. *Svarochnoye Proizvodstvo*, **2**, 12 – 14.
24. Savonov, Yu.N., Lazebnov, P.P., Aleksandrov, A.G. *et al.* (1982) Effect of yttrium om metallurgical processes in welding steels of austenitic class using electrodes with flurode-calcium coationg. *Avtomaticheskaya Svarka*, **7**, 26 – 28.
25. Lazebnov, P.P., Aleksandrov, A.G., Gorban, V.A. (1986) Effect of yttrium on electrochemical properties of Cr–Ni deposited metal in alkali media. *Svarochnoye Proizvodstvo*, **6**, 30 – 32.
26. Koshkin, B.N., Sidlin, Z.A., Mosolov, A.V. *et al.* (1981) *Corrosion resistance of welded joints of sparsely-alloyed stainless steels in aggressive media.* Moscow: NIITEKhIM.
27. Aleksandrov, A.G., Savonov, Yu.N., Vasilenko, G.I. *et al.* (1987) Corrosion resistance of welded joints of two-phase alloyed steels of Kh21N5T type. *Avtomaticheskaya Svarka*, **9**, 45 – 47.
28. Aleksandrov, A.G., Savonov, Yu.N., Ruban, V.T. *et al.* (1987) Effect of energy input on corrosion resistance of welded joints of austenitic-ferritic steel of 10Kh21N5T type. *Svarochnoye Proizvodstvo*, **7**, 9 – 11.
29. Aleksandrov, A.G., Savonov, Yu.N., Grishko, S.P. (1989) Optimization of chemical composition of metal welds from austenitic-ferritic Cr–Ni steels in alkali medium. *Ibid.*, **10**, 15 – 17.
30. Aleksandrov, A,G., Savonov, Yu.N. (1990) Corrosion resistance of weld metal of two-phase Cr–Ni steels with yttrium. *Ibid.*, **7**, 13 – 14.
31. Aleksandrov, A.G., Savonov, Yu.N. (1990) Corrosion resistance of welds of austenitic-ferritic steels in alkali medium. *Ibid.*, **8**, 15 – 16.
32. Aleksandrov, A.G., Savonov, Yu.N. (1998) Peculiarities of welding of 12Kh18N10T steel equipment for producing a sulphite cellulose. In: *New Materials in Metallurgy and Machine Building*. Zaporozhje: ZSTU.

CLADDING OF DRAUGHT EQUIPMENT BLADES

V.N. GORDIENKO and **A.A. SHUMILOV**
Zaporizhya State Technical University, Zaporizhya, Ukraine

ABSTRACT

Wear resistance of cladding consumables under gas-abrasive wear was studied. New cladding consumables in the form of flux-cored wires and coated electrodes were proposed, namely PP-150Kh12R4, PP-160Kh14R4MN, PP-80Kh12R3TA, EN-150Kh12R3TA, EN-180Kh14R4.

Key words: *cladding, wear resistance, abrasivity, fan*

The thermal power stations of Ukraine which fire solid fuel, currently produce up to 50 % of the total electric power. The effectiveness of their operation essentially depends on the characteristics of draught equipment, including such assemblies as mill exhauster fans and smoke exhausters (Table 1).

Wear of blades and other parts of the air path in fans and smoke exhausters under the impact of abrasive particles leads to shortening of the operational periods between repairs, marked deterioration of the draught equipment performance and, eventually, to considerable loss of electric power. In particular, in operation of 300 MW units in the thermal power stations the power losses can reach 15 to 20 MW because of insufficient draught of the smoke exhauster caused by intensive blade wear.

VM-180 mill exhaust fan (Figure 1) is a high-speed compressor unit of the centrifugal type with backward-curved blades. It collects air with coal dust of the finest fractions from the cyclones and supplies this mixture to the steam generator furnace. Between 15 and 30 % of the air coming to the furnace is transported through the mill exhauster fan blades. Weight percent concentration of dust in the drying agent (air + flue gases) can be up to 60 to 80 g/m^3. The high concentration of coal dust and considerable circumferential velocities of the blades are exactly the factors causing their intensive wear in operation. The mode of fracture of a blade without the protective cladding after six months of operation is shown in Figure 2. The temperature of the transported air varies between 100 and 120 °C [1].

Table 1. Specification of the equipment

Parameters	*VM-180 mill exhauster fan*	*DOD-31.5 smoke exhauster*
Efficiency, thous. m^3/h	180	870
Total pressure, GPa	107.9	367
Wheel diameter, m	1.92	3.15
Motor rotation frequency, s^{-1}	24.9	8.3
Electric motor power, kW	1250	–
Number of blades, pcs	16	40

Analysis of the coal dust samples leads to the conclusion that the fan blades are worn by the coal particles between 3000 and 50 μm and less in size. However, the major part of the dust, about 74 %, is made up by particles of 50 to 90 μm size. Coal grains of such dimensions are characterized by a rather high abrasivity, especially if they have sharp facets.

Two-stage axial DOD-31.5 smoke exhauster (Figure 3) is an important element of the gas-air path of an electric power station. It collects the flue gases from the air heater and feeds them to the chimney. Coal burning in boiler furnaces generates ash part of which is carried away by the flue gases. Special devices do not provide their complete cleaning. As a result, ash particles pene-

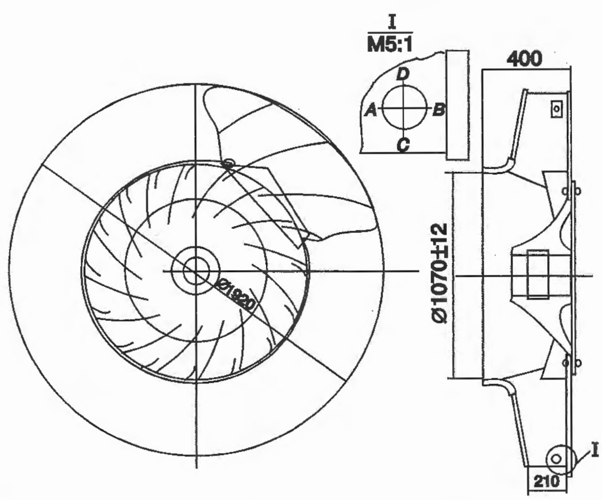

Figure 1. Mill exhauster fan impeller with samples mounted in the blades (*AB*, *CD* are the directions along which the profile of their worn surface was taken)

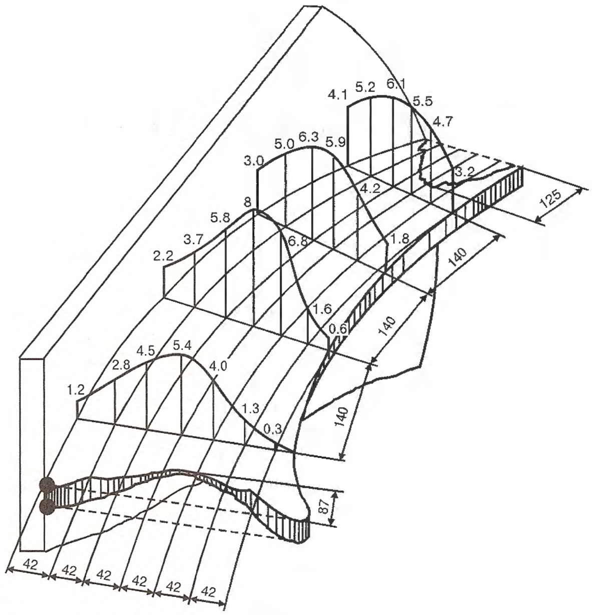

Figure 2. Mode of fracture of an unclad blade of VM-180 mill exhauster fan transporting coal dust (vertical lines show the linear wear values in mm)

trating into the smoke exhauster with the flue gases, cause intensive wear of the smoke exhauster blades (Figure 4) [1].

Screening of the ash samples showed that the blades of DOD-31.5 smoke exhauster are worn by the flow of flue gases containing ash particles of 5 to 300 μm size. Its main part, however (about 70 %) is made up by particles of 90 to 160 μm size. These particles have a spherical, and more seldom sharp-angled shape. Moreover, a magnetic fraction is found in the ash, which consists of magnetite and baked hematite.

The high abrasivity of the ash is related to the content of mineral admixtures in it, the quantity of which changes, depending on the kind of fuel and the field where it was produced. The mineral admixtures in coals most often consist of 95 % of silicon, aluminium, iron, calcium and magnesium compounds. The other 5 % are made up by vanadium, zinc, titanium, manganese and other compounds [2].

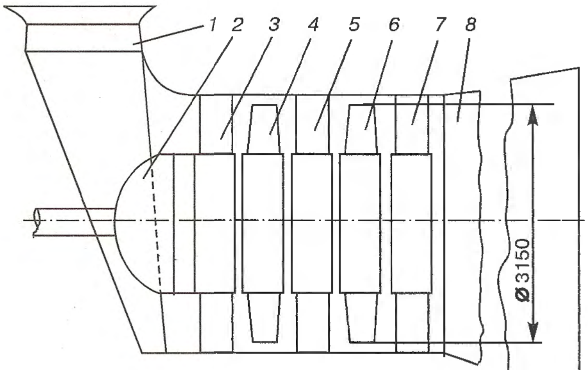

Figure 3. Two-stage axial DOD-31.5 smoke exhauster: *1* — inlet box; *2* — fairing; *3* — inlet vane device; *4* — first impeller; *5* — intermediate vane device; *6* — second impeller, *7* — straightening device; *8* — diffuser

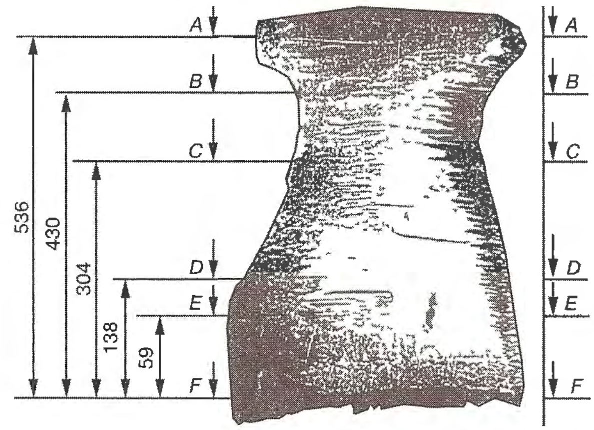

Figure 4. Mode of fracture of an unclad blade of DOD-31.5 smoke exhauster

In addition, the coals include alumina (Al_2O_3) and quartz (SiO_2) which have a high abrasivity. Their microhardness reaches 22 and 11 GPa, respectively.

In order to analyze the conditions of wear of the blades of the mill exhauster fan and smoke exhauster, it is necessary to know not only the dimensions and shape of the abrasive grains, but also such characteristics of the jet as the angle of incidence and collision velocity. Simultaneous consideration of these factors taking into account the curve of blade wear, enables determination of the parameter, namely velocity of the particles or their angle of incidence, which produces greater wear of a particular blade section.

In addition, the derived data are required for modelling the process of samples wear under the laboratory conditions [3].

Calculation of the triangles of velocities on the blade leading and trailing edges demonstrated that the mill exhaust fan blades are worn by sharp-angled particles of coal dust which at the moment of collision have the velocity of 145 to 212 m/s and angles of incidence of about 18 – 26°. Now the blades of axial DOD-31.5 smoke exhausters are exposed to the impact of spherical particles of the ash moving at the velocities of 72 to 140 m/s at angles of incidence of 10 – 38° [4].

Selection of steels and cladding alloys for the blades of mill exhauster fans and smoke exhausters can be performed by valid data on the nature of wear resistance dependence on the angle of incidence for different materials, as well as the velocity of collision of abrasive particles with the blade surface and angles of incidence at which the parts become worn under the actual conditions. In order

Table 2. Composition and properties of tested materials*

Batch No.	*Material*	*State*	*Fraction by weight, %*						
			C	*Si*	*Mn*	*Cr*	*V*	*Ti*	*B*
1	VK3M hard alloy	Brazing on St.3 steel	97 % WC + 3 % Co						
2	PP-AN170**	Cladding	0.70	0.60	0.60	20.00	–	0.2	3.0
3	Kh12F1 steel	Quenching from 1050 °C into oil	1.27	0.26	0.34	12.10	0.7	–	–
4	Kh12F1 steel	Quenching from 1175 °C into oil	1.27	0.26	0.34	12.10	0.7	–	–
5	Kh12F1 steel	Quenching from 1200 °C into oil	1.27	0.26	0.34	12.10	0.7	–	–
6	Kh12F1 steel	Quenching from 950 °C into oil	1.27	0.26	0.34	12.10	0.7	–	–
7	Kh12F1 steel (standard)	As-annealed	0.42 – 0.50	0.17 – 0.37	0.50 – 0.80	0.25	–	–	–

*Wear by coal dust under the conditions of production.
**Flux-cored wire cladding of St.3 steel.

Table 2 (cont.)

Batch No.	*Amount of carbide phase, %*	*HRC hardness*	*Specific wear, $\Delta P \cdot 10^{-4}$, g/h*	*Density, kg/m^3*	*Wear by volume, $\Delta V \cdot 10^{-4}$, mm^3/h*	*Relative wear resistance, ε*
1	97	90	0.271	15150	0.018	56.770
2	46 – 50	60	2.111	7370	0.285	3.586
3	14	61 – 63	3.065	7850	0.390	2.620
4	7	45 – 47	3.824	7850	0.489	2.090
5	5	38 – 40	4.026	7850	0.513	1.992
6	16	52 – 54	4.475	7850	0.570	1.754
7	–	–	8.023	7850	1.022	1.000

to derive such data, the mill exhaust fan blades were tested under the conditions of production.

Influence of the structural state of the base on the alloy wear resistance was studied for the case of Kh12F1 tool steel with heat treatment which provided a broad range of structures from the ferrite-pearlite to predominantly austenite structure.

In order to evaluate the influence of the carbide phase on the material wear resistance, alloys of 80Kh20R3T type were studied, which were produced in cladding with standard PP-AN170 flux-cored wire which yielded good results in wear by ash particles during operation of smoke exhauster blades. Another studied material was hard metal-ceramic VK3-M alloy based on tungsten monocarbide.

The level of wear resistance of Kh12F1 steel in different structural states after quenching from the temperature of 950, 1050, 1175, 1200 °C for producing the structures of troostite, martensite, metastable austenite with martensite and stable austenite, under the conditions of gas-abrasive wear, is characterized by the data in Table 2.

Under the conditions of production Kh12F1 steel has the highest wear resistance (ε = 2.62) after quenching from 1050 °C at *HRC* 63 hardness. Its structure consists of 67 % martensite, 19 – 20 % austenite and 13 – 14 % carbide phase. Troostite presence in the alloy matrix (batch 6 samples in Table 2) lowers its ability to resist the destructive action of the coal dust particles. Despite a comparatively high hardness (*HRC* 52 – 54), the wear resistance of the metal with troostite structure is low and is by just 75 % higher than that of the standard [4, 5].

Wear resistance of metastable austenite structure is by 19 % higher than that of the troostite structure, but almost 1.5 times lower than that of the martensite structure.

The influence of the amount of the carbide phase on wear resistance of the alloys in gas-abrasive wear was found in investigation of a standard PP-AN170 cladding alloy with about 50 % of the strengthening phase, as well as of metal-ceramic hard BM3-M alloy having a predominantly carbide structure (97 % carbides; see Table 2). It turned out that the alloys with the carbide structure have the highest wear resistance under the studied service conditions. So, wear resistance of the hard alloy when recalculated for volume loss, is 56.7 times higher than that of annealed steel 45. The relative wear resistance of the metal deposited with standard PP-

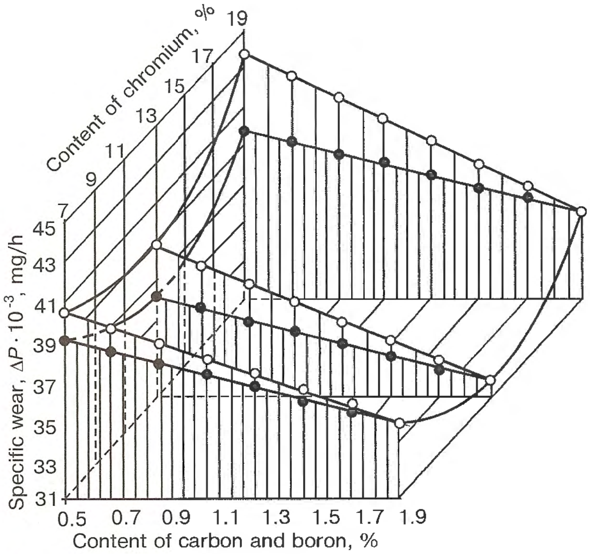

Figure 5. Influence of carbon, chromium and boron content on specific wear of the cladding metal (● – boron at 1.9 % C; ○ – carbon at 1.9 % B)

AN170 flux-cored wire, is up to 3.58 compared to the standard [5].

Wear of blades of mill exhauster fans by the coal dust flow is found in the absence of significant impact loads to which hard alloys are especially susceptible. It is known that they have the highest wear resistance under the impact of the sliding flow, when the wear process is reduced to scratching, and the fatigue phenomena develop only slightly.

Investigation of the laws of wear of the materials with markedly different physico-mechanical properties in a dust-laden gas-abrasive flow, enabled defining the requirements to the structure and properties of the alloys designed for operation under the conditions of intensive gas-abrasive wear. It is found that in order to achieve a high level of wear resistance under the impact of finely-dispersed particles of coal dust and ash, the deposited metal should have a high aggregate hardness. The alloy structure should contain not less than 50 – 70 % of the strengthening phase, uniformly distributed in the martensite-austenite matrix.

The eutectic and hypereutectic alloys which solidify with an excess carbide phase and have a relatively soft matrix, quite satisfactorily meet the above requirements.

Wear resistance of iron and carbon alloys with chromium and boron was studied to determine the optimal material.

Chromium content in the experimental alloys was changed in the range of 7 – 15 % and that of carbon and boron between 0.5 and 2.0 %.

Wear resistance testing was conducted in a laboratory unit of a pneumatic-mechanical type at 200 m/h velocity of the particle collision with the sample and angle of incidence $\alpha = 24°$. Quartz sand with 160 – 250 μm particle size from Novoselovsk quarry was used as the abrasive. 6 kg of abrasive passed through the nozzle during testing. Prior to that all the samples were subjected to running-in during 3 to 4 tests.

A three-dimensional model which characterizes the influence of carbon, chromium and boron on the specific wear value, is given in Figure 5. In the studied range of compositions the alloy wear resistance, with unchanged amount of other alloying elements, grows linearly both with the increase of carbon and of boron content. Dependence of specific wear on the content of chromium in the cladding metal with the same amounts of carbon and boron, is of a parabolic shape with the optimum in the range of 11 – 14 % chromium content.

The conducted investigations formed the basis for development of new highly wear-resistant cladding materials for cladding of the blades of fans and smoke exhausters, in the form of flux-cored wires and coated electrodes of PP-150Kh12R4, PP-160Kh14R4MN, PP-80Kh12R3TA, EN-150Kh12R3TA and EN-180Kh14R4 grades. Cladding with them allows a 1.5 to 2.2 times increase in wear resistance of blades compared to the standard cladding materials.

REFERENCES

1. Sherstyuk, A.N. (1957) *Fans and smoke exhausters*. Moscow-Leningrad: Gosenergoizdat.
2. (1963) *GOST 8184–70*. Bituminous coals and anthracite of the Donetsk coal-mining district. Moscow: Standartizdat.
3. Kleis, I.R. (1967) On some laws of impact wear. *Vestnik Mashinostroyeniya*, **8**, 52 – 54.
4. Popov, V.S., Gordienko, V.N., Stetsenko, A.I. (1977) Wear-resistant cladding of smoke exhauster blades. *Elektrich. Stantsii*, **5**, 79 – 80.
5. Popov, V.S., Gordienko, V.N. (1976) Investigation of wear of mill exhauster fan blades and selection of cladding materials. *Ibid.*, **8**, 14 – 16.

CAVITATION-CORROSION RESISTANCE OF SOME DEPOSITED STAINLESS STEELS AND ALLOYS

A.V. PATYUPKIN, A.S. RUDYCHEV and **O.G. BYKOVSKY**
Zaporizhya State Technical University, Zaporizhya, Ukraine

ABSTRACT

Some deposited stainless steels and alloys were tested in the impact-erosion testing facility. It is found that the corrosion factor plays the most important role in the process of cavitation-corrosion fracture of materials in an aggressive medium.

Key words: *compressor, cavitation erosion, corrosion, surfacing, modifying*

Rotary liquid-circular RZhK-1800/1.5 compressors are used in magnesium industry for chlorine production. Their main components (stationary casing, rotary rotor) are made of 10Kh18N9T steel and operate in a sulphuric acid solution with 92 to 98 % concentration. They are subjected to intensive cavitation-corrosion wear in service, which results in the compressor service life not exceeding 2000 h [1].

10Kh18N9T steel is highly resistant in sulphuric acid solutions only in the passivation zones [2, 3]. However, at cavitation-erosion impact the protective oxide film does not have enough time for complete restoration. There is practically no information on the joint action of cavitation and strongly corrosive medium on the metals. The currently available recommendations involve the use of steels of the type of 10Kh18N25M6, 10Kh23N28M3D3T, etc. for such service conditions [4]. They, however, are expensive and it is not rational to fully make the compressor parts of them. On the other hand, these parts can be surfaced, because the fractures are of a local nature and occur in the same areas.

In order to investigate the cavitation-corrosion resistance of some corrosion-resistant alloys, testing was conducted in a special impact-erosion facility [5] with the following parameters: jet flow velocity of 80 m/s; nozzle diameter of 5 mm; nozzle-to-sample distance of 5 mm; working fluid temperature of 50 to 60 °C.

Testing for corrosion losses was conducted by sample boiling for 24 h by the procedure of [6] in the following solution: 160 g of $CuSO_4 \cdot 5H_2O$ (GOST 4165–77) + 100 ml of sulphuric acid of 1.835 density (GOST 4204–77) + 1000 ml of water + copper chips.

10Kh18N9T steel in the form of rolled stock was taken as the standard.

Samples of 20×15×5 mm size for cavitation-corrosion resistance testing were cut out of the metal deposited manually with electrodes at reverse polarity direct current: $d = 4$ mm; $I_w = 120 - 130$ A; $U_a = 26 - 28$ V. Deposition was performed on 10Kh18N9T steel plates in two layers with forced cooling of the sample reverse side. Three to five samples of each composition were tested.

Electrode rods were produced by the hot extrusion method. In order to increase the yttrium transition coefficient at the metallurgical processing stage, the latter was deposited on the pouring ladle bottom only after preliminary deoxidation of the metal by aluminium, so that its assimilation by the

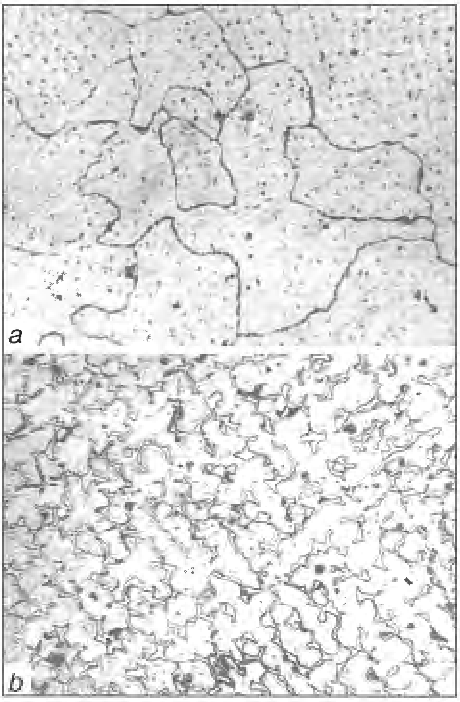

Structure of chromium-nickel deposited metal of 10Kh25N18M5 (*a*) and 10Kh25N18M5U (*b*) type (×200) (reduced by 3/5)

Dependence of cavitation-corrosion losses in deposited metal on the aggressive liquid kind and concentration

Deposited metal	*In-depth corrosion characteristic, mm/year*	*Weight loss in the testing medium after 10 h, g*		
		Process water	*Sulphuric acid concentration, wt.%*	
			92	*98*
10Kh18N9T (standard)	162.10	0.680	1.95	1.21
10Kh25N30G10M6D6T	98.50	0.350	1.49	0.72
08Kh12N8MTYu	59.70	0.310	1.42	0.72
10Kh18N25M6	48.05	0.470	1.30	0.62
10Kh23N28M3D3T	34.00	0.230	1.30	0.61
10Kh25N18M5	19.70	0.290	0.55	0.38
10Kh25N18M5U	0.33	0.028	0.48	0.11

steel was 70 to 80 %. Therefore, deposited metal alloying, also with yttrium, was performed through the rods with minimal losses.

Electrode coating (26 to 36 % marble, 18 to 22 % fluorspar, 38 to 40 % rutile, 8 to 12 % ferromanganese) was applied onto the rod by the dipping method. Rutile presence in the coating lowered the surface tension value, improved the weld formation and the slag crust separation. Ferromanganese addition improved the weld pool deoxidation, whereas the ratio of $CaCO_3$:CaF_2 = 1.5:1.0 was selected to ensure a higher coefficient of chromium and molybdenum assimilation with a low coefficient of silicon transfer.

According to the derived data (Table), cavitation input into the sample fracture is 6 to 34 %, while the influence of the corrosion factor is much greater — 66 to 94 %. With reduction of the sulphuric acid concentration, the deposited metal losses increase by more than 2 times.

It is known that the physical-chemical properties inherent to individual alloying elements, are also transferred to the alloy to a certain degree. So, the alloy fracture resistance is increased with the increase of chromium content in it [3, 7], this being confirmed by the testing results (see Table).

Presence of up to 13 % chromium in the composition, promotes the formation on the metal surface of a passive layer of oxides, practically insoluble in corrosive media.

In practical work, molybdenum, vanadium and niobium are added to the alloys, which strengthen the steel both at the expense of distortion of the crystallographic lattice of α-solid solution (08Kh12N8MTYu), and formation of dispersed strengthening phases, namely carbides and carbonitrides [8].

Addition of about 25% nickel to two-component Fe–Cr alloys also promotes a significant increase in their corrosion resistance [2].

It is rational to use such systems as Cr–Ni–Mo, Cr–Ni–N–Mo, Cr–Ni–N–V for service under the conditions of cavitation-corrosion wear [9, 10].

Titanium and aluminium in steel have a strong ferritizing action. So, addition of 0.4 to 0.5 % Ti or Al to the steel leads to formation of 20 % ferrite, thus lowering the strength properties of the materials [11].

The corrosion resistance of these steels is essentially enhanced with the increase of nickel content in chromium-nickel steels and their additional alloying with molybdenum and copper [2]. So, in 10Kh23N28M3D3T steel the in-depth corrosion characteristic is almost 5 times lower than that of the standard (see Table).

Samples made of 10Kh25N18M5 alloy turned out to be the most resistant to corrosion, this being, probably, due to the degree of the material alloying with chromium. Higher resistance of 08Kh12N8MTYu alloy, unlike 10Kh25N30G10M6D6T alloy, is attributable to the fact that addition of aluminium, nickel and molybdenum to the alloy provides the strength properties which are due to the dispersion-strengthening effect in ageing. In addition to that, $Ni_3(Al)$ intermetallics and a finely-dispersed R-phase of $(FeCo)_{15}Cr_{18}Mo_{10}$ composition uniformly precipitating on the defects of crystalline structure of martensite, are formed.

Decrease of 10Kh25N30G10M6D6T alloy corrosion resistance is related to addition of manganese to this alloy, which lowers the degree of the alloy passivity [3].

Additional alloying of 10Kh25N18M5 alloy with yttrium leads to a higher cavitation-corrosion resistance, this being due not only to lowering of steel contamination with non-metallic inclusions [12], but also to reduction of surface tension and critical nucleus size, increase of the number of solidification centers and structure refinement (Figure).

The deposited metal with the highest resistance values has the following composition (%): Cr — 24.8; Ni — 17.7; Mo — 4.5; Mn — 2.2; Si — 0.47; C — 0.07; S — 0.012; P — 0.014; N — 0.06; Y — 0.02.

The high cavitation-erosion resistance of Cr–Ni–Mo system alloys is largely due to addition of REM, including yttrium, into their composition, they essentially lowering the deposited layer contamination with non-metallic inclusions and promoting the refinement of the structure.

CONCLUSIONS

1. The corrosion factor has the principal role in the process of cavitation-corrosion fracture of materials in an aggressive medium.

2. The highest cavitation-corrosion resistance is found in Y-modified Cr–Ni–Mo system alloy at the expense of an essential reduction of the deposited metal contamination with non-metallic inclusions and structure refinement.

REFERENCES

1. Razikov, M.I., Efimenko, S.A., Fomenko, V.D. *et al.* (1972) Causes for intensive wear of the cones and blades of the rotor and covers of the chlorine compressor casing. *Tsvetnaya Metallurgia*, **19**, 38.
2. (1970) *Corrosion and protection of chemical apparatuses*. Ed. by A.M. Sukhotin, V.S. Zotikov. Leningrad: Khimia.
3. Tomashov, N.D., Chernova, G.P. (1973) *Corrosion and corrosion-resistant alloys*. Moscow: Metallurgia.
4. Fomenko, V.D., Nasekan, A.F., Rudychev, A.S. *et al.* (1979) Materials for surfacing the components of equipment operating in sulphuric acid production. *Tsvetnaya Metallurgia*, **11**, 37 – 38.
5. Fomenko, V.D., Shakiro, G.F., Rudychev, A.S. *et al.* *Unit for material testing for cavitation-erosion resistance*. USSR author's certificate **563605**, Int. Cl. G 01 N 17/00. Publ. 30.06.77.
6. (1990) *GOST 6032–89*. Corrosion-resistant steels and alloys. Methods of intercrystalline corrosion testing. Moscow: Izd. Standartov.
7. Kakhovsky, N.I. (1968) *Welding of stainless steels*. Kyiv: Tekhnika.
8. Alekseenko, M.F. (1962) *Structure and properties of high-temperature structural and stainless steels*. Moscow: Oborongiz.
9. Perkas, M.D., Kardonsky, V.M. (1970) *High-strength maraging steels*. Moscow: Metallurgia.
10. Lanskaya, K.A. (1976) *High-chromium high-temperature steels*. Moscow: Metallurgia.
11. Pinkovsky, I.V. (1980) *Investigation of cavitation wear and development of sparsely-alloyed cavitation-resistant materials*. Diss. of Cand. of Sci. (Eng.). Zaporozhje.
12. Shulte, Yu.A., Volchok, I.P., Tsarev, A.V. (1973) Investigation and introduction of a technology of production of steels and alloys with additives of yttrium, and other REM for parts of mining equipment. Zaporozhje: Zaporozh. Metallurg. Inst.

FEATURES OF WELD AND HAZ FORMATION IN GAS-SHIELDED PULSED TWIN-ARC WELDING IN HIGH-STRENGTH LOW-ALLOYED STEELS

N.M. VOROPAY and **P.P. PROTSENKO**
The E.O. Paton Electric Welding Institute, NASU, Kyiv, Ukraine

ABSTRACT

The process of pulsed twin-arc welding is characterized by a separate feed of current pulses to electrically isolated consumable electrodes, the arcs of which form the common weld pool. Studies of the effect of parameters of twin-arc welding on the penetrating power of the arc, weld formation, sizes of the HAZ, structure and properties of welded joints in high-strength low-alloyed steels with improved thermal characteristics are described.

Key words: *twin-arc welding, current pulses, feed mechanism, power source, metal penetration, weld formation, thermal cycle, macrosections*

The technological capabilities of mechanized arc welding are greatly expanded in application of twin-arc processes [1 – 3]. The idea of using twin electrodes to increase the efficiency of arc welding was first put forward by B.E. Paton already in 1947 [4]. Twin-wire submerged-arc welding has been making steady progress since that time as can be seen from publications [5 – 8]. Multi-wire submerged-arc welding process became accepted in industry mostly in making longitudinal welds on large-diameter pipes, thus allowing a 2 to 3 times increase of welding speed and an essential improvement of welded joint quality.

Attempts have also been made to ensure the stability of twin-arc CO_2 welding process [9]. The power to the arcs was supplied from one power source with a common current supply to both electrodes. This welding process did not become widely accepted, except for performance of technological welds in pipe welding, because of a greater metal spatter due to electromagnetic interaction of closely located arcs.

Over the recent years, gas-shielded consumable-electrode multi-arc welding has attracted interest again in connection with development of easily controlled transistorized and thyristorized power sources and computerized systems of mode parameters adjustment [10 – 15]. The equipment mentioned in these papers almost two times increases the speed of welding aluminium alloys and alloyed steels 2 to 3 mm thick. PWI studied some aspects of the combined consumable- and nonconsumable-electrode twin-arc welding which consists in separate feeding of current pulses to each electrode [16].

The information in [10 – 16] mostly is of promotional nature. There are no data on the essence of twin-arc welding processes, optimal mode parameters and their influence on the arc penetrability, weld formation, structure and properties of welded joints.

This paper is a study of the features and technological capabilities of gas-shielded consumable-electrode pulsed twin-arc welding process for the case of heat-treated high-strength low-alloyed steels.

In view of a great diversity of multi-arc welding processes, pulsed twin-arc welding was selected for study. The process, essentially, consists of the following. Pulses (isolated or in packs) of current of an adjustable amplitude, duration and frequency, are fed to electrically insulated from each other consumable electrodes *1* and *2* (Figure 1), which are, as a rule, arranged along the weld axis. Under the impact of these pulses, arcs forming a common weld pool are also separately and alternatively excited between each of electrodes *1* and *2* and base metal *3*. Electrode wires (of the same or different composition and diameter) are fed separately by mechanisms *4* and *5*. Current pulses to the arcs are supplied from two sources *6* and *7* through synchronization module *8*. Shielding gas (Ar, CO_2, Ar + 25 % CO_2) is supplied through common oval nozzle *9*.

An experimental set up incorporating an all-purpose OI-126 power source has been developed for gas-shielded consumable-electrode pulsed twin-arc welding. The power source consists of welding transformer TDFZh-1002, thyristor power unit, control module, panels for switching the operational modes and current pulse distribution. Both arcs are excited by the arc initiator module consisting of two step-up transformers. As a result, pulsed voltage of 3 to 4 kV of 200 kHz frequency, maintaining a stable arcing in welding, is supplied through parallel circuits of the oscillator to arc gaps between the electrodes and workpiece. Electric circuit of OI-126 power source allows performing a separate feed of same and different polarity current pulses to both electrodes by a preset program, a smooth increase of welding current at the process start and its decrease in crater welding up.

The specification of such a power source envisages adjustment of the current pulse amplitude between 150 and 1000 A in the range of current pulse time and pause repetition rates of 0.02 to 2.00 s and 5 to 50 Hz pulse feed frequency. Variation of these parameters and combinations of isolated pulses with several DC and AC pulses using OI-126 source produces different variants of twin-arc processes. Separate feed of 1.2 to 2.0 mm electrode wires is performed with drives used in series-produced semi-automatic welding machines. A specialized twin-wire torch has a common water-cooled case which incorporates two insulated from each other guides for wire feed and current supply. The electrode spacing is adjustable in the range of 2 to 10 mm by replacing the washers and changing the electrode stick-out.

Preliminary technological testing of the developed equipment has confirmed the high stability of both arcs running in a rather broad range of welding modes. Use of a separate power supply to the arcs in pulsed twin-arc welding permitted complete elimination of their electromagnetic interaction even with a small electrode spacing. It should be noted that in pulsed twin-arc welding the number of process parameters is greater than in the regular single-arc welding. Besides the diameters and feed rates of electrode wires, as well as the welding current and arc voltages, the amplitude, time and repetition rate of the current pulses fed to each electrode become extremely important with the process under consideration.

Let us analyze the features of base metal penetration in consumable-electrode pulsed twin-arc welding with electrodes located at a certain distance C from each other. For this purpose let us assume the following designations: I_{a1} and I_{a2} are the amplitudes of current pulses on electrodes *1* and *2*, with respective current pulse times τ_1 and τ_2. Then, the period of the cycle of current pulse variation $t = \tau_1 + \tau_2$, current pulse repetition rate $f_p = 1/t$, while the rigidity of the mode $G = \tau_1/\tau_2$, by analogy with the traditional pulsed-arc welding.

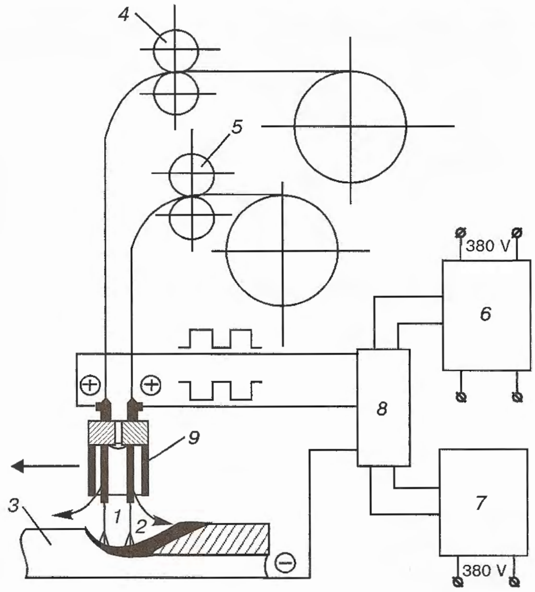

Figure 1. Schematic of the process of twin-arc welding with separate feed of current pulses (for designations see the text)

With the steady welding process, during the time of the current pulse fed to the first electrode in the welding direction, heat $Q_1 = q_1\tau_1$ is applied to the base and the electrode metal, leading to the metal melting to form the weld pool. Under the impact of powerful current pulses and appropriate arc pressure proportional to the square of current, the molten metal is intensively ousted from under the first arc base to the weld pool tail part. This creates a gradient of molten metal levels in the head and tail parts of the melting space. Just a thin film of the melt contained by surface tension forces, remains on the crater surface. During the current pulse fed to the second electrode, a new portion of heat $Q_2 = q_2\tau_2$ is applied to the base and the electrode metals, thus increasing the penetration depth. The arc active spot is displaced by a value equal to the electrode spacing. The second arc while promoting further ousting of the metal from the pool head part into the tail part, maintains the equilibrium between gas-dynamic pressures of both arcs and hydrostatic pressure of molten metal in the solidification zone. Power supply to both arcs with periodically fed current pulses, provides a minimal thickness of the interlayer of liquid metal under the arcs and reduces the heat losses for metal overheating and evaporation in the active spots.

The total amount of heat during the time of the cycle of change of current pulses of both arcs can be given as:

$$Q_{tot} = Q_1 + Q_2 = q_1\tau_1 + q_2\tau_2. \quad (1)$$

Then, the amount of heat per a unit of weld length l is equal to

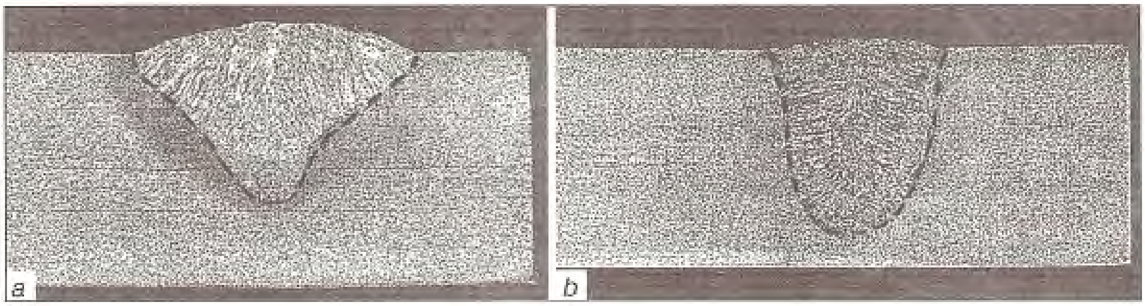

Figure 2. Macrosections of deposited metal in single-arc (*a*) and pulsed twin-arc (*b*) welding (09G2S steel, $\delta = 12$ mm; for mode parameters see the text)

$$Q_{tot} = \frac{q_1\tau_1 + q_2\tau_2}{v_w(\tau_1 + \tau_2)}. \qquad (2)$$

If the power of the arc of the first electrode is much smaller than the power of the arc of the second electrode ($q_1/q_2 \to 0$), relationship (2) will correspond to the variant of one periodically running DC pulsed arc. Considering that $q_1 = \eta_1 I_{a1} U_1$ and $q_2 = \eta_2 I_{a2} U_2$, let us write expression (2) in the following form:

$$Q_{tot} = \frac{\eta_1 I_{a1} U_1 \tau_1 + \eta_2 I_{a2} U_2 \tau_2}{v_w(\tau_1 + \tau_2)}. \qquad (3)$$

Assuming that $U_1 = U_2 = U_{arc}$ and $\eta_1 = \eta_2 = \eta_{arc}$, equation (3) takes the following form:

$$Q_{tot} = \frac{\eta_{arc} U_{arc}(I_{a1}\tau_1 + I_{a2}\tau_2)}{v_w(\tau_1 + \tau_2)}. \qquad (4)$$

Let us consider some examples of investigation of the technological capability of consumable-electrode pulsed twin-arc welding process. The main part of the experiments were performed on heat-treated low-alloyed steels of 09G2S (GOST 19282–73) and 09G2SYuCh (TU 14-227-280–83) type.

Case 1. Beads were deposited by single-arc and pulsed twin-arc welding on 10×300×600 mm plates of 09G2S steel with grooves 6 mm deep and 55° groove angle. Sv-08KhG2SNMT wire of 2 mm diameter was used in both cases. The rationality of its application for welding thermostrengthened low-alloyed steels is substantiated in [17]. The shielding gas (CO_2) flow rate varied between 16 and 30 l/min, depending on the welding modes. The current pulse parameters in twin-arc welding were $I_{a1} = I_{a2} = 600$ A, $U_{arc1} = U_{arc2} = 40$ V, $\tau_1 = \tau_2 = 0.1$ s, $G = 1$.

Five reverse polarity current pulses of 0.02 s duration were actually fed from OI-126 source to each electrode during 0.1 s. Electrode spacing in the tests was kept constant and equal to 6 mm. In single-arc welding $I_w = 600$ A and $U_{arc} = 40$ V were set. During the experiments just one parameter, namely welding speed, v_w, was changed in the range from 10 to 60 m/h. The shape of the produced bead macrosections was characterized by penetration depth h and weld width b.

Figure 2 gives the typical shapes of the beads made under comparable conditions of single-arc and pulsed twin-arc welding at 40 m/h speed. In pulsed twin-arc welding process, the penetration depth as a rule is by 1.2 to 1.3 times greater than in single-arc process with all the parameters studied (Figure 3, *a*). The weld width is noticeably reduced in this case. The tempo of h change with welding speed variation is nonuniform for both processes, namely in transition from v_w of 10 – 20 m/h to v_w of 40 m/h, h is somewhat increased, and then decreases again with further increase of v_w. This can be explained as follows. At relatively small welding speeds, a rather thick interlayer of molten metal is found under the arc column, hindering the arc heat transfer to the unmolten base metal. Increase of welding speed up to 40 m/h leads to the arc being deflected backward, ousting of the molten metal into the weld pool tail part and thinning of the molten interlayer. This results in an improvement of the conditions of heat transfer from the arc to the base metal, and increased penetration depth. In pulsed twin-arc welding the arc pressure on the liquid interlayer is much greater due to the large amplitudes of current pulses, thus leading to deeper penetration and narrower weld. In this case, uniform weld formation with fine-rippled surface and smooth transitions to the base metal is achieved in the optimal welding modes.

Case 2. Unlike case 1 $v_w = 60$ m/h was set, while the current pulse amplitude was varied in the range of 300 to 600 A. It was found (Figure 3, *b*) that with the increase of current from 400 to 600 A, the penetration depth increases practically linearly, both in the case of pulsed twin-arc and single-arc welding. With the optimal values of arc voltage, the weld width changes in a similar fashion. The experimental results demonstrated that the use of electrode wire of 1.6 mm instead of 2.0 mm diameter, in both cases increases the base metal penetration depth by not less than 1.5 times. On the other hand, application of 3 mm wire reduces h by almost 2 times with a slight widening

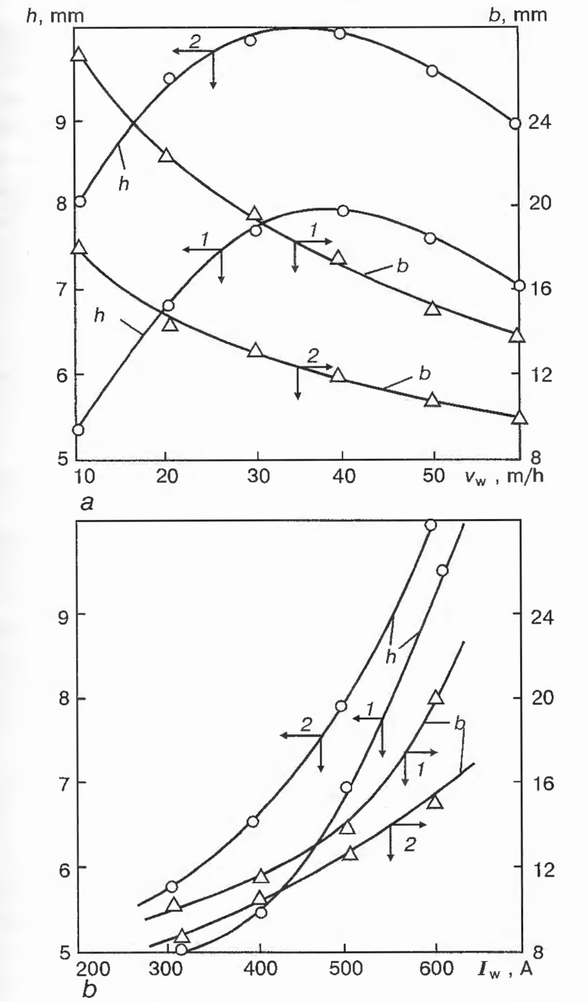

Figure 3. Influence of welding speed (a) and welding current (b) on weld dimensions in single-arc (*1*) and pulsed twin-arc (*2*) welding

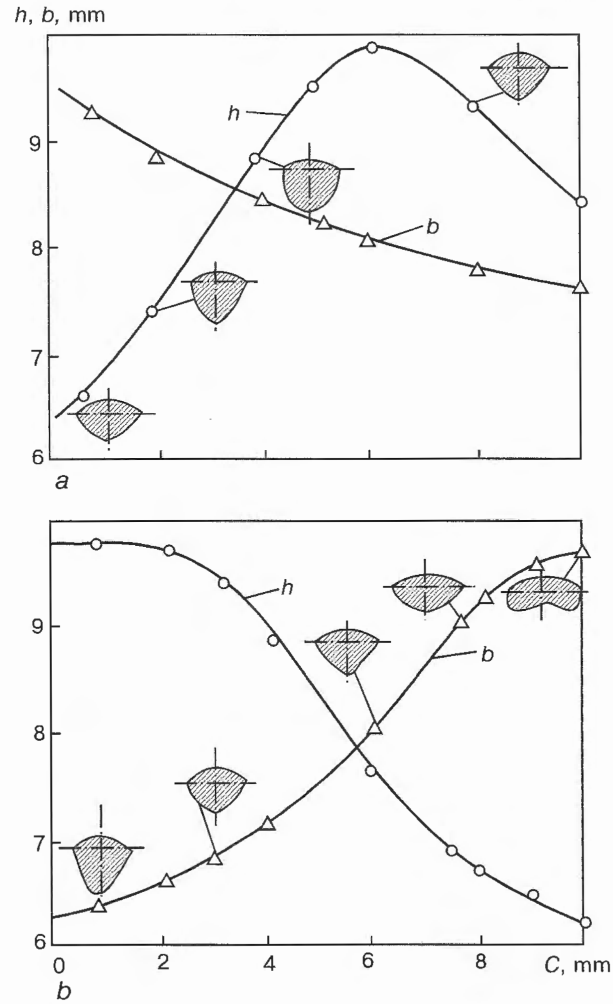

Figure 4. Influence of electrode spacing C on penetration depth h and width b with the longitudinal (a) and transverse (b) arrangement of the electrodes

of the weld. It is also found that the shape of the welds made by the processes being compared, largely depends on arc voltage. Also, as demonstrated by the results of the conducted experiments, the arc voltage primarily influences the weld width and to a smaller degree the penetration depth.

Case 3. Electrode spacing is the twin-arc welding parameter which is little studied. Therefore, the beads were deposited at $I_{a1} = I_{a2} = 600$ A, $U_{arc1} = U_{arc2} = 40$ V, $\tau_1 = \tau_2 = 0.1$ s, $G = 1$, $v_w = 60$ m/h, varying electrode spacing C in the range of 2 to 10 mm. The appropriate experimental data for the longitudinal and transverse arrangement of the arcs, are given in Figure 4. With the longitudinal arrangement of the electrodes (Figure 4, a), the metal penetration depth h increases with the increase of C parameter from 1 to 6 mm, and with further increase of C, it decreases to 8 to 10 mm. The situation is totally different with the transverse arrangement of the electrodes (Figure 4, b). With C parameter rise, h noticeably decreases, while b increases.

Case 4. Butt welds on 10×300×600 mm plates of 09G2SYuCh steel were welded with the longitudinal arrangement of electrodes and V-shaped edge preparation. During welding of the first weld which has the function of a backing weld, current pulses $I_{a1} = 200$ A ($U_{arc1} = 24$ V; $\tau_1 = 1$ s) were fed to the front electrode of 1.2 mm diameter. For the second electrode of 2 mm diameter, these parameters corresponded to $I_{a2} = 500$ A, $U_{arc2} = 36$ V, $\tau_2 = 1$ s.

A specific nature of weld formation during welding in the above modes was found. When weak current pulses were fed to the first electrode, a uniform melting of lower edges of the joint with a V-shaped groove and solidification of the weld root metal took place. A relatively powerful current pulse fed to the second electrode, partially melts the solidified bead and additionally fills the V-shaped groove to the specified depth. This results

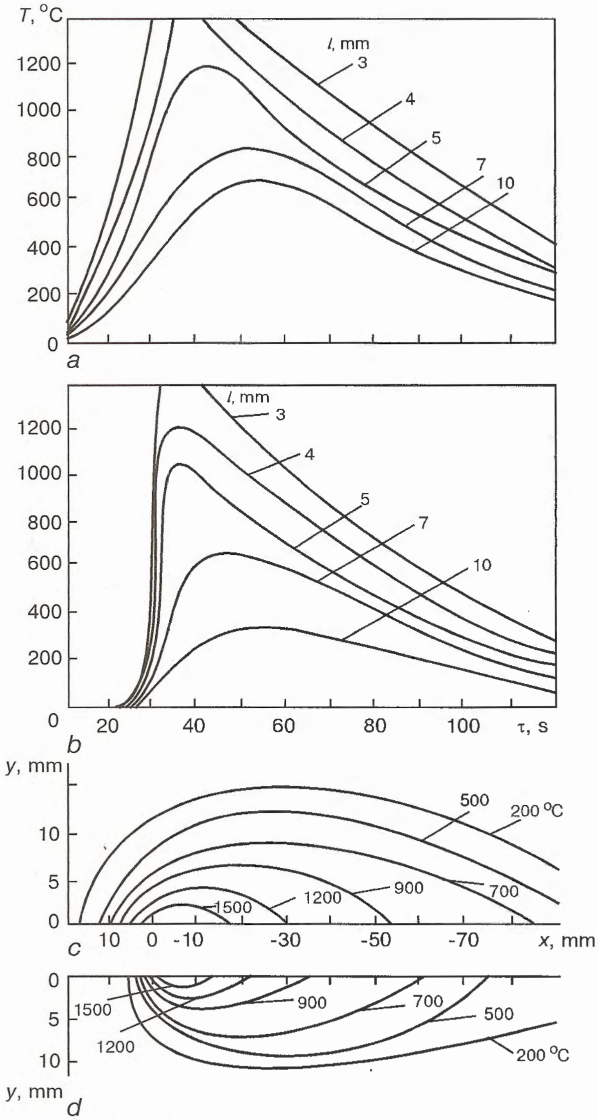

Figure 5. The thermal cycles and isotherms of base metal heating (09G2S steel, δ = 8 mm) in single- (*a*, *c*) and twin-arc (*b*, *d*) CO_2 welding (for mode parameters see the text)

in achievement of the required quality of weld formation without the application of technological backing. Further layers of the deposited metal can be applied in one pass by any technology, namely automatic submerged-arc welding or gas-shielded pulsed twin-arc welding with higher parameters.

It was also interesting to evaluate the temperature-time conditions in the HAZ of the welded joints produced by single- and twin-arc welding. Temperature recording in an oscillograph in points located at a certain distance from the weld axis (3; 4; 5; 7; 10 mm) was performed for this purpose. N-102 mirror-galvanometer oscillograph with tungsten-rhenium thermocouples of 0.12 mm diameter was used fort his purpose. The depth of holes for the thermocouples was equal to approximately one third of the metal thickness, their diameter being 0.5 mm.

Figure 5 presents the thermal cycles and isotherms of base metal heating in single-arc and pulsed twin-arc welding in CO_2 of butt joints of thermostrengthened 09G2S steel (δ = 8 mm) with Sv-08KhG2SNMT wire of 2 mm diameter. To achieve complete penetration of the edges, the following welding modes were used in the experiments:

in single-arc process I_w = 600 A; U_{arc} = 38 V; v_w = 20 m/h; $Q_{sh.g}$ = 18 l/min; q/v_w = = 30535 J/cm;

in twin-arc process on each electrode I_a = = 600 A; U_{arc} = 38 V; $\tau_1 = \tau_2$ = 0.05 s; v_w = 36 m/h; $Q_{sh.g}$ = 24 l/min; q/v_w = 17100 J/cm.

It is found that in pulsed twin-arc welding, the rate of heating of individual sections of the HAZ, $w_{ih} = dT_i/d\tau_i$, is essentially higher than in single-arc welding (Figure 5). So, for instance, for a point with the thermocouple located near the fusion zone (at 3 mm distance from the weld axis), in single-arc welding w_{ih} = 60 °C/s, and in twin-arc welding w_{ih} > 1000 °C/s. In this case, the duration of the metal soaking in the high-temperature regions (600 to 1400 °C) in twin-arc welding is reduced by 1.5 to 3 times, and the maximal temperature of heating T_{max} for the points with thermocouples located at 5, 7 and 10 mm distance from the weld axis, drops by 150 to 300 °C. The rates of cooling of the HAZ metal w_{ic} are practically the same in the welding processes being compared. Near the fusion zone in the temperature range of 500 to 800 °C they are not more than 8 to 12 °C/s. This is attributable to the fact that in the high-temperature regions (> 800 °C) the coefficient of heat conductivity of iron decreases 3 to 4 times. The HAZ region heated up to the temperature above 800 °C in welding, prevents heat removal from the heat source into the base metal [18]. According to [19, 20] such cooling rates do not have any significant influence on impact toughness of welded joints of thermostrengthened 09G2S and 09G2SYuCh steels.

From the results of metallographic investigations and the derived heating isotherms, the width of the HAZ for the isotherm with T = 500 °C was 12 and 8 mm in single-arc and pulsed twin-arc welding, respectively. The width of the overheated region (coarse-grained zone) which is in the temperature range from 1200 °C up to the melting temperature, is not more than 0.6 mm in twin-arc welding, while in single-arc welding it is 1.5 to 2.0 mm. The difference in the dimensions of the appropriate zones where the coarse-grained austenite structure is usually formed, is also noticeable in the isotherms of the HAZ heating limited by temperatures of 900 to 1200 °C (normalizing zone). This is also true for the zones of incomplete recrystallization (700 to 900 °C) and ageing (500 to 700 °C).

Twin-arc welding of thermostrengthened low-alloyed steels provides the capability of formation of a favourable fine-grained structure of weld metal at the expense of the pulsed action of the arcs, increase of the rate of temperature rise, and shortening of the time of the weld and HAZ metal staying at elevated temperatures. In 09G2S steel welds, made by twin-arc welding, the amount of martensite, bainite and residual austenite is minimal (not more than 5 %). These are hardening structures uniformly distributed in the soft ferrite base, thus promoting the achievement of a high impact toughness of the weld metal in a broad temperature range. So, for instance, when CO_2 pulsed twin-arc welding with Sv-08KhG2SNMT wire is used, the impact toughness of the metal of the weld on thermostrengthened 09G2SYuCh steel at −70 °C reaches *KCV* 40 J/cm² (Figure 6). For the HAZ this value is even higher.

The developed method of pulsed twin-arc welding can find application in fabrication of critical metal structures of high-strength low-alloyed steels in such industries as chemical and transportation engineering, ship-building, in production of welded pipes, as well as in industrial construction.

The technological capabilities of pulsed twin-arc welding are far from being limited by the examples given here. The specific features of melting and transfer of the electrode metal under the conditions of separate feed of current pulses to each electrode could not be covered in view of the limited scope of the paper. Investigation of the effectiveness of this process in mechanized welding and surfacing of medium- and high-alloyed steels, non-ferrous metals and alloys is also of interest. In our opinion use of pulsed twin-arc welding can turn out to be effective for making welds in different positions in space. The algorithms of welding process control can be different, in particular they can be related to the welding speed and electrode wire feed rate.

CONCLUSIONS

1. The process of consumable-electrode pulsed twin-arc welding features an independent and alternative feeding of current pulses (of adjustable amplitude, duration and frequency) to the arcs, separate feed of electrode wires (of the same or different diameter and composition), arcs running in a common weld pool with a longitudinal or transverse arrangement of the electrodes.

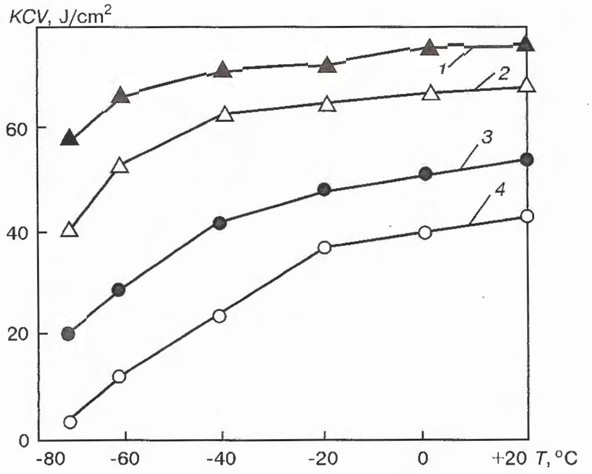

Figure 6. Impact toughness of the HAZ (*1, 3*) and weld metal (*2, 4*) on thermostrengthened 09G2SYuCh steel in single-arc (*3, 4*) and pulsed twin-arc (*1, 2*) welding (CO_2, Sv-08KhG2SNMT wire, 2 mm dia.)

2. Application of a longitudinal arrangement of the electrodes creates favourable conditions for intensive ousting of the liquid metal from the weld pool head part into the tail part, as well as for maintaining a stable equilibrium between the gas-dynamic pressures of both arcs and hydrostatic pressure of liquid metal in the solidification zone. This enhances the penetrability of the heat source and improves weld formation in welding with higher parameters.

3. The weld shape greatly depends both on the energy parameters of the process (amplitude, duration and frequency of current pulses of each arc, welding speed, heat input) and on the electrode spacing, as well as on their arrangement relative to the weld axis. The longitudinal arrangement of the electrodes leads to deeper penetration and weld narrowing. With the transverse arrangement of the electrodes, the results are opposite.

4. The following advantages of the considered welding process have been revealed compared to the traditional technologies:

complete elimination of electromagnetic interaction of the arcs forming a common weld pool;

increase of base metal penetration depth and weld narrowing;

two-times reduction of the heat input into the base metal and appropriate narrowing of the HAZ;

ability of a sound formation of welds without technological backing.

5. Gas-shielded pulsed twin-arc welding provides higher properties of ductility and cold resistance of welded joints of high-strength heat-treated low-alloyed steels due to formation of a fine-grained structure of the weld metal and HAZ.

REFERENCES

1. (1974) *Technology of electric fusion welding of metals and alloys*. Ed. by B.E. Paton. Moscow: Mashinostroyeniye.
2. Medovar, B.N. (1950) High-speed twin-arc automatic welding. *Avtogen. Delo*, **11**, 20 – 23.
3. (1953) *Automatic electric-arc welding*. Ed. by B.E. Paton. Kyiv-Moscow: Mashgiz.
4. Paton, B.E. (1947) *Welding heads and current supply to them*. Kyiv: AN Ukr.SSR.
5. Mandelberg, S.L., Lopata, V.E. (1962) On connection of welding transformers in high-speed twin-arc welding. *Avtomaticheskaya Svarka*, **10**, 20 – 23.
6. Paton, B.E., Mandelberg, S.L., Sidorenko, B.G. (1971) Some features of weld formation in higher-speed welding. *Ibid.*, **8**, 1 – 6.
7. Sidorenko, B.G., Mandelberg, S.L. (1988) Selection of the optimal number of electrodes in high-speed multi-arc welding. *Ibid.*, **2**, 53 – 55.
8. Mandelberg, S.L. (1965) High-speed multi-arc welding with transverse oscillations of the electrode. *Ibid.*, **2**, 8 – 13.
9. Fainberg, L.I., Rybakov, A.A., Mandelberg, S.L. (1975) CO_2 twin-arc welding at a higher speed. *Ibid.*, **2**, 35 – 38.
10. Hackl, H. (1997) TIME TWIN – Schneller MSG – Schweissen mit zwei Drahtelektroden. *Schweiss- und Prueftechnik*, **5**, 71 – 73.
11. (1998) New technological process of «Fronius» company. *Avtomaticheskaya Svarka*, **2**, 69 – 70.
12. Killing, R. (1997) Das MAG-Mehrdrahtschweissen. *Praktiker*, **2**, 243 – 245.
13. (1996) KUKA two-wire MAG welding system doubles welding speeds. *Ind. Robot*, **6**, 42.
14. Lassaline, E., Zajaczkowski, B., North, T. (1989) Narrow groove twin-wire GMAW of high-strength steel. *Welding J.*, **9**, 53 – 58.
15. (1996) MIG/MAG-Hochleistungsschweissen mit TANDEM Technik. *Schweiss- und Pueftechnik*, **9**, 150.
16. Voropay, N.M., Lesnykh, V.V., Mishenkov, V.A. (1994) Combined process of non-consumable- and consumable-electrode arc welding and surfacing. *Avtomaticheskaya Svarka*, **4**, 56 – 57.
17. Protsenko, P.P., Privalov, N.T. (2000) Technological properties of Sv-08KhG2SNMT electrode wire in gas-shielded welding of high-strength low-alloyed steels. *Ibid.*, **6**, 18 – 23.
18. Dudko, D.A., Savitsky, A.M., Savitsky, M.M. *et al.* (1998) Features of thermal processes in welding with thermal cycling. *Ibid.*, **4**, 8 – 12.
19. Demchenko, Yu.V., Asnis, A.E., Ivashchenko, G.A. (1983) Influence of the thermal cycle of welding on the properties of the HAZ of 16G2AF and 09G2S steel joints. *Ibid.*, **11**, 70 – 71.
20. Egorova, S.V., Sterenbogen, Yu.A., Yurchishin, A.V. *et al.* (1987) Weldability of low-alloyed steels strengthened by normalizing from an intercritical temperature range. *Ibid.*, **2**, 20 – 23, 31.

FORMATION OF AEROSOLS IN CO_2 MODULATED-CURRENT WELDING

O.G. LEVCHENKO
The E.O.Paton Electric Welding Institute, NASU, Kyiv, Ukraine

ABSTRACT

It is shown that the method of a modulated-current welding makes it possible to decrease the intensity of evolution of a hard constituent of welding aerosols (HCWA) and content of manganese in it as compared with welding at a continuous current. At the modulated-current welding these characteristics are determined not only by a mean power of the arc, but also by a frequency of impulses.

Key words: *welding, modulated current, welding aerosols, intensity of HCWA evolution*

One of the ways of improving the hygienic characteristics of the arc welding processes is the application of special pulsed-current sources. This makes it possible to decrease the excessive energy of the arc, that causes the intensive evaporation of melting materials, and to control also the electrode metal transfer and to minimize its spattering [1]. The modulated-current welding [2], can improve the hygienic characteristics of this process as compared with a continuous-current welding using a periodic changing of the welding current level [3].

The present work was aimed at the investigation of hygienic characteristics of the above-mentioned welding process, and also at the defining of possibilities of decreasing the HCWA evolutions by a selection of an optimum condition of the mechanized CO_2 welding. For this purpose, the dependencies of characteristics of levels of HCWA evolutions (intensity of aerosol formation v_a, specific aerosol evolution G_a) and content of manganese [Mn] in it on the parameters of the welding condition at a modulated current (current I_i and voltage U_i of the impulse, impulse duration τ_i) were investigated. Welding in CO_2 was performed using a semi-automatic machine A-547Um with a low-frequency modulator SU-256U3. Electrode wire Sv-08G2S of 1.2 mm diameter and parent metal VSt.3 were used. The conditions of welding with a modulated current of 50 Hz frequency are given in Table. In welding at direct current of a reversed polarity (for comparison) the welding current was varied within 150 – 255 A at 26 V arc voltage. The level of evolutions of HCWA and content of manganese in it were determined using the generally-accepted methodologies [4, 5].

As a result, the following values were obtained:

at DC welding (I_w = 150 A, U_{arc} = 26 V) v_a = = 0.51 g/min, G_a = 15.8 g/kg, [Mn] = 8.9 mass %;

at modulated-current welding (I_i =220 A, I_p = = 100 A, U_i = 26 V, U_p = 15 V, $\tau_i = \tau_p$ = 0.5 s) v_a = 0.48 g/min, G_a = 12.4 g/kg, [Mn] = = 5.7 mass %.

Thus, in welding at conditions with an approximately equal average current the values of level of evolution of HCWA and manganese content in it is higher for the direct current than in case of using the modulated current.

During periodic reduction of the strength of the modulated current in pauses (at equal average values of impulse current and direct current) the modulated-current welding provides the lower intensity of the HCWA formation, except the case of DC welding at I_w = 255 A (Figure 1, *a*). It is clear that the decrease in a total arc power at the expense of pauses reduces the excess of energy forming in welding with a continuous current and used for metal overheating and evaporation. The manganese content in HCWA composition is lower than in DC welding when the modulated current is used at different conditions (Figure 1, *b*).

The level of HCWA evolutions in a shielded-gas DC welding is determined not only by the arc power but also by a mode of the electrode metal transfer.

Parameters of modulated-current welding conditions

I_i, A	I_p, A	U_i, V	U_p, V	τ_i, s	τ_p, s
150	100	24	15	0.1	0.1
200	100	24	15	0.1	0.1
260	120	24	15	0.1	0.1
150	100	26	15	0.5	0.5
200	100	26	15	0.5	0.5
250	120	26	15	0.5	0.5
150	100	30	15	1.0	1.0
220	100	30	15	1.0	1.0
250	120	30	15	1.0	1.0

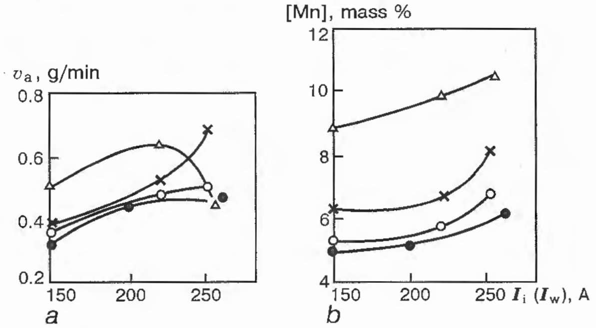

Figure 1. Dependence of intensity of formation of HCWA (*a*) and manganese content in it (*b*) on welding current in welding at direct current (Δ) and modulated current with an equal duration of impulses and pauses (● — 1 s, ○ – 0.5 s, × — 0.1 s)

Moreover, the dependence of the intensity of HCWA evolution on the welding current has an extreme nature: there is a maximum which corresponds to the highest spattering of the electrode metal, and a minimum, which corresponds to a fine-drop transfer without short-circuits [6]. At DC welding the minimum levels of HCWA evolutions are observed at increased welding current (225 A) (Figure 1, *a*). In modulated-current welding the increase in an impulse current increases the intensity of the HCWA formation (Figure 2, *a*). Here, the electrode metal is transferred with forced short-circuits, and the growth in an impulse current leads to the intensification of explosions of metal bridge in the arc gap and, consequently, to the large ejection of metal vapours beyond the arc. The increase in an impulse voltage also leads to the growth of the HCWA evolution (Figure 2, *b*). With increase in duration of similar impulses and pauses the intensity of the HCWA evolution is decreased (Figure 2, *c*).

The investigations of influence of parameters of the modulated-current welding conditions on the content of manganese in HCWA (Figure 3) show that it is possible to reduce the manganese evolution within the wide ranges, for example, from 11.3 to 4.4 % , i.e. by 2.5 times, by selection of the modulation conditions. Thus, in welding at low voltage of impulse (24 V) with a current increase the manganese content in HCWA is increased negligibly, i.e. from 4.4 to 6.1 %, and at high impulse voltage (30 V) — from 7.5 to 11.3 % (Figure 3, *a, b*). The growth in arc voltage leads to the increase in its length and, consequently, in time of transfer and evaporation of drops of the electrode metal. As in welding, in particular with a modulated current, the conditions of evaporation in the arc gap differ significantly from the equilibrium evaporation, then the content of easily-evaporating manganese in aerosol will also be determined mainly by the peculiarities of evaporation during the arc process [7]. These conditions are determined by an arc length, presence of short-circuits and their frequency, size of drops of the electrode metal, and also by the time of their existence and evaporation. In short-circuit welding the metal evaporation has an explosion mode. The content of an easily-evaporating manganese in a pair has no time during a short time of explosion to be increased to the value that corresponds to a partial pressure. With increase of the arc voltage the arc length, drop size, time of its evaporation are increased, and the frequency of short circuits of the arc gap is reduced. This promotes the approach of the evaporation conditions to equilibrium conditions at which the content of manganese in aerosol is greatly increased (tending to a calculated content) [7].

Hence, the conclusion can be made that the application of the modulated-current welding makes it possible to reduce the manganese content in HCWA composition by using the process with forced short circuits, increase in frequency of short circuits, decrease in arc length and drop size.

The growth in duration of impulses leads to the decrease in manganese content in HCWA (Figure 3, *c*), though the mean arc power is not changed. Probably, this is stipulated by the effect of frequency of impulses on the frequency of short

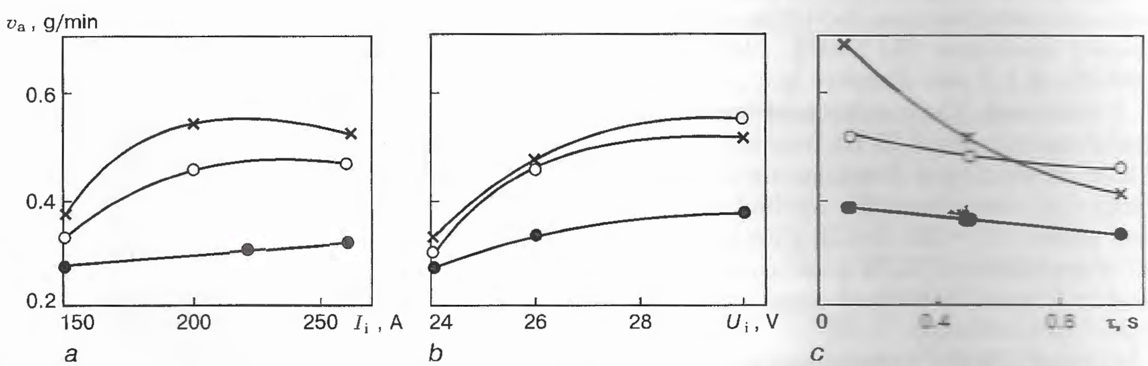

Figure 2. Dependence of intensity of formation of HCWA: *a* — on strength of impulse current (at impulse voltages: ● — 24, ○ — 26, × — 30 V); *b* — on impulse voltage; *c* — on duration of equal impulses (*b, c* — at current of impulses: ● — 150, ○ — 200 – 220, × — 260 – 270 A)

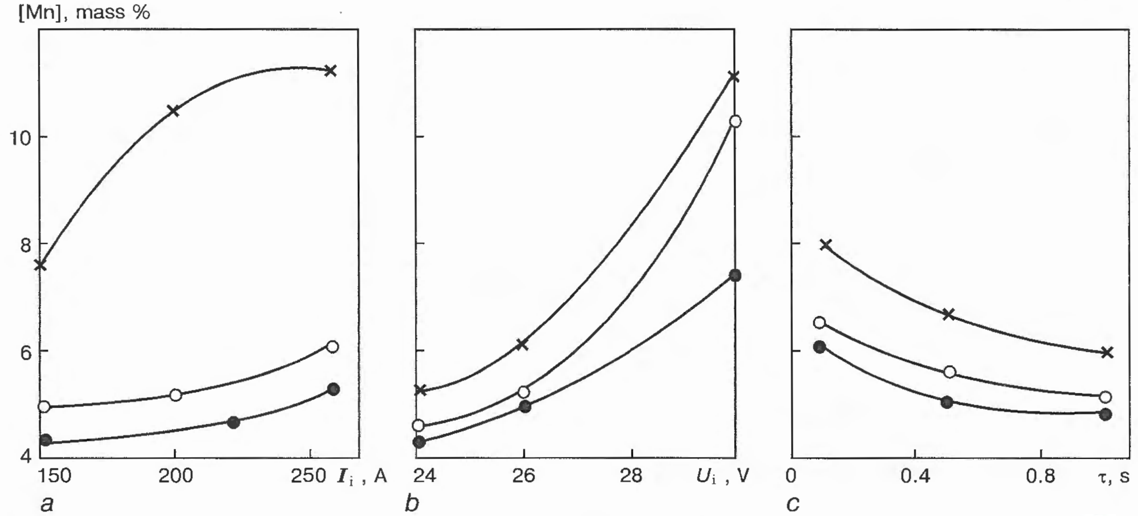

Figure 3. Dependence of content of manganese in HCWA: *a* — on strength of impulse current (at impulses voltages: ● — 24, ○ — 26, × — 30 V); *b* — on impulse voltage; *c* — on duration of equal impulses (*b*, *c* — at currents of impulses: ● — 150, ○ — 200 – 220; × — 260 – 270 A)

circuits. The modulated current impulses promote the drop detachment from the electrode, but the frequency of the imposed impulses is not always coincided with frequency of the drop transfer from the electrode to the pool. With the increase in the frequency of impulses the content of manganese in HCWA is increased. In welding at a continuous current it is maximum (Figure 1, *b*). This testifies that with increase in the frequency of impulses and also in transition to welding at a continuous current the effect of impulses on the frequency of transfer of the electrode metal drops is reduced and the evaporation approaches the equilibrium. Therefore, the manganese content in HCWA can be reduced by control of the frequency of impulses of the modulated current, thus promoting the better detachment of drop from the electrode and increase of frequency of their transfer to the pool.

CONCLUSIONS

1. Method of a modulated-current welding makes it possible to reduce the intensity of evolution of HCWA and content of manganese in it as compared with DC welding. Decrease in total arc power at the expense of pauses reduces the excess of energy, observed in a continuous welding and used for overheating and evaporation of the materials melted.

2. At the mentioned method of welding the intensity of evolution of HCWA and manganese content in it is determined not only by the average arc power but also by a frequency of impulses. These characteristics are reduced with a decrease in current and voltage of impulses, and also with increase of their duration.

3. Decrease in manganese content in aerosol in modulated-current welding is attained at the expense of an equilibrium evaporation of metal due to a presence of forced short circuits of the arc gap, caused by an impulse modulation of the current.

REFERENCES

1. Levchenko, O.G. (1998) Technological methods of reducing the level of formation of welding aerosol. Review. *Svarochnoye Proizvodstvo*, **3**, 32 – 38.
2. Mirlin, G.A., Ageev, V.I., Barashev, V.V. (1980) Arc welding with a modulated current. *Ibid.*, **8**, 16 – 17.
3. Golovatyuk, A.P., Sidoruk, V.S., Levchenko, O.G. *et al.* (1985) Intensity of formation of aerosols in manual welding with a modulated current. *Avtomaticheskaya Svarka*, **2**, 39 – 40.
4. (1980) *MR No.1924–78*. Hygienic assessment of welding consumables and methods of welding, surfacing and cutting of metals. Moscow: Minzdrav SSSR.
5. (1990) *MR No.4945–88*. Determination of harmful substances in welding aerosol (solid phase and gases). Moscow: Minzdrav SSSR.
6. Levchenko, O.G. (1986) Effect of composition of shielding gas and welding conditions of gross evolutions of welding aerosol. *Avtomaticheskaya Svarka*, **1**, 72 – 74.
7. Podgaetsky, V.V., Golovatyuk, A.P., Levchenko, O.G. (1989) About mechanism of formation of welding aerosol and prediction of its composition in CO_2 welding. *Ibid.*, **8**, 9 – 12.

STABILITY OF ARC PROCESS IN WIDE-LAYER SURFACING OF CYLINDER SURFACES

A.P. PAKHOLYUK[1] and **G.A. KIRILYUK**[2]
[1]Lviv State Agricultural University, Lviv, Ukraine
[2]The E.O.Paton Electric Welding Institute, NASU, Kyiv, Ukraine

ABSTRACT

Dependence of a stable melting of a self-shielding flux-cored wire for the conditions of a wide-layer surfacing on the condition parameters is established. A mathematical model is presented and a procedure of selection of parameters of this surfacing conditions is suggested.

Key words: *wide-layer surfacing, stability, electrode oscillations, curvilinear trajectory, radius*

The highly-efficient electric arc wide-layer surfacing with a self-shielding flux-cored wire is based on the oscillations of the electrode end transverse the vector of the surfacing speed at an amplitude equal to a half of the width B of the bead deposited. Here, the condition parameters should provide the weld pool equal to the width of the bead deposited. These parameters include a wire feed speed $v_{w.f}$, arc voltage U_a, surfacing speed v_s, mean rate of electrode oscillation v_o, its shifting from zenith e, electrode stickout L_e, radius of electrode oscillations R_o and rate of its displacement at extreme positions v (Figure 1).

The electrode oscillations can be performed along the straight or curvilinear trajectories. When surfacing the surfaces confined by flanges or other design elements (pins of crankshafts, rollers), a curvilenear trajectory is simplier, as it simplifies the surfacing of a fillet region. However, here the electrode deviation to the edge is accompanied by changing the value of the electrode stickout L'_e, elongation of the welding arc and, thus, by violation of conditionally stationary process of its burning. In surfacing with a flux-cored wire the change in voltage and current leads to non-uniform melting of a sheath and powdered core of the wire, and also changes the conditions of saturation of the molten metal with gases, thus leading to the porosity formation.

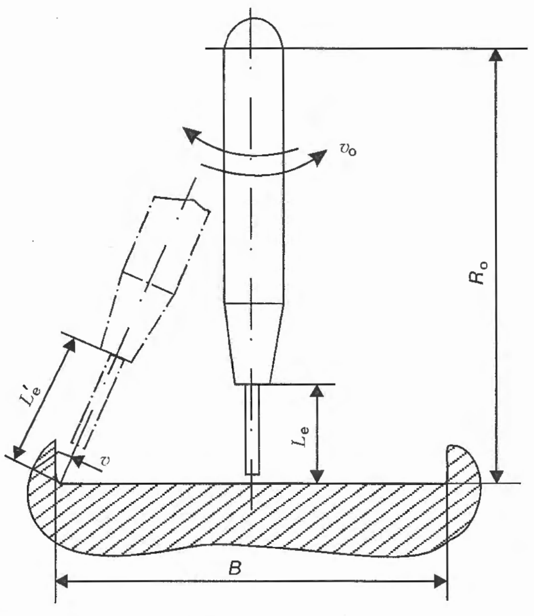

Figure 1. Scheme of electrode end oscillations

Therefore, during invesigation of the condition parameters of such surfacing and their selection in practice it is necessary to evaluate quantitatively the stability of the process depending on the condition parameters.

It was not possible to use the statistical evaluation of the process of the electrode melting [1] and assessment of the stability of arc burning by a mean rate of changing the conductivity in the arc gap for the processes with periodic short circuits [2], because the process of melting with a self-shielding wire occurs almost without short circuits.

The stability of the arc process is evaluated by a root-mean-square amplitude of current oscillations CV for a definite period by formula

$$CV = \left(\left(\sum_{i=1}^{k} a_{i\max}^2/k\right)^{0.5} - \left(\sum_{i=1}^{k} a_{i\min}^2/k\right)^{0.5}\right)/I_w,$$

where $a_{i\max}$, $a_{i\min}$ is the difference, respectively, between the minimum and maximum values of current in a separate period and its mean value in experiment, A; k is the number of periods; I_w is the mean value of current, A.

Taking into account the complex and non-linear effect of parameters studied on the stability of arc burning the calculated model was selected in the form of a polynomial of the second order. Experiments for evaluating parameters were performed according to a design of dimension $n = 8$ hartly which included a fractional replica 2, centers of hyperfaces and a center of the design, for the following ranges of the condition parameters: $v_{w.f} = 0.04 - 0.11$ m/s; $U_a = 23 - 29$ V; $v_s = 0.001 - 0.003$ m/s; $v_o = 0.02 - 0.09$ m/s; $e = 8 - 16$ mm; $R_o = 80 - 145$ mm; $L_e = 16 - 30$ mm. To make the experiments more convenient the ratio $m = v/2.5\, v_o$, equal to 0 – 0.6 was selected as a variable parameter of the condition, but not the rate of electrode end displacement in extreme positions, v.

The change of current and voltage in a stable process (end of surfacing) of the experiment were recorded on an oscillogram. To determine the maximum and minimum values in a separate period and its mean value in the experiment the lengths of oscillograms of 500 mm length (10 – 15 periods) which included a moment of electrode location in extreme position were considered (Figure 2). Surfacing was performed with 2 mm diameter self-shielding wire PP-Np-30Kh4G2SM using 75 mm diameter samples.

Change in CV of a root-mean-square amplitude of oscillations of welding current in experiments had positive and negative signs. The negative values CV were typical of experiments in which the wire feed speed was minimum and the arc voltage was maximum. In addition, the wire melting was ahead of its feeding and the current decrease due a self-adjustment of arc was higher than its increase at the moment of the electrode drop transition to the weld pool. The arc was stable and the deposited metal was of the high quality in experiments, the root-mean-square amplitude of current oscillation varied within 0 – 10 % of the current mean value.

Model of welding current stability CV has been developed by the method of multidimensional regressive computer analysis:

$$CV \cdot 10^3 = 283.3 - 380.52\, v_{w.f} - 6.24 U_a - 304.2\, v_o + 6.52\, e - 4.04 R_o + 8.1 L_e + 32.5\, v_{w.f}.$$

$$U_a = 77112 v_{w.f}\, v_s - 23.4\, v_{w.f}\, e - 503\, v_s\, e + 0.026 U_a\, R_o - 0.013 R_o\, e - 0.266 L_e\, U_a + 7.16 L_e\, v_o - 0.76 L_e\, e - 146.2 v_{w.f}\, m + 2737152 v_s^2 + 0.015 R_o^2 + 19.9\, m^2.$$

Here, the coefficient of correlation $R = 0.96$, residual deviation $\sigma_0 = 6.22$.

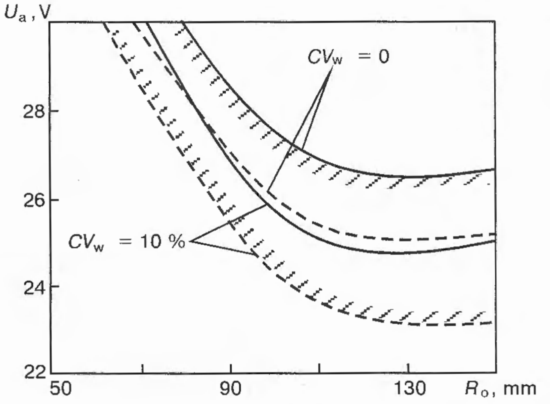

Figure 3. Effect of radius R_o of electrode oscillation and arc voltage U_a on the stability of arc process at the following parameters: $v_o = 0.02$ (solid) and 0.09 (dashed line), m/s; $v_{w.f} = 0.105$ m/s; $v_s = 0.0015$ m/s; $L_e = 22$ mm; $e = 8.5$; $v = 0.04$ m/s

The model adequacy was evaluated by the Fisher's criterion. The obtained calculated value 1.65 is less than a table 3.7 value, that does not contradict the hypothesis of the model adequacy at the level $\alpha = 0.05$. Boundary values of arc voltage and radius of electrode oscillations for the 0.018 – 0.074 m/s interval of rate of oscillations are shown in Figure 3. Relative dispersion of calculated values was $\sigma_c^2 = 0.72$. The achievement of stability of the process at small radii of oscillations at the expense of the voltage increase is associated most probably with an increase of the arc length at extreme positions of the electrode (by 4.6 mm at 80 mm radius of oscillations and 55 mm width of the deposited layer). With voltage increase the arc gap is increased and its relative changes become less than those which are compensated in the process of a self-adjustment, i.e. the arc will burn more stable.

Thus, after determining the wire feed speed and surfacing speed by calculations using sizes of the metal layer deposted and taking the values of other condition parameters of the wide-layer surfacing from technological and design conditions, it is possible to predict the stability of the arc process and the quality of the deposited layer of metal by comparing the expected change in CV within the interval 0 – 10 %.

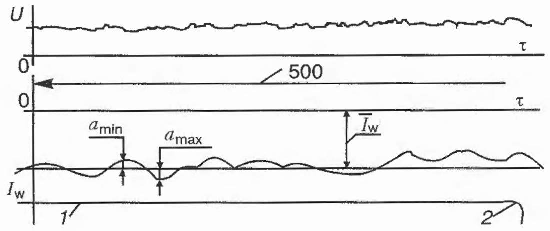

Figure 2. Length of current and voltage oscillogram (recording rate 250 mm/s): *1* — characteristic of electrode position; *2* — electrode in extreme position

CONCLUSIONS

1. In wide-layer surfacing with a self-shielding flux-cored wire with a curvilinear trajectory of transverse oscillations of electrode the process of a stable self-adjustment of the arc is possible, when the root-mean-square amplitude of current oscillations is 0 – 10 % of its mean value.

2. Stable process of melting with a self-shielding flux-cored wire in a wide-layer surfacing within the arc voltage 23 – 30 V is possible at radii of oscillations of the electrode end of more than 60 mm, the increase in radius for 10 mm makes it possible to decrease the voltage by 1 V. At radii of more than 110 mm the process is stable within the range of arc voltages 23 – 27 V.

REFERENCES

1. Sytnik, V.A., Makarov, V.K., Drozdov, A.P. *et al.* (1976) Determination of optimum surfacing conditions using the method of a rational design of experiments. *Svarochnoye Proizvodstvo*, **7**, 26 – 28.
2. Pokhodnya, I.K., Marchenko, A.V., Gorpenyuk, V.N. *et al.* (1979) Study of alternating current arc stability. In: *Proc. of Int. Conf. on Arc Physics and Weld Pool Behaviour*, London, 1979, May 8 – 10. London.

ELECTRON BEAM BRAZE WELDING OF COMPRESSOR IMPELLERS*

L.W. MYERS[1] and **G. LaFLAMME**[2]
[1]Dresser-Rand Co., USA
[2]PTR-Precision Technologies, Inc., USA

ABSTRACT

The development of a unique welding process which combines electron beam welding and brazing in one operation is described for application to centrifugal compressor impellers. The first phase of the testing program (reported in this paper) consisted of welding T-samples to develop welding conditions, axial and bending fatigue, metallurgical investigation, and hardness testing. Upon completion of testing, prototype impellers were fabricated to prove the process on production parts, and these impellers were also destructively examined after overspeed testing. All test results have been excellent, and the process is being used to produce impellers.

Key words: *electron beam braze welding, compressor impellers, fillet weld, slot weld*

Compressor impellers consist of only 3 major components — the disc (hub), cover (shroud), and blades (Figure 1). The blades are attached to the disc either by welding, machining from a solid forging, or integrally cast with the disc. The cover is usually joined to the blades by welding or vacuum furnace brazing. Dresser-Rand has a long history of experience with welding impellers, and is a recognized leader in welded impeller technology. Some of the welding processes utilized are the internal fillet weld, the slot weld, and the electron beam weld. Each of these weld processes has advantages as well as practical limits to its application. Upon review of the existing weld processes, it became apparent that the electron beam weld process held substantial potential for productivity and quality improvements beyond the potential of the other processes. For this reason, the electron beam weld method was studied for ways to expand and optimize the range of it's traditional application, including elimination of the notch effect caused by the unfused area of the weld joint (Figure 2).

A brainstorming session was held to develop an improved electron beam welding method. This session resulted in a variety of possible solutions. The first and most obvious solution was to refine weld techniques to weld closer to the edge of the blade by manipulating the angle that the electron beam penetrated through the cover and into the blade. This approach was unsuccessful, and deemed to be impractical due to the shape of the weld plume as it developed in the cover prior to entering the blade,

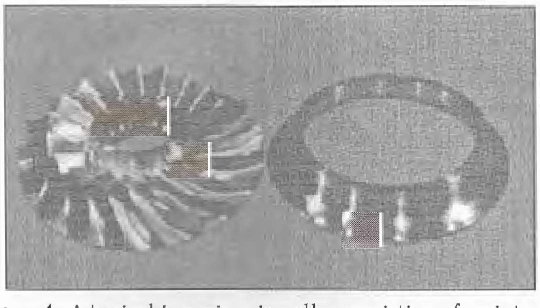

Figure 1. A typical two-piece impeller consisting of an integral machined bladed disc and separate cover

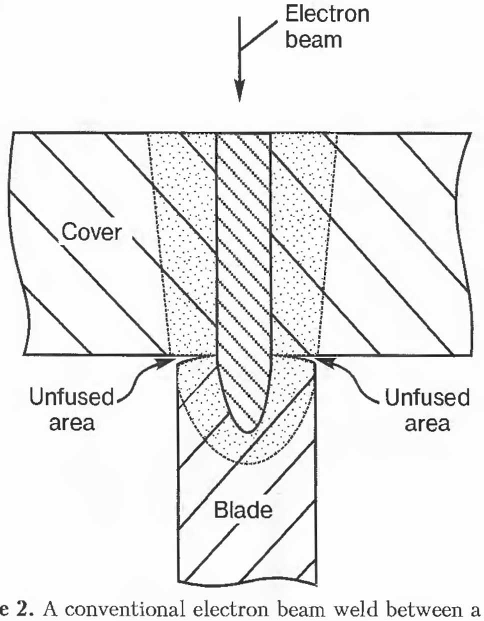

Figure 2. A conventional electron beam weld between a cover and blade showing the fused and unfused areas

* The paper was presented at the International Conference «Welded structures», Kyiv, Ukraine, 10 – 12 October, 2000.

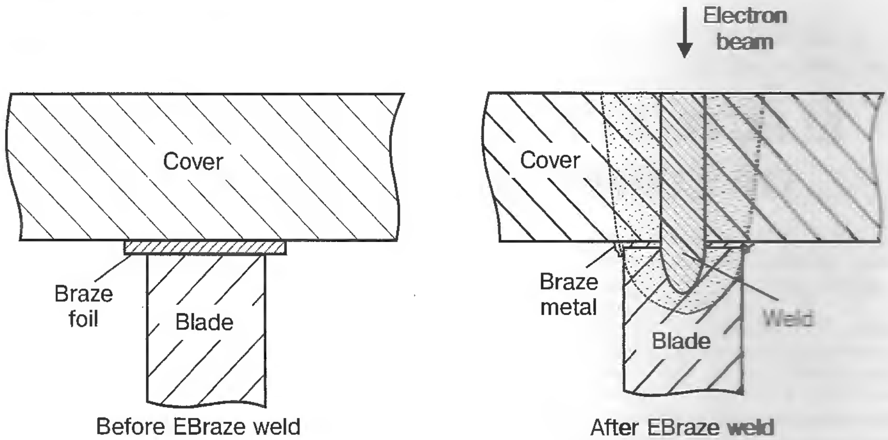

Figure 3. Expected configuration of a typical EBraze welded joint

as well as the increased distance that the beam had to travel, which required that the power of the beam be adjusted more radically than was required for the more normal weld path.

The second approach was borrowed from the vacuum furnace braze process which was also being evaluated simultaneously. The «what if» question that was asked during the brainstorming session was, what would happen if we put a piece of braze foil between the cover and blade, and then proceeded to electron beam weld right through it? Since the braze alloy melted at a lower temperature than the steel cover and blades, it was hoped that the molten braze alloy would fill the unwelded gap on both sides of the welded joint, resolidify, and fuse the cover and blade together in the formerly unwelded areas. It was expected that not only would there be some strength gained from the fusion of the unwelded areas by the braze alloy, but a major side benefit would be the reduction and/or elimination of the classic stress riser normally attributed to the unwelded areas.

After discussing this idea with the electron beam weld machine manufacturers, it was decided to prepare some sample pieces and test the process. There were unknowns associated with the behavior of the braze alloy when intermixed with the molten weld metal. It was decided to use the same material prepared in the same way as the earlier weld joint fatigue test samples, so that any differences in behavior could be directly attributed to the weld joint, not some other varying parameter. There were also unknowns associated with the electron beam penetrating different materials. Nevertheless, the samples quickly proved that the process worked (Figure 3). The fatigue test results bore out the contention that the stress riser was not only reduced, but that additional strength was evident from the braze alloy bonding the cover and blade in the formerly unfused area. The term «EBraze Weld Process» was created by Dresser-Rand to name this new process.

The remainder of the paper describes the details of the weld process development and testing program.

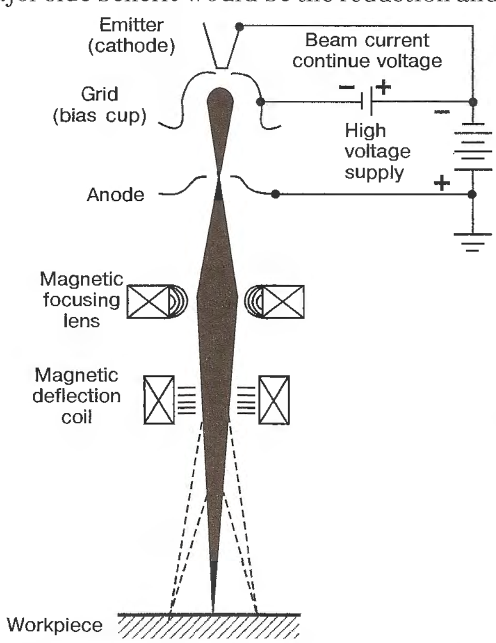

Figure 4. A schematic of the electron beam process [1]

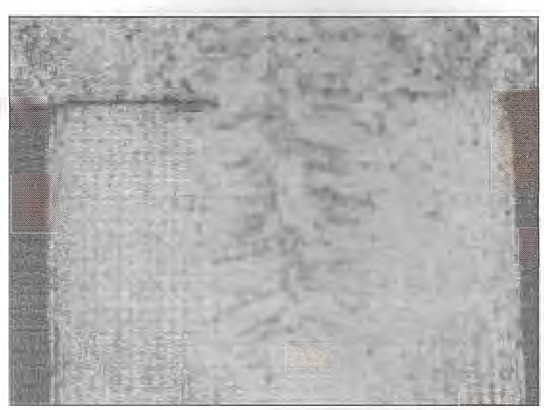

Figure 5. Typical cross-section of an electron beam welded joint. Notice the unfused areas on both sides of the weld

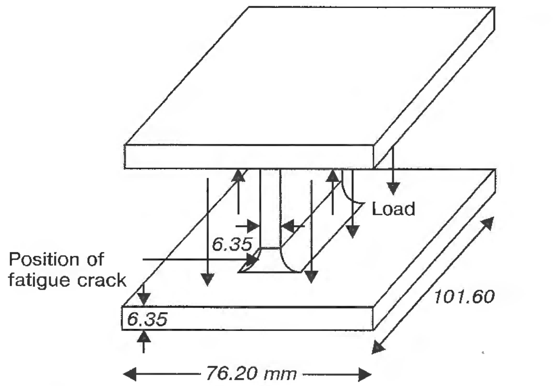

Figure 6. Axial tension specimen geometry and its fatigue loading

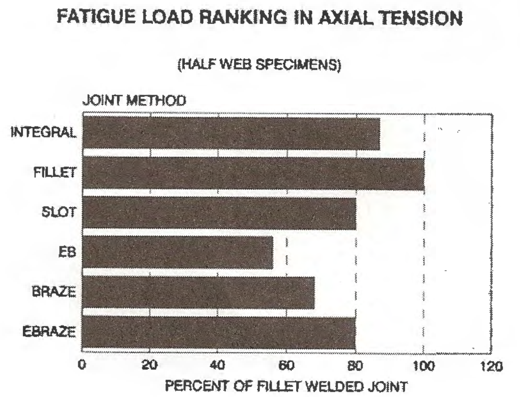

Figure 8. Fatigue load carrying performance of the axial tension specimens

Weld process development. Electron beam (EB) welding is accomplished with a stream of high velocity electrons which is formed into a concentrated beam to provide a heating source. The process, illustrated in Figure 4, produces intense local heating through the combined action of the stream of electrons. Each electron penetrates its own short distance into the workpiece and gives up its kinetic energy in the form of heat. With a sufficiently high volume of electrons (there are approximately 6.3×10^{15} electrons per second in a 1 mA current stream), a hole can be melted through the workpiece. This hole is called a keyhole, and as the beam is moved along the work, the melted material flows around the keyhole from front to back. If the keyhole is moved along a tightly fitup joint, a weld between the two components is achieved. EB welding has several major advantages. It can produce deep, narrow, and almost parallel-sided welds with low total heat input and comparatively narrow HAZ. The depth to width ratio can be in excess of 10 to 1 (Figure 5).

Testing program. The testing program attempted to simulate the mechanical performance of the EBraze welded joints in impellers using small scale I-beam specimens. It is a well known fact that a majority of impeller fatigue failures occur at impeller blade/cover or blade/disc joints. These failures are often located at either a blade leading edge (impeller eye), or a blade trailing edge. Stress analysis revealed that the centrifugal and gas pressure forces acting on these locations are different. At the impeller eye, the tensile loading is believed to be a dominant force, while the bending/shear loading should be the acting force at the impeller outer diameter. Therefore, the specimens were tested either in axial tension across the web (impeller blade) of the I-beam or by bending/shear loading of the I-beam web.

The geometry described as half web axial tension test specimen is shown in Figure 6. Pictured in Figure 7 is the full-web bending/shear test specimen geometry. The purpose of the program is to establish a performance ranking of the EBraze welding process and several conventional impeller joining methods in terms of fatigue load carrying capability.

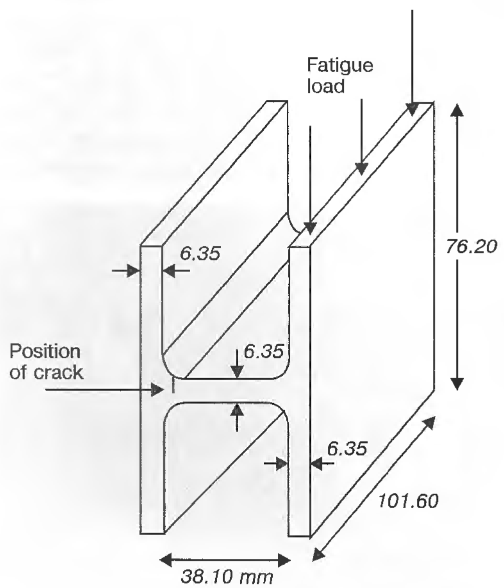

Figure 7. Bending/shear specimen geometry and its fatigue loading

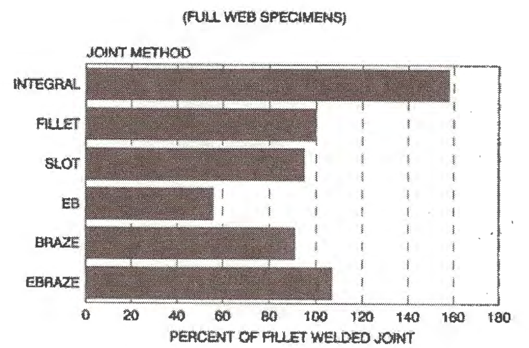

Figure 9. Fatigue load carrying performance of the bending/shear specimens

Table 1. Test results for the axial tension specimens

Joint method	*Mean fatigue load (lbf)* and $2\cdot10^6$ cycles*	*No. of specimens tested*
Integral	2850	14
Fillet	3262	19
Slot	2595	19
EB	1838	31
Braze	2225	20
EBraze	2603	18

*lbf = $21\cdot10^3$ MPa.

Table 2. Test results for the bending/shear specimens

Joint method	*Mean fatigue load (lbf)* and $2\cdot10^6$ cycles*	*No. of specimens tested*
Integral	1853	18
Fillet	1170	19
Slot	1136	21
EB	650	33
Braze	1063	18
EBraze	1252	16

*lbf = $21\cdot10^3$ MPa.

During both axial tension and bending/shear fatigue test, an R-ratio of 0.1 was maintained based on the nature of the simulation. (R-ratio is a ratio of minimum stress to maximum stress during a fatigue test.)

The failure condition in fatigue was defined by the loss of load controllability due to the large deflection of the cracked assembly. In practice this resulted in nearly 90 % of the joint area cracking in axial tension and approximately 60 % of the joint area cracking in bending/shear. Very little additional life to a complete separation would be expected beyond the chosen cutoff point.

All of the fatigue tests were specified according to the staircase method as described in ASTM STP 91A for a mean fatigue load at $2\cdot10^6$ cycles [2].

Fatigue test results. The results giving mean fatigue loads at $2\cdot10^6$ cycles for each joint method are shown in Tables 1, 2. Fatigue crack locations depend upon loading and joint type, but were repeatable.

Since the mean fatigue load values in this test are meaningless unless compared to each other, we used the fillet welded values as a benchmark to derive the performance rankings of the all joint methods (Figures 8, 9).

Metallurgical analysis. There are a number of areas to investigate in the EBraze welding process as a welding method. The most obvious one is the role of the melted braze metal inside the weld joint. In general, a lower melting temperature metal should not be mixed within a higher melting temperature parent metal during its welding. In many documented incidents, a low melting temperature alloy causes cracking in the steel welds. The braze alloy used in the EBraze welding process is a commercial brazing alloy. The reason that the low melting temperature metal cracking in the welds did not occur in this process could be contributed to a very low solubility of gold in iron and its absence in the parent metal grain boundaries. Another area to investigate is the possibility of forming certain phases in or near the weld that could lead to some «hard spots» in a subsequent heat treatment. Again, the low solubility of gold in iron made this scenario impossible. In addition, diffusion of a large amount of nickel from the braze metal into the nearby parent metal or the weld to form hard spots does not take place because the large nickel atomic size prevents it from migrating into the parent metal [3]. A destructive sectioning and a hardness survey of a fully heat-treated EBraze welded impeller proved that the above mentioned concerns are unnecessary (Figure 10).

In a typical EBraze welded joint (Figures 11, 12), a conventional electron beam weld formed at the center location in relation to the thickness of the blade. A layer of braze metal was also observed in formerly unfused areas in a typical electron beam

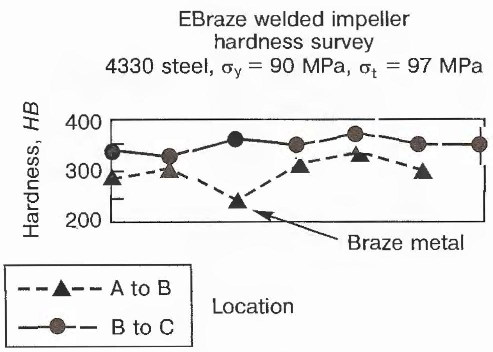

Figure 10. Hardness survey of the joint from Figure 11. The hardness values are converted from KHN_{300} values

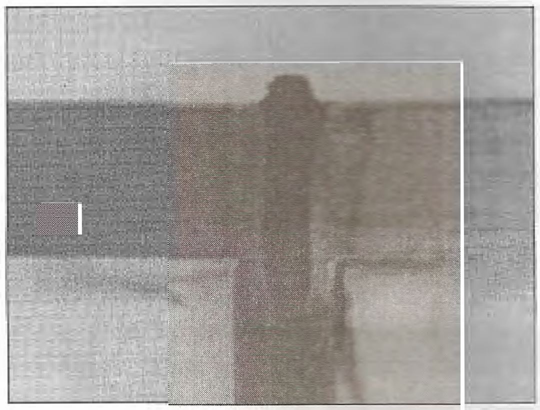

Figure 11. A typical EBraze welded joint (≈ ×3)

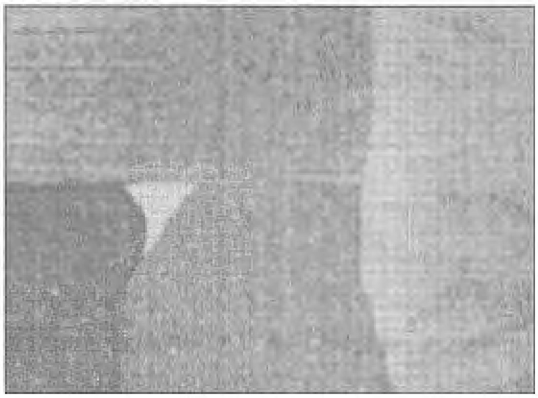

Figure 12. A close-up view of the joint in Figure 11. Notice a fillet was formed and the gap between the pieces was fused by the braze metal (×25)

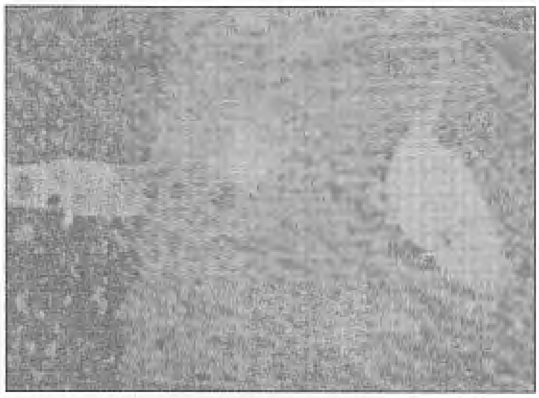

Figure 13. A close-up view of the weld in Figure 12. Notice that the morphology of two gold nodules were «trapped» in the weld, but did not cause any cracks (×200)

welded joint to form a conventional brazed joint. Some braze metal was «squeezed» out from the joint during the weld solidification process. One interesting observation in the analysis is the thickness of the braze layer. The braze foil started with several thousandths of a thick and the final brazed layer is less than 0.025 mm thick. It is believed that the cover and the blade were pulled together during the electron beam weld solidification process. It is a potentially significant benefit for the welding technique since machining tolerance requirements may not be as critical compared to that in the brazing process. A closer examination found that some braze metal was «trapped» inside the weld and formed gold nodules (Figure 13). However, these small areas are ductile and coherent with the weld microstructure.

Impeller test. In order to prove that this process is practical in impeller fabrication, a 381 mm diameter impeller made of 4330 steel with a three-dimensional blade design was manufactured using the EBraze welding process. Extensive analyses were performed to investigate the feasibility of the process, follow-up treatment, the integrity of the welded impeller, and to explore the optimal processing parameters. The impeller was EBraze welded, heat treated to 90 MPa yield strength, final machined, ultrasonic inspected using the C-scan technique to detect any lack of bond or cracking in the joint, and oversped at 18,000 rpm. This impeller was then sectioned to correlate the C-scan results with the weld/fusion condition, and the hardness survey was conducted (Figure 10).

CONCLUSIONS

As can be seen in the foregoing paper, the EBraze welding process developed by Dresser-Rand represents a significant step forward in the technology of metals joining, and in particular to the application of fabricated centrifugal compressor impellers. The test program proved the process produced impellers with fatigue strength as good as or better than that of impellers welded by the more conventional welding processes, that the process is metallurgically sound, and that the welding parameters were capable of producing a production impeller with acceptable quality.

As of this writing, several hundred impellers have been manufactured using the EBraze welding process, passed in-house NDT and inspections, and are in service around the world.

Further development testing is also in progress in such areas as corrosion and impact testing, as well as testing the process on other commonly used impeller materials such as AISI-410 stainless steel, 17-4 and 15-5 PH stainless steels, and Cartech 625+. Although not yet complete, the preliminary results from many of these tests are quite positive, and will certainly be the subject of future technical papers on this subject.

To complement the development testing, a significant amount of analytical work was undertaken as well. The analyses consisted of traditional 3-D FEA, elasto-plastic FEA, transient thermal FEA, and fracture mechanics analysis. Much of this analytical work was groundbreaking in nature and provided a sound technical foundation to support the process development.

Finally, on behalf of Dresser-Rand, the authors wish to acknowledge and thank the Edison Welding Institute and PTR-Precision Technologies, Inc., without whose cooperation and assistance, this development would not have been possible.

REFERENCES

1. (1991) *Welding Handbook*. Ed. by R.L. O'Brien. AWS.
2. (1962) *A guide for fatigue testing and the statistical analysis of fatigue data*. Committee E-9 on Fatigue. ASTM.
3. Tolle, M.C., Kassner, M.E., Cerri, E. *et al.* (1995) Mechanical behavior and microstructure of Au–Ni Brazes. *Metallurgical and Materials Transaction A*, 4, 941.